NASA CR-134678

QUATERNARY AND QUINARY MODIFICATIONS OF EUTECTIC SUPERALLOYS STRENGTHENED BY δ, Ni_3Cb LAMELLAE AND γ', Ni_3Al PRECIPITATES

by

F.D. Lemkey and G. McCarthy

UNITED AIRCRAFT RESEARCH LABORATORIES
EAST HARTFORD, CONNECTICUT 06108
UARL R911698-13

Prepared for

NATIONAL AERONAUTICS AND SPACE ADMINISTRATION
Fredric H. Harf, Project Manager

NASA Lewis Research Center
Contract NAS 3-17785

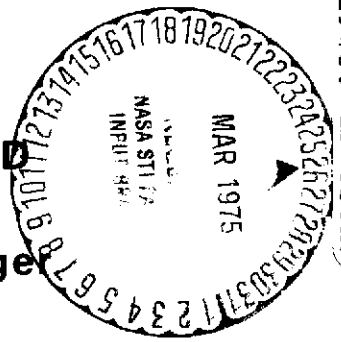

1. Report No.	2. Government Accession No.	3. Recipient's Catalog No.
NASA CR-134678		

4. Title and Subtitle	5. Report Date
QUATERNARY AND QUINARY MODIFICATIONS OF EUTECTIC SUPERALLOYS STRENGTHENED BY δ, Ni_3Cb LAMELLAE AND γ', Ni_3Al PRECIPITATES	February 1975
	6. Performing Organization Code

7. Author(s)	8. Performing Organization Report No.
F. D. Lemkey and G. McCarthy	R911698-13
	10. Work Unit No.

9. Performing Organization Name and Address	11. Contract or Grant No.
United Aircraft Research Laboratories East Hartford, Connecticut	NAS3-17785
	13. Type of Report and Period Covered Contractor Report

12. Sponsoring Agency Name and Address	14. Sponsoring Agency Code
National Aeronautics and Space Administration Washington, D. C. 20546	

15. Supplementary Notes

Project Manager, Fredric H. Harf, Materials and Structures Division, NASA Lewis Research Center, Cleveland, Ohio

16. Abstract

By means of a compositional and heat treatment optimization program based on the quaternary γ/γ'-δ, Ni-19.7 w/o Cb-6.0 w/o Cr-2.5 w/o Al, a tantalum modified γ/γ'-δ alloy with improved shear and creep strength combined with better cyclic oxidation resistance was identified. In this study quinary additions including W, Mo, Re, Co, Ti, Ta, Si, and B as well as quaternary adjustments and heat treatment were investigated. The tantalum modified γ/γ'-δ alloy, Ni-17.9 w/o Cb-6.0 w/o Cr-2.5 w/o Al-3.0 w/o Ta, possessed a slightly higher liquidus temperature and exhibited rupture strength exceeding NASA VIA by approximately three and one-half Larson-Miller parameters (C = 20) above 1000°C. Although improvements in longitudinal mechanical properties were achieved, the shear and transverse strength property goals of the program were not met and present a continuing challenge to the alloy metallurgist.

17. Key Words (Suggested by Author(s))		18. Distribution Statement
Solidification	Directional Solidification	Unclassified - Unlimited
Eutectic Alloys	Composites	
Nickel Alloys	Refractory Compounds	

19. Security Classif. (of this report)	20. Security Classif. (of this page)	21. No. of Pages	22. Price*
Unclassified	Unclassified	137	5.75

* For sale by the National Technical Information Service, Springfield, Virginia 22151

Report N911698-13

Quaternary and Quinary Modifications of Eutectic Superalloys Strengthened by δ, Ni_3Cb Lamellae and γ', Ni_3Al Precipitates

TABLE OF CONTENTS

TABLE OF CONTENTS (Cont'd)

LIST OF TABLES

LIST OF ILLUSTRATIONS

LIST OF ILLUSTRATIONS (Cont'd)

LIST OF ILLUSTRATIONS (Cont'd)

LIST OF ILLUSTRATIONS (Cont'd)

LIST OF ILLUSTRATIONS (Cont'd)

LIST OF ILLUSTRATIONS (Cont'd)

SUMMARY

The purpose of this program was to develop by iterative experimental adjustments of both composition and heat treatment, an improved γ/γ'-δ alloy based on Ni-19.7 w/o Cb-6.0 w/o Cr-2.5 w/o Al. The optimized alloy was expected to maintain useful high temperature properties to 1200°C (2192°F) and exceed the rupture strength of NASA VIA by at least two Larson-Miller units above 700°C (1290°F). Gains in intrinsic oxidation resistance and isotropy of critical mechanical properties (i.e. shear and tensile strength/ductility) were also sought.

Quaternary modifications and quinary additions from the elements Co, Ti, Mo, W, Re, Ta, B, and Si to the base line quaternary Ni, Cb, Cr, Al alloy were examined for various concentrations. While certain elements were added to improve the balance of mechanical properties, maximum phase stability was also sought from minimization of the γ/γ' lattice parameter mismatch by compositional control. Alloy additions which exceeded the solid solubility limits of either phase and resulted in the formation of additional phases upon freezing were not considered within the scope of this program. Extensive alloying was possible for elements which exhibited a wide solubility range in both phases, e.g. Co, Ti, and Ta. On the other hand, limited substitution of W, Mo, Re, Si and B was possible for elements whose solid solubility was restricted especially in the δ phase. These alloying paths permitted changes in the composition and volume fraction of all the pertinent phases, i.e. γ, γ' and δ.

The substitution of three weight percent tantalum on an equiatomic basis for columbium provided the most promising alloy modification, i.e. Ni-17.9 w/o Cb-3.0 w/o Ta-6.0 w/o Cr-2.5 w/o Al. This alloy possessed a higher liquidus temperature, improved shear at intermediate temperature and creep rupture strength (exceeding NASA VIA by more than three parameters above 815°C) combined with an unexpected but significant improvement in cyclic oxidation resistance. No damage to the elevated temperature rupture properties after 3000 thermal exposures between 400°C minimum/1120°C maximum in 2.1 minute cycles was observed. The alloy failed however to meet the transverse strength and ductility and the elevated temperature shear strength goals of the program. Widmanstätten precipitates were observed in both the tantalum modified and base line γ/γ'-δ alloys after extended (1500 hrs) exposures to 850 and 900°C respectively. The presence of such Widmanstätten δ within γ/γ' was somewhat deleterious to the low temperature fracture toughness.

After systematically screening γ/γ'-δ alloy modifications for comparative shear, tensile, rupture and oxidation properties, one promising alloy was chosen and evaluated subsequently in greater detail. Heat treatment of the quaternary base line γ/γ'-δ alloy, Ni-19.7 w/o Cb-6.0 w/o Cr-2.5 w/o Al, indicated that although useful changes in the strength and ductility at low and intermediate temperatures were effected, no improvement at elevated temperature properties was observed.

I. INTRODUCTION

Even though there have been and continue to be concentrated research and development programs on other, more refractory materials, nickel-base alloys must still be considered paramount for present and near term high temperature gas turbine applications. Toward this end the United Aircraft Research Laboratories have pioneered new families of directionally solidified alloys termed 'Eutectic Superalloys' which may permit a 60-110°C (100-200°F) increase in allowable metal temperature over current superalloys. One such alloy within the γ/γ'-δ system, Ni-19.7 w/o Cb-6.0 w/o Cr-2.5 w/o Al, optimized under Contract NAS3-15562 (Ref. 1), was found to be superior to all advanced nickel-base superalloys in tension and in creep. Although the longitudinal mechanical properties of this alloy were outstanding, improvements in creep and shear strength together with gains in intrinsic oxidation resistance and γ/γ' phase stability are envisioned by further adjustments of the quaternary composition and/or by quinary additions. This 'enlightened empirical' approach forms the basis of this program. A parallel activity, which will ultimately lead to engine component testing of this alloy system, proceeds under Contract NAS3-17811 with Pratt and Whitney Aircraft (Ref. 2) entitled "Alloy and Structural Optimization of a Directionally Solidified Lamellar Eutectic Alloy".

Currently, superalloys make up approximately 50% of the weight of advanced gas turbine engines. Most of these alloys are modifications of a nichrome matrix hardened by γ', but with further additions of Co, Fe, W, Mo, V, Ti, Nb, Ta, B, Zr, C and Mn. Thus, today's superalloys are known for their complexity and their compositions have evolved empirically over the last thirty years. This trend might be expected to continue in the development of recently identified eutectic systems (Ref. 3), resulting in adjustments in composition to meet the demands of the physical, mechanical, and chemical use criteria. The exploration of new and modified 'eutectic' alloy systems, uniquely conceived to achieve superior high temperature strength together with a favorable balance of properties to meet other selective use criteria, has only just begun.

Identified under NAS3-15562 (Ref. 1) were simple ternary monovariant γ/γ'-δ eutectic alloys encompassing the compositional range 1.0-3.0 percent by weight aluminum and 20-22 percent by weight columbium with a balance of nickel, which displayed promise for further optimization. One outstanding feature of these alloys was the great insensitivity of their directional microstructure to growth parameters which have allowed them to be directionally solidified at velocities exceeding 100 cm/hr with a planar growth interface under a thermal gradient of ~300°C/cm. Their compositional uniformity after directional freezing was another outstanding feature.

To understand why this is so, one must relate the significant variables affecting the structure of biphase eutectic type alloys. As derived from the principles of constitutional supercooling (Ref. 4), the range of solidification conditions which permit aligned lamellar growth is qualitatively described by the relation:

$$\frac{G}{R} \geq \frac{\Delta T}{K}$$

where G is the thermal gradient in the liquid, R is the solidification velocity, ΔT is the freezing range of the alloy, and K is a constant which includes the solute diffusion coefficient and distribution coefficients. This relationship says that if one wishes to generate aligned biphase structures in any given γ/γ'-δ alloy either (1) an increase in G, (2) a decrease in R, or (3) a decrease in ΔT is required so that the G/R ratio exceeds some critical value for the particular alloy system. If the value of G/R is less than this critical value the alloy will solidify such that a cellular or dendritic microstructure is produced. For the ternary γ/γ'-δ monovariant alloys, none of which possesses a melting range greater than 5 degrees celsius, the critical value of G/R is ~3°C hr cm^{-2}. With respect to the foundryman's endeavors to control microstructure in a complex shape such as a turbine blade, this property is a highly desirable one.

The in situ composites resulting from the directional growth of these monovariant γ/γ'-δ alloys were found to be ductile, with fracture elongations as high as 30%, and much tougher than current superalloys, e.g. impact energies of 13 J (19.9 ft-lbs) compared to 4 J (3 ft-lbs) for Mar-M200 on half size Charpy specimens. These alloys were also very creep resistant at elevated temperature, exceeding the rupture life of current superalloys (100 hr 1093°C (2000°F) and 14 x 10^7 N/m^2 (20 ksi)).

In order to improve the oxidation/corrosion resistance of these alloys, chromium was added up to approximately 15% by weight. Attendant with additions of chromium is an increasing melting range of the alloy which increases the difficulty of directional processing. One alloy, Ni-19.7 w/o Cb-6.0 w/o Cr-2.5 w/o Al, has a useful balance of properties, e.g. superior creep strength, useful ductility, good oxidation resistance and acceptable processability. The critical G/R value for this alloy was >40°C hr cm^{-2}. The routinely controlled solidification of this alloy in the laboratory with no elaborate temperature control resulted in 15-20 cm (6-8 in.) long ingots displaying little macrosegregation, and few microstructural perturbations along their length. However, there is no way of quantitatively "scaling up" the results of these small scale laboratory experiments to absolutely predict the conditions that will give optimum results in large, more complex castings, e.g. cluster investment castings. This is because the various

physical growth parameters such as temperature gradient, rate of removal of heat, and convection of the liquid metal, depend in different ways on the shape and dimensions of the mold. Such problems will be solved either by ingenious application of solidification principles combined with careful experiment, or by computational analyses based primarily on empirical data.

The design of an improved γ/γ'-δ alloy will in general follow an 'enlightened empirical' route. Alloy theory alone, used to predict increased mechanical properties will not suffice, but evolutionary improvements will soon come to a stop if theoretical insight is not used as a guide for the experimental approach. Besides the alloy compositional adjustments for property enhancement, the importance of heat treatment of any modified γ/γ'-δ alloy cannot be overlooked. Because of the complex compositions of these alloys, a wide variance in properties may be achieved by the use of different heat treatments. The optimum heat treatment cycle for each new alloy will thus depend upon the property requiring optimization. In general, the following design steps will be taken to increase longitudinal creep strength and bring about a favorable balance of physical, mechanical, and chemical properties required for engine application:

1. Solid solution harden γ
2. Solid solution harden γ'
3. Increase volume percent γ'
4. Increase volume percent δ
5. Decrease γ/γ' ripening rate by decreasing Δa or $(a_\gamma - a_{\gamma'})$
6. Align lamellae at maximum freezing velocity.

The overall objective of this program was to develop, by means of optimization of composition and heat treatment, an improved γ/γ'-δ alloy based on Ni-19.7 w/o Cb-6.0 w/o Cr-2.5 w/o Al with greater potential for use in advanced gas turbine engines.

The properties of the alloys produced and tested were compared against the following goals:

(1) A tensile strength of not less than 250 MN/m^2 (36,300 psi) at 1200°C (2192°F).

(2) A rupture strength exceeding the Larson-Miller parameters of NASA VIA alloy by at least two units at all temperatures above 700°C (1290°F), (Parameter = $1.8\ T\ (20 + \log t) \times 10^{-3}$ where T = temperature in °K, and t = time in hrs).

(3) Tensile and rupture ductility as measured by elongation and reduction of area, of at least 5% over the entire temperature range from room temperature to 1200°C (2192°F).

(4) Resistance to thermal fatigue cracking and delamination under conditions of thermal cycling as evidenced by post exposure microstructure and stress rupture properties.

(5) Phase stability after long exposure to elevated temperatures as evidenced by microstructure and room temperature tensile ductility.

(6) Improved cyclic oxidation resistance over that produced for the base alloy in Contract NAS3-15562. The formation of an adherent scale of Al_2O_3 should be promoted.

(7) Longitudinal shear yield strength properties equivalent to not less than 40% of the longitudinal yield strength properties over the entire temperature range to 1200°C.

(8) Transverse tensile strength and ductility equivalent to not less than 80% of the longitudinal tensile strength in the range to 1200°C (2192°F).

II. EXPERIMENTAL PROCEDURES

2.1 Melting and Solidification

Master melts of the various alloys investigated were made in new recrystallized alumina crucibles in a Heraeus vacuum induction melting furnace powered by a 30 kw motor generator and pumped by a 25 cm (10 in.) vacuum system. The system was exhausted to approximately 0.001 N/m^2 (10^{-5} torr) and then back filled with high purity argon to provide a dynamic 200 liters per hr (~7 cfh) inert cover at atmospheric pressure. Power to the furnace coil was slowly increased until melting of the nickel, chromium and columbium charge material was achieved. Aluminum was then added separately to the melt. Subsequently the melt was held at a constant temperature of ~1400°C (2550°F) for a 15-20 min homogenization period prior to pouring into copper chill molds. The purity of the starting materials used is presented in Table I. Impurities detected by atomic absorption analysis are noted therein.

Each resulting cast alloy bar was usually directionally solidified vertically within a nominally 1.25 cm (1/2 in.) dia 99.7% recrystallized alumina cylindrical crucible whose wall thickness was nominally 2 mm. Vertical controlled solidification (upward moving liquid-solid interface) of the alloys under moderate thermal gradients was accomplished within a dynamic argon atmosphere in one of two identical graphite resistance furnaces. The alumina crucible, either open at both ends or closed at one end, containing the melt was supported on a movable water cooled pedestal as illustrated in Fig. 1. Crucible lowering rates were varied by means of a variable speed motor and a step function gear reducer from 1 to 20 cm/hr. The maximum melt temperatures observed on the surface of the melt were approximately 1650°C with the furnace control being accomplished automatically by a Milletron two color (ratio) optical pyrometer whose electronic servo loop monitors a saturable core reactor regulated 35 Kva power supply. The large thermal mass of these resistance furnaces provides the stability required for the linear movement of the liquid-solid interface.

Vertical controlled solidification was also accomplished in a high gradient apparatus described in Ref. 5. In this setup a known mass of alloy typically 200 gms, contained in a both ends open or one end closed cylindrical alumina crucible, is positioned within the induction coil, water spray ring, and constant water level tank as illustrated in Fig. 2. With the impinging water spray turned on, melting is accomplished by inductive coupling with the stationary graphite sleeve. Power requirements are established from empirical trials or experiments instrumented with thermocouples. The freezing is controlled by the withdrawal of the Al_2O_3 crucible through the water spray ring. In this setup thermal gradients in

Table I

Purity of Charge Elements
in ppm

	Nickel[1]	Chromium H. P. Flake[2]	Columbium[3]	Aluminum[4]	Cobalt[5]	Tantalum[6]	Molybdenum[7]	Titanium[8]	Rhenium[9]	Tungsten[10]	Boron[11]	Silicon[12]
Al	100	<2	<20	bal.	-	-	-	-	-	-	-	-
B	-	-	<1	-	-	-	-	-	-	-	99.8	-
C	-	10	35	-	60	<30	10	-	-	-	-	-
Ca	-	-	<20	-	-	<10	-	-	-	-	-	-
Cb	-	-	bal.	-	-	262	-	-	-	-	-	-
Cd	-	-	<5	-	-	-	-	-	-	-	-	-
Co	-	-	<10	-	-	<5	-	-	-	-	-	-
Cr	-	-	<20	-	-	-	-	-	-	-	-	-
Cu	1	2	<40	-	30	-	-	1	-	-	-	-
Fe	200	<2	<50	2	40	<15	20	5	-	-	-	-
H	-	<60	2.4	-	-	5	-	-	-	-	-	-
Hf	-	-	<50	-	-	-	-	-	-	-	-	-
Mg	10	-	<20	2	-	<5	-	1	-	-	-	-
Mn	-	-	<20	-	9	-	-	1	-	-	-	-
Mo	-	-	<20	-	-	<10	-	-	-	-	-	-
N	-	<30	33	-	-	25	-	-	-	-	-	-
Ni	bal.	-	<20	-	440	<10	<10	-	-	-	-	-
O	-	<600	<150	-	-	<50	-	-	-	-	-	-
Pb	-	<2	<20	-	3	-	-	-	-	-	-	-
Re	-	-	-	-	-	-	-	-	99.9+	-	-	-
S	-	<30	-	-	20	-	-	-	-	-	-	-
Si	100	<10	<50	-	20	<10	10	1	-	-	-	97+
Sn	-	-	<10	-	-	-	-	200	-	-	-	-
Ta	-	-	<110	-	-	-	-	-	-	-	-	-
Ti	-	-	<40	-	-	-	-	-	-	-	-	-
V	-	-	<20	-	-	<10	-	-	-	--	-	-
W	<100	-	43	-	-	140	-	-	-	99.9+	-	-
Zn	-	-	-	-	60	-	-	-	-	-	-	-
Zr	-	-	<100	-	-	-	-	-	-	-	-	-

[1]United Mineral & Chemical Corp.
[2]Shieldalloy Corp.
[3]Wah Chang Corp.
[4]Gallard Schlesinger Chemical Mfg. Corp.
[5]African Metals Corp.
[6]Wah-Chang Corp.
[7]Amax Specialty Metals
[8]Johnson Mathey Corp.
[9]Cleveland Refractory Metals
[10]Phillips-Elmet Corp.
[11]United Mineral & Chemical Co.
[12]Fischer Chemical

FIG. 1

GRAPHITE DIRECTIONAL SOLIDIFICATION FURNACE

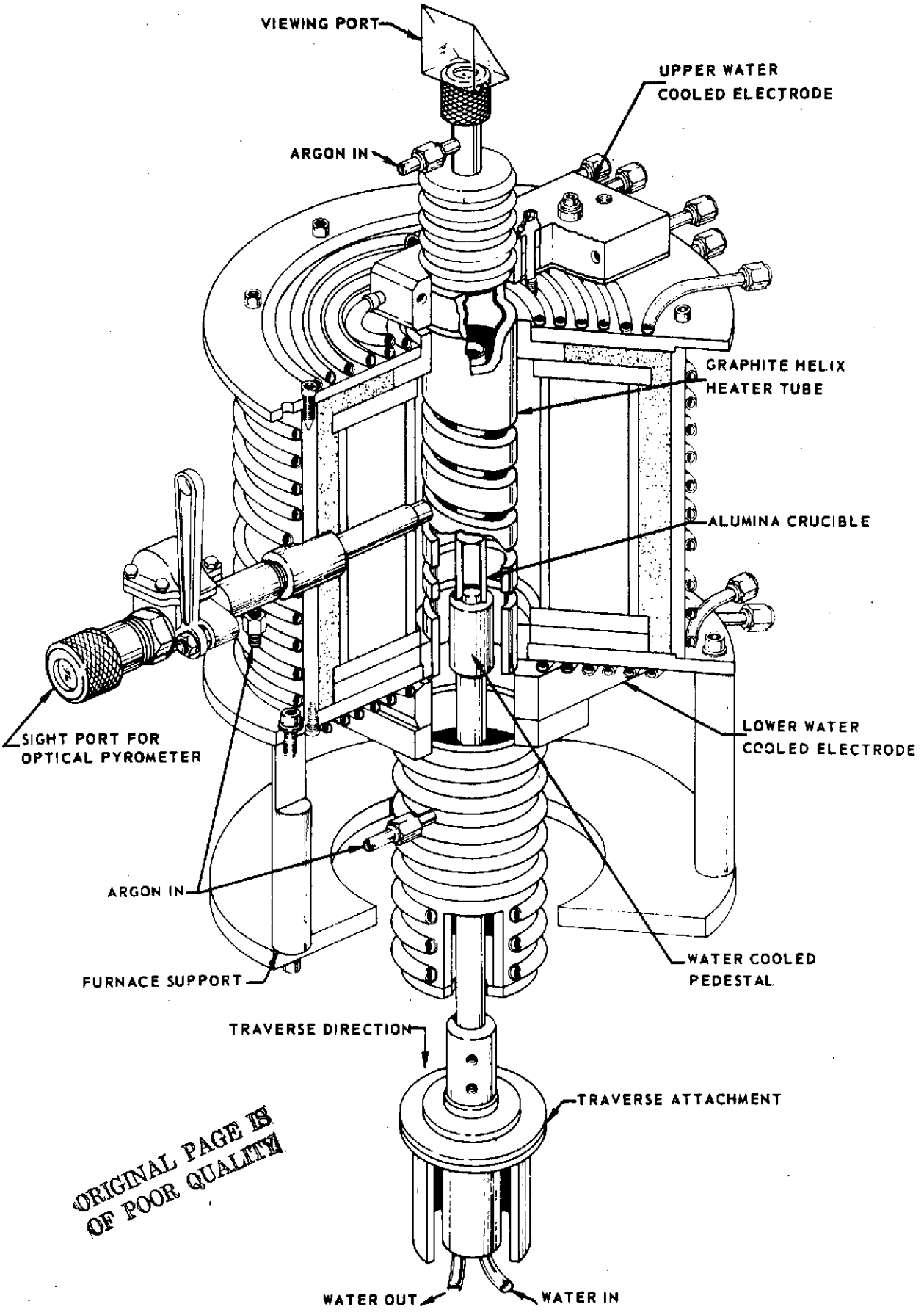

FIG. 2

HIGH THERMAL GRADIENT DIRECTIONAL SOLIDIFICATION APPARATUS

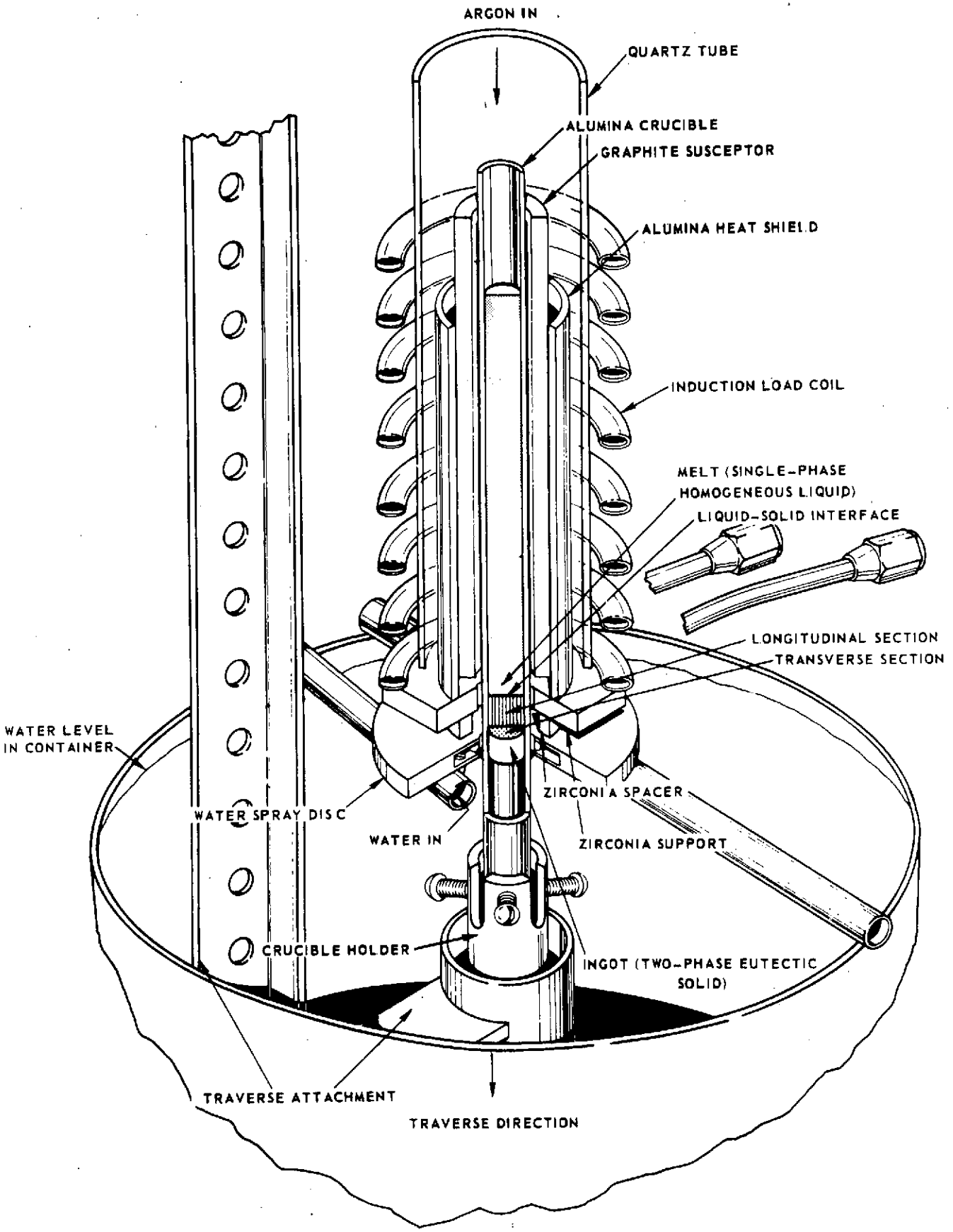

the liquid of approximately 250-350°C/cm were routinely achieved. Excluding small end affected regions the rate of freezing is found to be equal to the velocity of crucible withdrawal over the entire specimen length solidified. Each directionally solidified bar was given a laboratory number and each subdivided specimen was identified by a dash (-01, -02, etc.) and numbered from the end first solidified.

The maximum superheat of the melt was monitored by an optical pyrometer and held to approximately 400°C. This technique permitted the containment of the alloys within commercial Al_2O_3 tubes without serious metal-mold reaction and resulted in fully aligned 1.25 cm dia by 18 cm long cylindrical bars. Some vertical cracking of the oxide tubes resulted from the severe thermal shock of the water spray. However, complete loss of the melt or vertical lines of severe local oxidation from cracks occurred in less than 10% of the total experiments after experience was gained. During the second task of the contract a total of 40 directionally solidified bars were prepared without run-out failures.

2.2 Differential Thermal Analysis

The liquidus and solidus temperatures of certain quinary modified alloys of the system Ni-Cb-Cr-Al were determined using a differential thermal analysis apparatus. Heating and cooling of the sample was accomplished in argon at a rate of 3°C/min. The platinum vs platinum-10% rhodium thermocouple used was calibrated against a pure silver standard and the accuracy of the temperatures measured was within $\pm$2°C. The liquidus temperature was normally determined during cooling and the solidus during heating from the respective exothermic and endothermic inflections of the temperature-differential temperature traces.

2.3 Chemical Analyses

Wet chemical analyses were performed on specimens taken from the steady state growth area of a directionally solidified bar. The sample was dissolved in a nitric acid-hydrofluoric acid solution and fumed with sulfuric acid. After dissolution Cb was precipitated with cupferron. The precipitate was ignited and dissolved by fusion with potassium pyrosulfate. The Cb was then hydrolyzed and the precipitate ignited and weighed as Cb_2O_5. The filtrate from the hydrolysis and the cupferron precipitation were combined and evaporated to destroy the excess cupferron. After diluting to a convenient volume, a sample was taken for each Ni, Al, and Cr analysis procedure. Chromium was determined by a ferrous sulfate permanganate titration after persulfate oxidation to a chromate. Nickel was precipitated as the glyoximate. Finally, after a mercury cathodic electrolysis to remove nickel and chromium, aluminum was determined by E.D.T.A. titration.

As wet chemical analysis is a tedious and expensive destructive process, the use of X-ray fluorescence analysis was employed as an alternative nondestructive and less expensive technique. Under a separate program (Ref. 6), the X-ray

fluorescence (XRF) intensities of Co, Ni, Fe, Mo, Zr, V, Al, Ti, Cr, Nb, W, and Ta in approximately 75 analyzed samples were recorded. These samples included Ni-base alloys obtained from the National Bureau of Standards, Carpenter Technology, and those previously analyzed by wet chemical means for NASA at UARL. A least mean square fit of intensities versus concentration was obtained using a multi-element regression program on a PDP-6 time share computer. After obtaining the sample XRF's intensities, they were entered into the program to obtain the calculated concentration.

X-ray fluorescence analyses at 1.27 cm (1/2 in.) intervals were performed over the entire length of d.s. (Ni-19.7 w/o Cb-6.0 w/o Cr-2.5 w/o Al) alloy bars. A 0.95 cm (3/8 in.) dia window was used in recording the X-ray fluorescence intensities. Measurements were made by translating a typically 15.2 cm (6 in.) long specimen with a ground longitudinal flat under the window.

2.4 Tensile Testing

Tensile specimens, ground from unidirectionally solidified bars, were oriented in such a way that the load would be applied parallel to the growth direction. Tensile tests of 1.27 cm (0.5 in.) gage length and 0.36 cm (0.140 in.) diameter samples were conducted in accordance with ASTM specification E21-69 (Ref. 7) from room temperature to 1235°C (2200°F) in air using a Tinius-Olsen four-screw machine at strain rates of 0.01 and 0.05 min^{-1}. The temperature was controlled to within ± 3°C and monitored during each test. Strain was measured at room temperature with two element averaging strain gages positioned 180° apart and by total crosshead deflection as measured by an LVDT (linear variable differential transformer) extensometer at elevated temperature. Ultimate strain and reduction in area values were made from measurements of the gage length and area before and after testing.

Measurements of the offset yield and elastic modulus at temperatures of 750, 815, 870, 925, 1000, 1050, 1100, 1150, and 1200°C were made using specimens (Fig. 3) containing ridges defining the 1.27 cm (0.5 in.) gage length which permitted direct strain measurements using 304 stainless steel extension rods coupled to a pair of averaging LVDT extensometers.

2.5 Stress Rupture and Creep Rupture Testing

Stress rupture tests were performed at 1149°C (2100°F) in vacuum. These tests were performed in accordance with ASTM E139-69 as applicable, with specimens of gage diameter 0.28 cm (0.110 in.) and gage length 1.27 cm (0.50 in.) with 5/16-18 threaded ends. A redesign of the stress rupture and creep specimens from one with a 1.27 cm (0.50 in.) long, 0.32 cm (0.125 in.) diameter gage and 1/4-20-NC3 threaded end was necessitated from thread shear failures observed after

TENSION TEST SPECIMEN

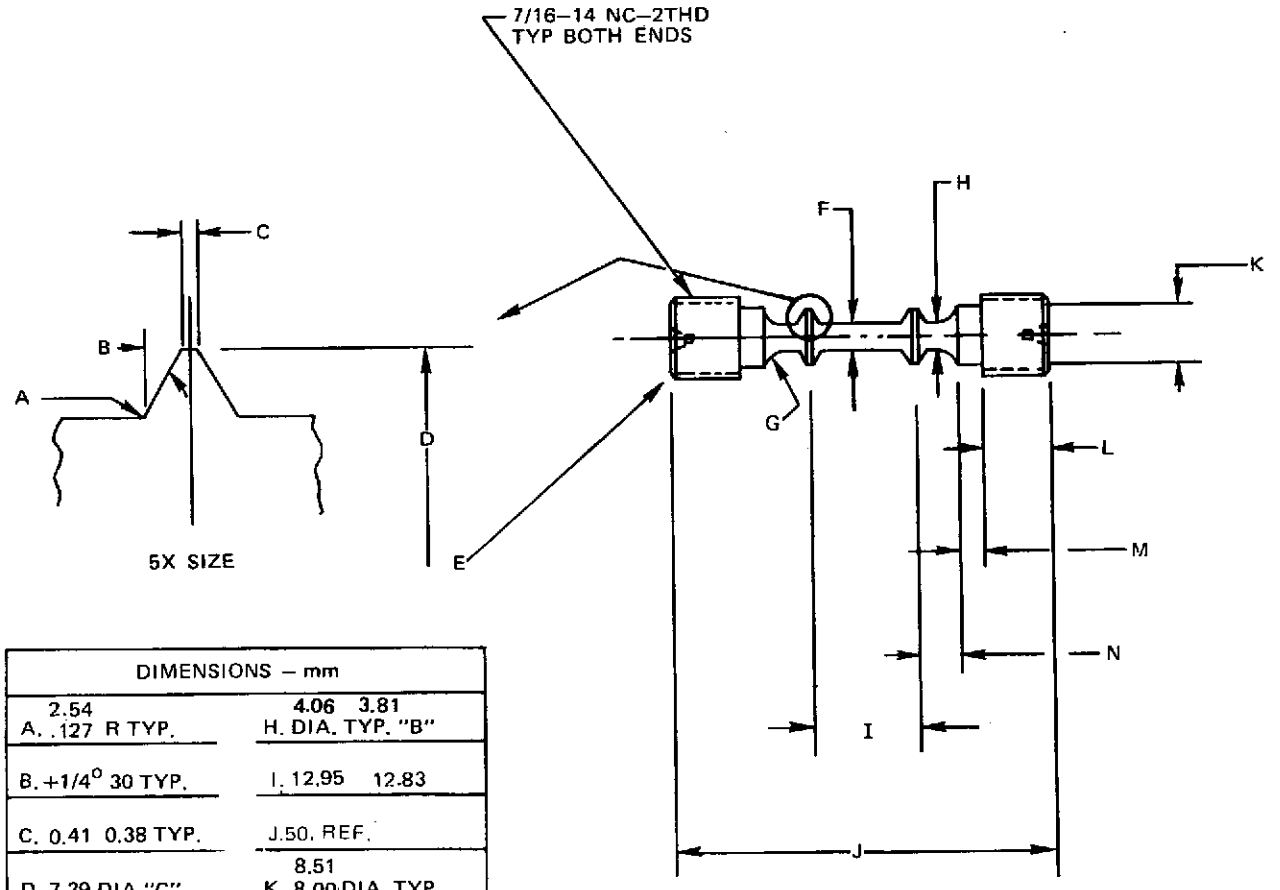

DIMENSIONS – mm	
A. 2.54 .127 R TYP.	H. 4.06 3.81 DIA. TYP. "B"
B. +1/4° 30 TYP.	I. 12.95 12.83
C. 0.41 0.38 TYP.	J. 50. REF.
D. 7.39 DIA "C"	K. 8.51 8.00 DIA. TYP.
E. 0.76 x 45° TYP	L. 9.78 9.27 TYP.
F. 3.58 3.53 "A" dia	M. 2.16 1.65 TYP.
G. 3.18 R (MIN) TYP.	N. 7.75 7.24 TYP.

DIMENSIONS – INCHES	
A. 0.10 0.005 R. TYP.	H. 0.160 0.150 DIA. TYP "B"
B. + 1/4° 30 TYP.	I. 0.510 0.505
C. 0.016 0.015 TYP.	J. 2. REF.
D. 0.291 DIA. "C"	K. 0.335 0.315 DIA. TYP
E. 0.030 x 45° TYP	L. 0.385 0.365 TYP.
F. 0.141 0.139 "A" DIA.	M. 0.085 0.065 TYP.
G. 0.125 R. (MIN) TYP.	N. 0.305 0.285 TYP.

FIG. 3

prolonged times under load at 1149°C (2100°F). Crosshead extension was measured during the test and elongation and reduction of area were measured on the fractured halves. Tests were conducted as shown in Fig. 4, in a chrome plated stainless steel vacuum chamber. Heating was accomplished with a tantalum resistance furnace. Temperature was controlled with a tungsten rhenium thermocouple and vacuum to 10^{-4} N/m^2 (10^{-6} torr) was standard.

Creep rupture tests were also conducted in accordance with ASTM specifications E139-69 on ridged specimens of dimensions shown in Fig. 5. Tests were performed in the same vacuum chamber used for the stress rupture experiments. Continuous creep measurements were made with an LVDT extensometer within the environment. Because the presence of the extensometer rods disrupted the uniformity of the temperature gradient at the maximum exposure temperature employed, i.e. 1200°C, radiation baffling was added to modify the specimen temperature profile so that failures occurred within the gage length. All creep tests were performed using continuously recording thermocouples attached to the center of the gage and to the fillet region near the top threaded end.

2.6 Longitudinal Shear

Test specimens of directionally solidified bars were ground to the shape illustrated in Fig. 6, for measurement of the longitudinal shear strength (parallel to the growth direction and phase alignment). The specimens consisted of a .64 cm (1/4 in.) diameter bolt shank with two 0.32 cm (1/8 in.) thick heads (one at each end of the shank) which were attached to a fixture shown in Fig. 7. The fixture was composed of two high temperature slotted button head adapters and split ring washers to insure full bearing on the specimen heads. Longitudinal shear tests were conducted in air at a loading rate of 0.025 cm/min (0.01 in./min) using a Tinius-Olsen four screw machine.

2.7 Thermal Cyclic Testing

The quaternary base line alloy (Ni-19.7 w/o Cb-6.0 w/o Cr-2.5 w/o Al) and quinary modified alloys were thermally cycled 3000 times between 400°C (750°F) and 1121°C (2050°F) in an automatic self-resistance heated, thermal cycling apparatus (Fig. 8) as described elsewhere in greater detail (Ref. 6). The specimen temperature was monitored by the output of a thermocouple welded at the center of the heat zone and each thermal cycle as well as the specimen extension was continuously monitored. The cycles were of approximately 2 minutes duration and produced heating and cooling rates of 25°C/sec (45°F/sec).

FIG. 4

CREEP RUPTURE TESTER

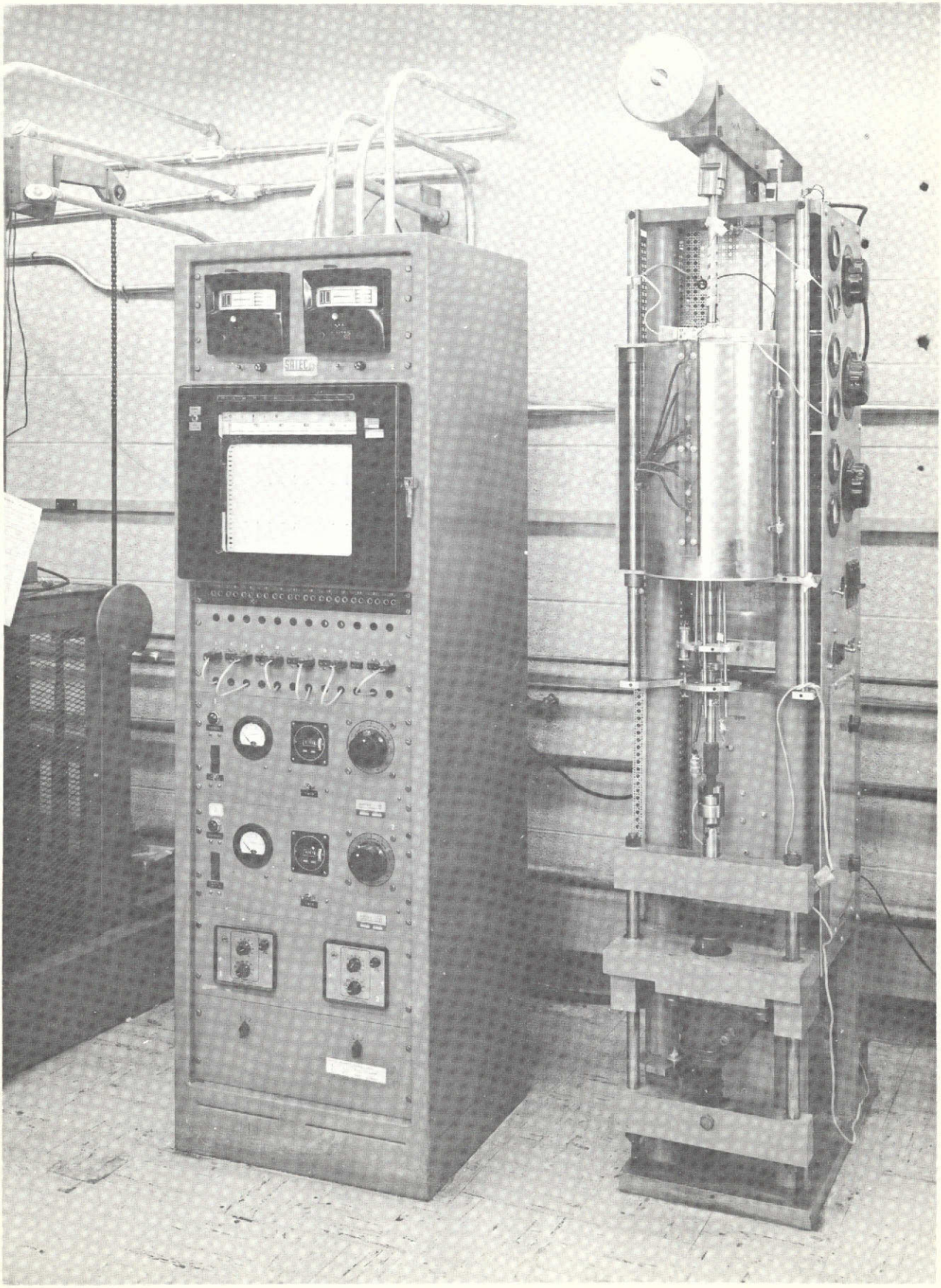

CREEP TEST SPECIMEN

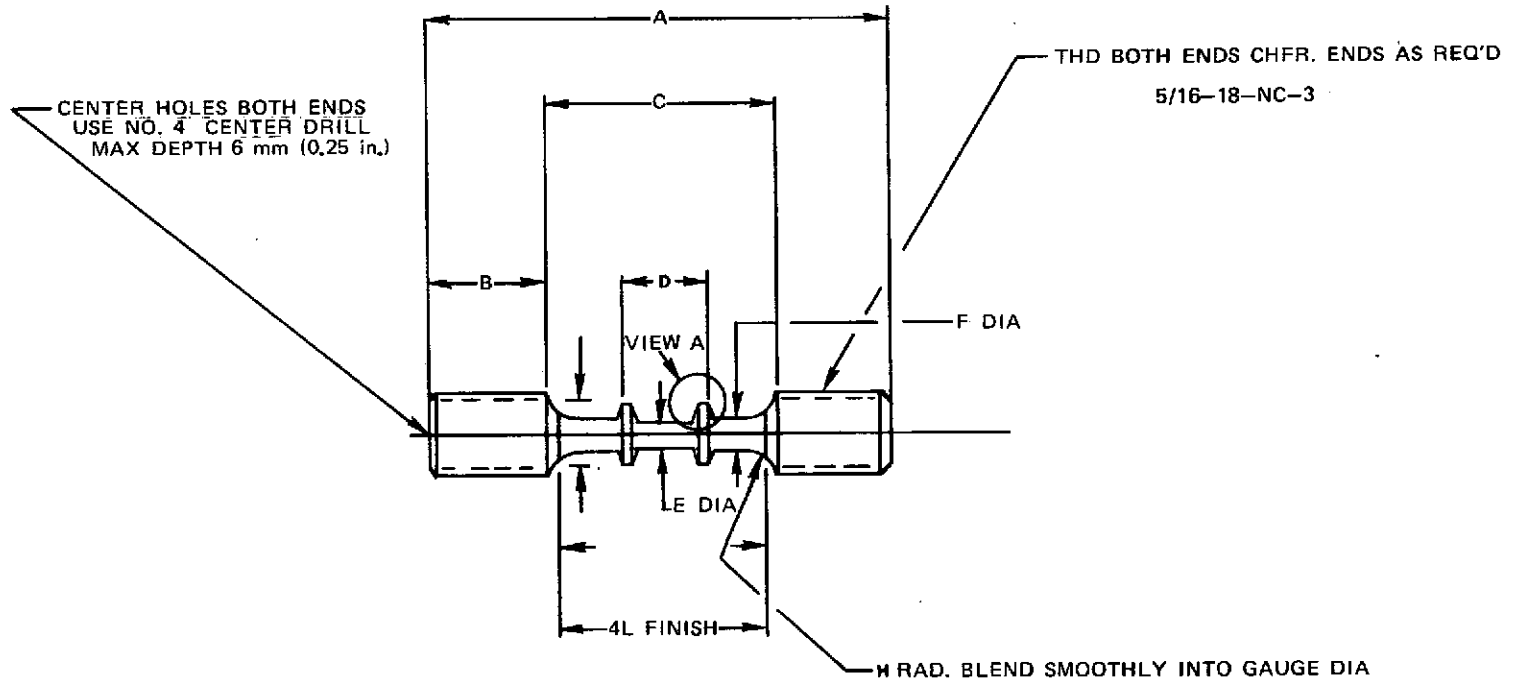

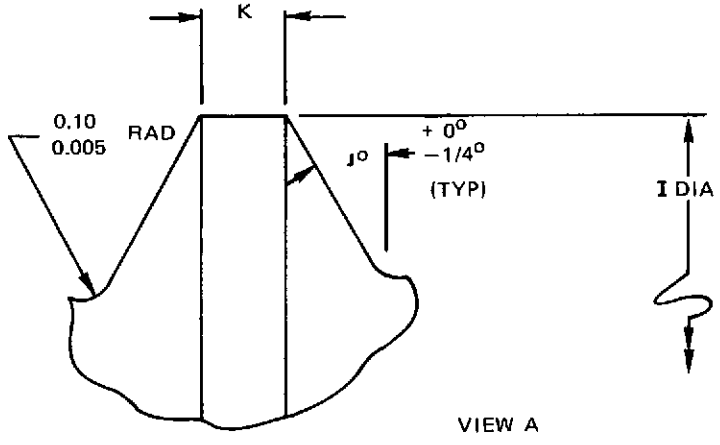

NO UNDERCUTTING PERMITTED BLEND SMOOTHLY

NOTE:
1. IDENTIFY ONE END BY NUMBER

SPECIMEN DIMENSIONS – mm			
A. 57.15		H. 5.08	
B. 12.7		I. 4.41	
C. 31.75		J. 30° + 0° − 1/4°	
D. 12.7		K. 0.40	
E. 2.78			
F. 3.18			
G. 0.10 (0.005) RADIANS			

ALL DIMENSIONS ± 0.013

SPECIMEN DIMENSIONS – INCHES			
A. 2.250		H. 0.200	
B. 0.500		I. 0.1735	
C. 1.250		J. 30° + 0° −1/4°	
D. 0.500		K. 0.0155	
E. 0.1100			
F. 0.1250			
G. 0.10 (0.005) RADIANS			

ALL DIMENSIONS ± 0.0005

FIG. 5

LONGITUDINAL SHEAR SPECIMEN

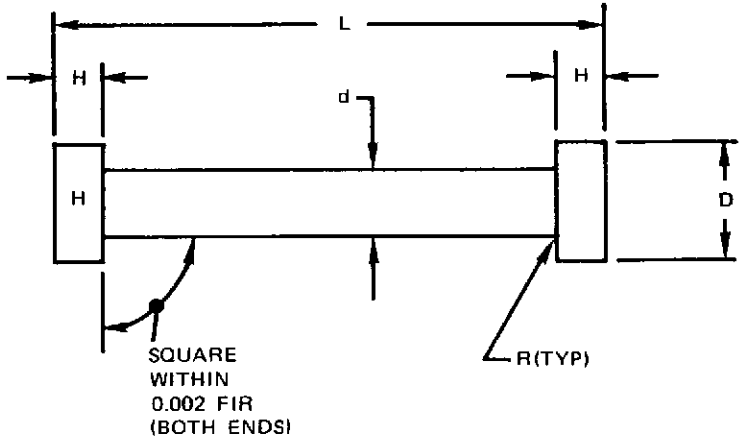

L	AS IS	AS IS
H	0.125 $^{+\ 0.005}_{-0.000}$	3.18 mm $^{+0.013}_{-0.000}$
D	AS IS (½IN.DIA.MAX)	12.7 mm
d	0.250 $^{+\ 0.002}_{-0.000}$ DIA	6.36 mm $^{+0.005}_{-0.000}$
R	0.020 0.015 IN.	0.051 mm 0.038 mm

FIG. 6

FIG. 7

LONGITUDINAL SHEAR FIXTURE

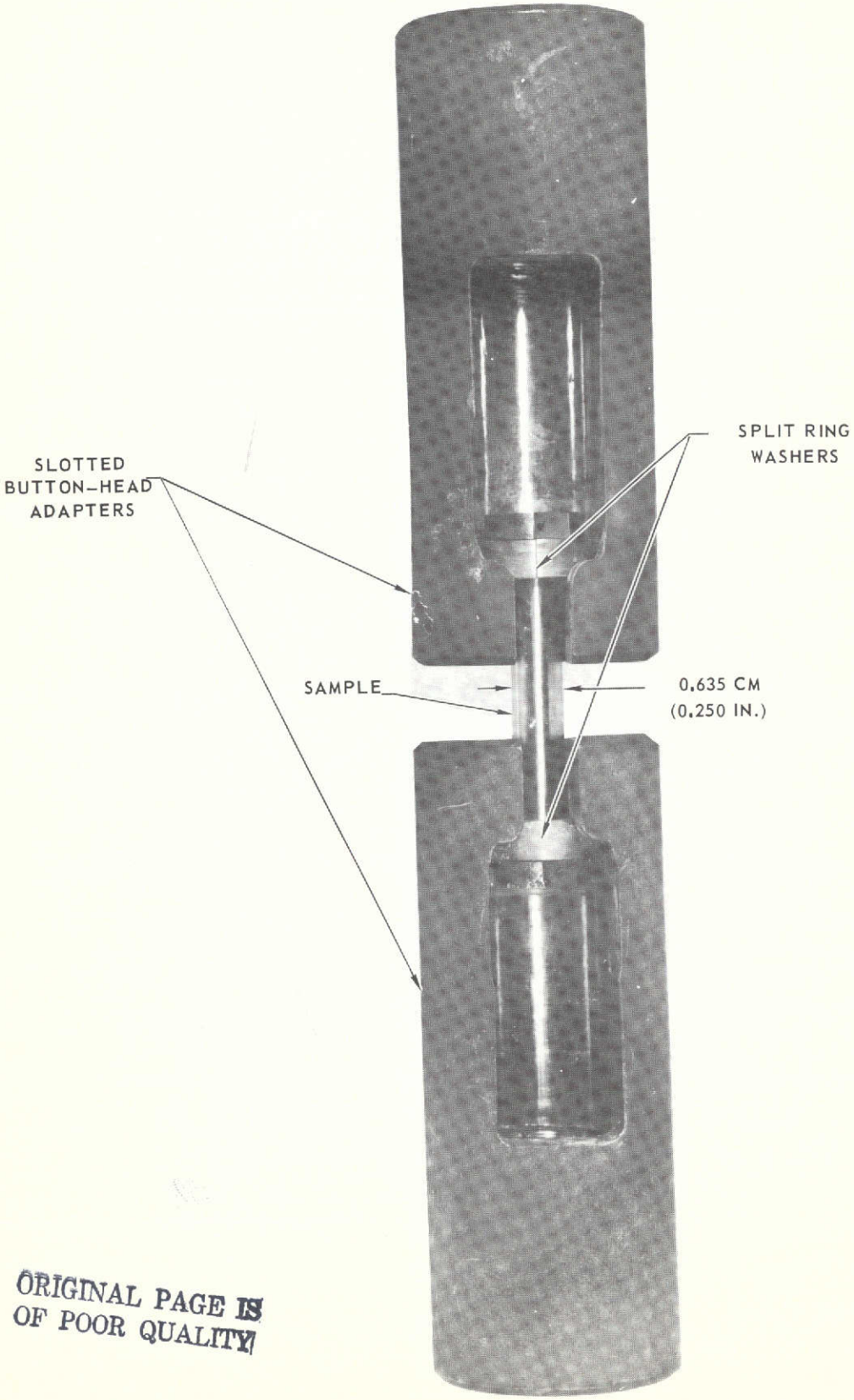

RL-71-243

FIG. 8

AUTOMATED CYCLIC OXIDATION TEST EQUIPMENT

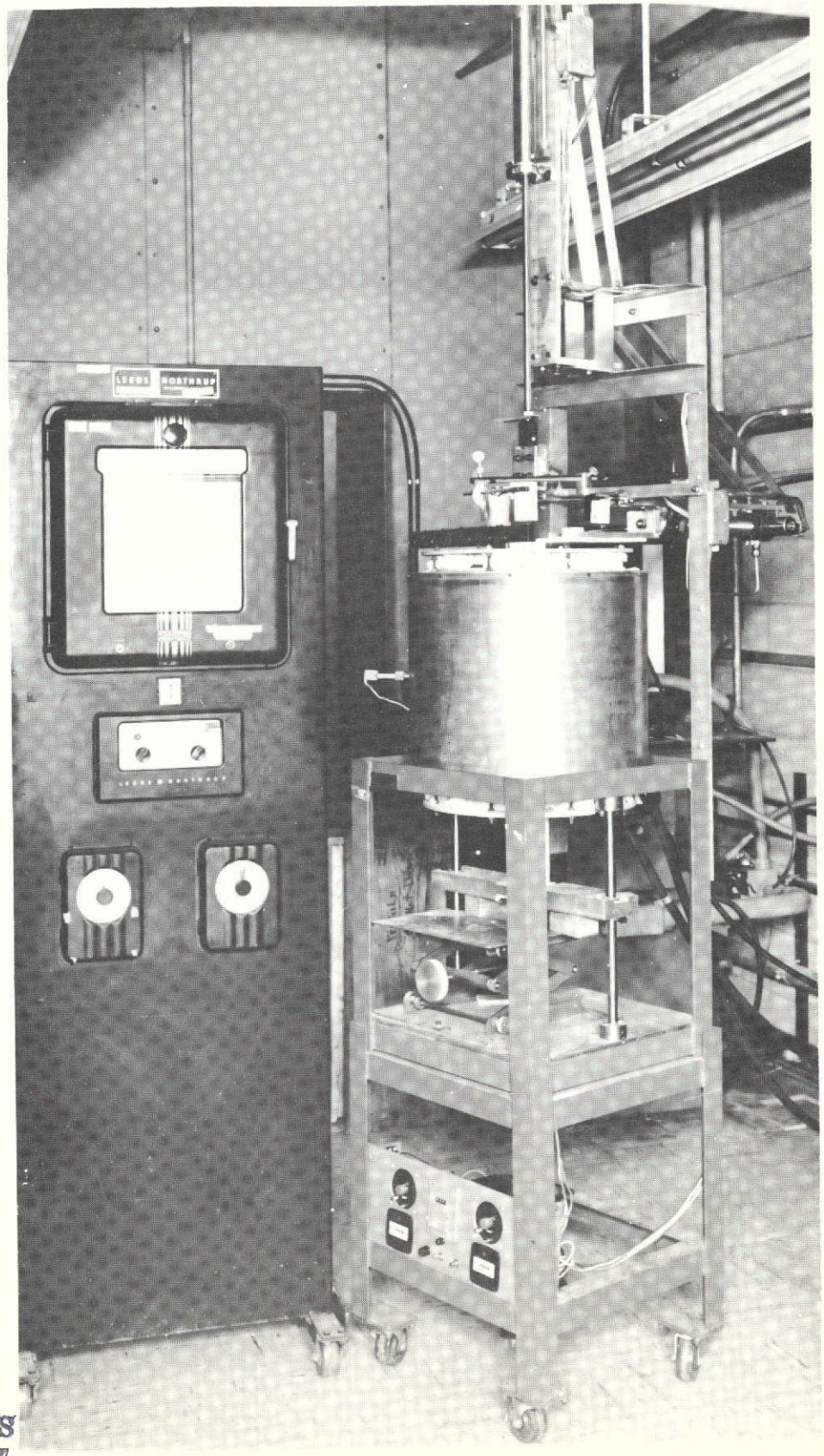

2.8 Thin Foil Preparation Technique

Preparation of thin foils was performed in three steps: First, a 0.6 mm thick transverse slice was cut from the directionally solidified ingot and mechanically ground and polished into four 3.0 mm discs, ~0.2 mm thick. The second step involved dimpling the discs to a minimum thickness of ~0.07 mm. This is achieved in a room temperature electrolyte consisting of 10% sulfuric acid in methanol, at cell settings of 85V and 0.02A. The third and final thinning step was performed in a solution comprised of 87% CH_3OH, 8% H_2SO_4, 3% HNC_3 + 2% HF. This solution was cooled to -18°C (~0°F) at the start of final thinning and attempts were made to keep it below -12°C (+10°F) until perforation occurred. Cell settings were held at 8V and .15A using a 6 cm^2 sheet of platinum as the cathode.

2.9 Oxidation Test Procedure

2.9.1 Isothermal

Test coupons, nominally 2.5 x 1.3 x 0.13 cm (1 x 0.5 x 0.050 in.), were ground and lapped with 600 grit paper and cleaned with trichloroethylene. The long dimension of the coupon lay in the eutectic growth direction. Separate coupons were contained in ~1.9 cm (~3/4 in.) O.D. x 2.86 cm (1 1/8 in.) high cylindrical alumina crucibles and exposed continuously in still air for times of 5, 50, 200 and 500 hrs at 760°, 1000°, and 1100°C. The crucibles were previously heated to constant weight for 24 hrs at 1250°C. The weight change (including spall weight) and the spall weight were determined after each exposure. The depletion zone thickness was determined by measuring the microstructurally unaffected thickness normal to the largest faces of the test coupon and computing on the basis of one side. Changes in each sample's total thickness were measured microstructurally on mounted and polished cross sections as well as by micrometer after each exposure. Microstructure stability, scale adhesion and oxide penetration paths were observed and recorded.

III. RESULTS AND DISCUSSION

3.1 Alloy Studies

3.1.1 Background Phase Equilibria

It is now known that numerous compositions in the quaternary system Ni-Al-Cb-Cr may be directionally solidified to form aligned biphase composite structures of δ-Ni_3Cb lamellae within a γ/γ' matrix (Ref. 1). These compositions were geometrically defined previously as those residing on a liquidus surface and each alloy thereon solidified according to the bivariant eutectic reaction (Fig. 9), i.e. $L \rightleftarrows \gamma + \delta$. The liquidus surface was bounded by the invariant eutectics, $\gamma + \delta$, at Ni-22.4 w/o Cb (Refs. 7-13), $\gamma + \gamma' + \delta$, at Ni-20.7 w/o Cb-3.2 w/o Al (Refs. 14-16), and $\gamma + \delta + \beta$, at Ni-20.2 w/o Cb-27.6 w/o Cr (Refs. 17-19).

As explained in the Introduction, the starting point (base alloy) was the bivariant eutectic composition Ni-19.7 w/o Cb-6.0 w/o Cr-2.5 w/o Al. The iterative optimization alloying plan required that each new bi- or multivariant eutectic composition solidify within the equilibrium space wherein:

$$L \xrightarrow{\Delta T} \gamma + \delta \xrightarrow{\text{solid state}} \gamma/\gamma' + \delta$$

Alloy modifications and additions which introduce primary phases or which exceed the solubility limits of either phase (γ or δ) derived from the melt and result in the formation of additional phases on freezing were considered to fall outside the current program definition. Because of the above microstructural requirement for each modified alloy, fractional factorial, Latin square (Ref. 20) and Box-Wilson (Ref. 21) techniques and strategies were judged difficult to apply due to complex interdependence of the elements (independent variables) on morphology and the compromise among several mechanical and physical properties (dependent variables). Metallurgical judgement based on existing binary and ternary equilibrium diagrams formed the basis of further alloy improvement.

3.1.2 Alloy Modifications and Additions

Two types of alloying were considered for the base line quaternary to achieve a turbine blade alloy with improved strength and oxidation resistance. First adjustments in the aluminum and chromium content were made to enhance the intrinsic oxidation of the matrix γ/γ' phases by promoting the formation of an external Al_2O_3 scale. Information gained from previous oxide mapping of the various scales on ternary Ni-Cr-Al alloys (Ref. 22) provided direction in the design of compositions which form Al_2O_3. However, the constraint to produce

FIG. 9

POLYTHERMAL PROJECTION SHOWING BIVARIANT EUTECTIC SURFACE WHEREIN $L \rightleftharpoons \gamma + \delta$

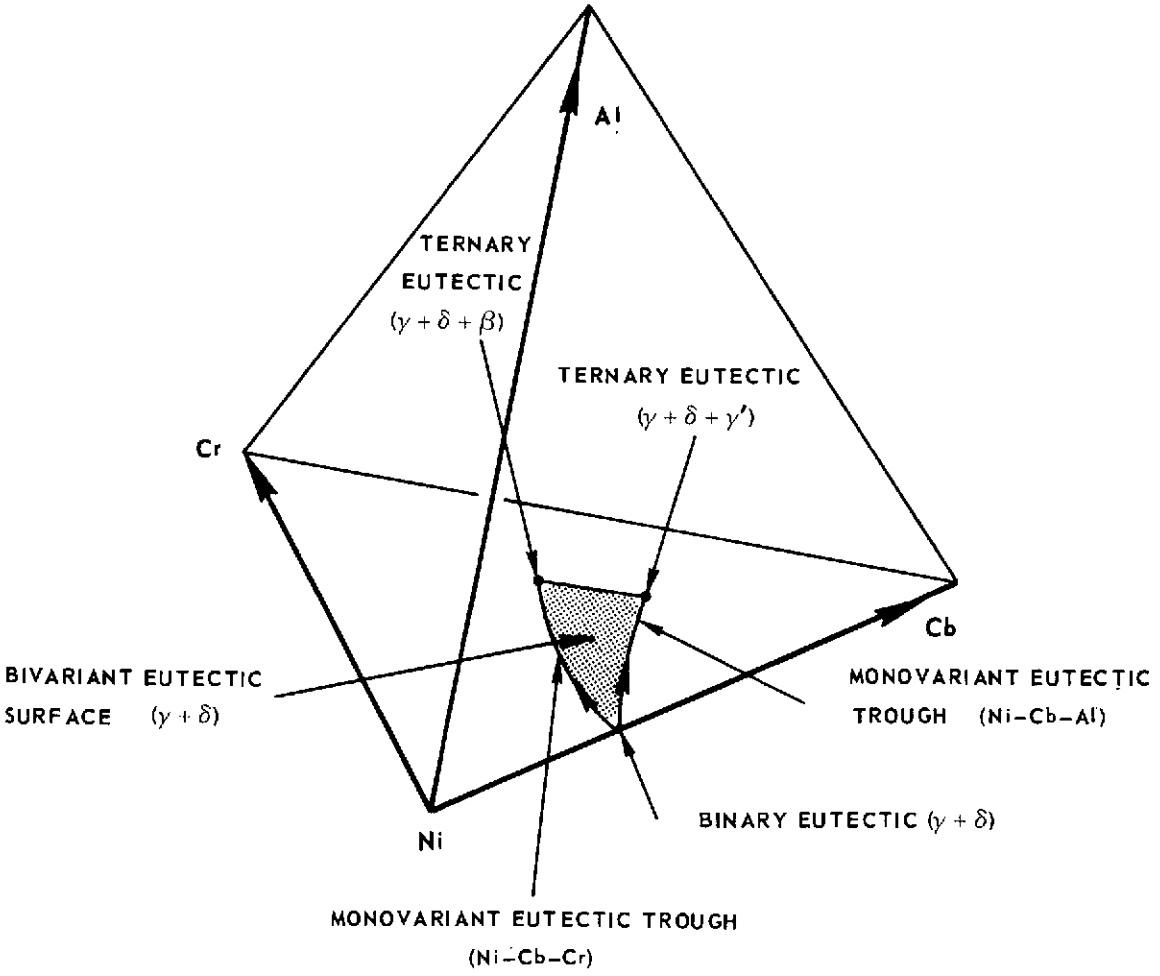

aligned lamellar structures thermodynamically precluded the introduction of more than 3.2 w/o Al and 12 w/o Cr. Thus, although α-Al_2O_3 was detected by X-ray diffraction of the spalled oxide products, more complex oxides and the presence of $NiCbO_4$ was found as is discussed elsewhere.

The second path involved the substitution of a quinary alloying element for one or more of the elements in the quaternary eutectic (Ni,Cb,Cr,Al). A total of eight elements (Co,Ti,Mo,W,Re,Ta,B and Si) were substituted at varying levels to obtain further property improvements. Both the matrix and the intermetallic compound Ni_3Cb were affected by each elemental substitution. Depending on the respective solubilities exhibited in binary and ternary systems, the partitioning of each alloy substitution could be estimated provided some phase diagram information on the system was available.

Molybdenum, tungsten, and rhenium were substituted in small amounts for nickel to solid solution strengthen the gamma phase as these elements differ from nickel by 1 to 13 percent in atomic diameter. From the experiments of Pelloux and Grant (Ref. 23) and Parker and Hazlett (Ref. 24) solute hardening can be related to this atomic diameter oversize as measured by lattice expansion. Furthermore, above 0.6 T_m and within the range of high temperature creep, gamma phase strength is dependent on diffusional processes. The slow diffusing elements, molybdenum, tungsten and rhenium would be expected to be most potent hardeners in that they increase the strength of the interatomic bonds in the solid solution lattice (Refs. 25-26). In fact, beneficial effects of the former two elements on the high temperature strength of Ni-Cr-Cb alloys have been reported (Ref. 27). There is, however, little known concerning the solubility of Mo, W, and Re in δ-Ni_3Cb but each is miscible in gamma nickel to an extent greater than the amount substituted, i.e. one weight percent.

Cobalt was added primarily to increase the volume percentage of δ-Ni_3Cb as it is mutually soluble in both phases and was previously noted to raise the γ' solutioning temperatures of nickel base superalloys (Ref. 24). Cobalt substitutes for Ni atoms in the Ni_3Cb compound.

As well as affecting the solubilities and volume fraction of matrix and reinforcing phases, tantalum and titanium additions would be expected to affect the size, distribution and hardness of the γ' precipitates (Ref. 24). Both Ta and Ti extensively substitute for Cb in the Ni_3Cb compound (Refs. 28-29) and would be expected to act beneficially in solid solution hardening of δ. Although the compounds Ni_3Cb, Ni_3Ti and Ni_3Ta form a continuous series of solid solutions, they are not isomorphous in structure as reported by I. I. Kornilov (Ref. 28). The crystal structure of Ni_3Cb and Ni_3Ta is orthorhombic and that of Ni_3Ti is hexagonal.

Finally, small additions of Si and B were added to improve the oxidation resistance and strengthen grain boundaries respectively. Previous work by Lowell and Miner (Ref. 30) indicated the marked favorable effect of Si on the cyclic alloy depletion zone thickness of B-1900 at 1100°C even though the same oxides formed on alloys prepared with and without Si. Small additions of boron as well as Hf and Zr have been observed for numerous years to promote grain boundary strengthening in complex nickel base superalloys.

While certain elemental additions were expected to promote improved high temperature stability and strength, greatest creep resistance was believed achievable with minimization of γ/γ' lattice parameter mismatch (Ref. 31). Thus, alloying additions were evaluated as to the extent they changed the lattice constants of both phases.

The role of the γ' dispersion on structural stability is a particularly subtle question. On thermal exposures above ~0.6 T_m, the γ' ripens at a significant rate. Therefore, modifications to the base line quaternary γ/γ'-δ composition that minimize γ' ripening should optimize high creep resistance. The particle size distribution for γ/γ' type alloys was derived by Wagner (Ref. 32) and states that:

$$\bar{r}^3 = \frac{8\ DS\ \gamma\ \Omega\ t}{9\ K\ T}$$

where r is the mean particle radius of the distribution, D is the solute diffusion coefficient, S the normal solubility, γ the interfacial energy, Ω the atomic volume of the particles and t time. Although it is difficult to measure the values of the interfacial energy it will be considered that the smaller the misfit between γ/γ' the smaller the interfacial energy. Thus, retardation of γ' ripening would be favored by minimizing the lattice parameter misfit and by partitioning more of the slower diffusing elements to γ' thereby decreasing D.

A compilation of the effects of various solutes on the measured lattice parameter of γ-nickel and γ'-Ni_3Al are shown in Figs. 10 and 11 (Refs. 34,35). From these measurements and assumptions concerning the preferential partitioning of certain quinary additions to the γ, γ', and δ phases one can calculate the lattice parameter, $\bar{a}$, of the γ and γ' phases from the solid solution relationship:

$$\bar{a} = a_o + \sum_{i=1}^{n} C_i\ K_i$$

where a_o = lattice parameter of phase pure γ or γ', n = number of elements, C_i = atomic fraction of the particular element and K_i = compositional dependence (slope) of particular element on the lattice parameter of phase pure γ or γ'.

FIG. 10

THE LATTICE SPACINGS OF NICKEL SOLID SOLUTIONS AS A FUNCTION OF COMPOSITION

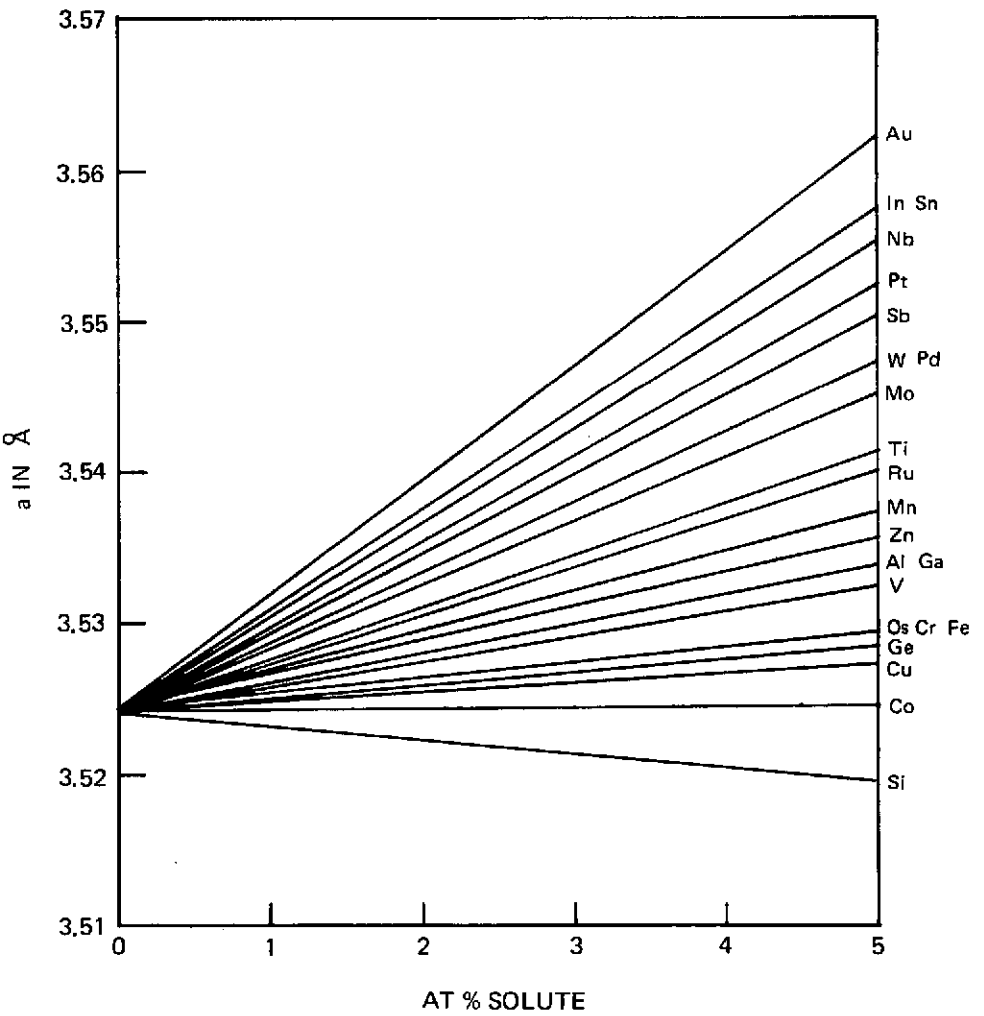

N03–260–1

FIG. 11

THE LATTICE SPACINGS OF NICKEL ALUMINIDE $Ni_3Al(\gamma')$ SOLUTIONS AS A FUNCTION OF COMPOSITION

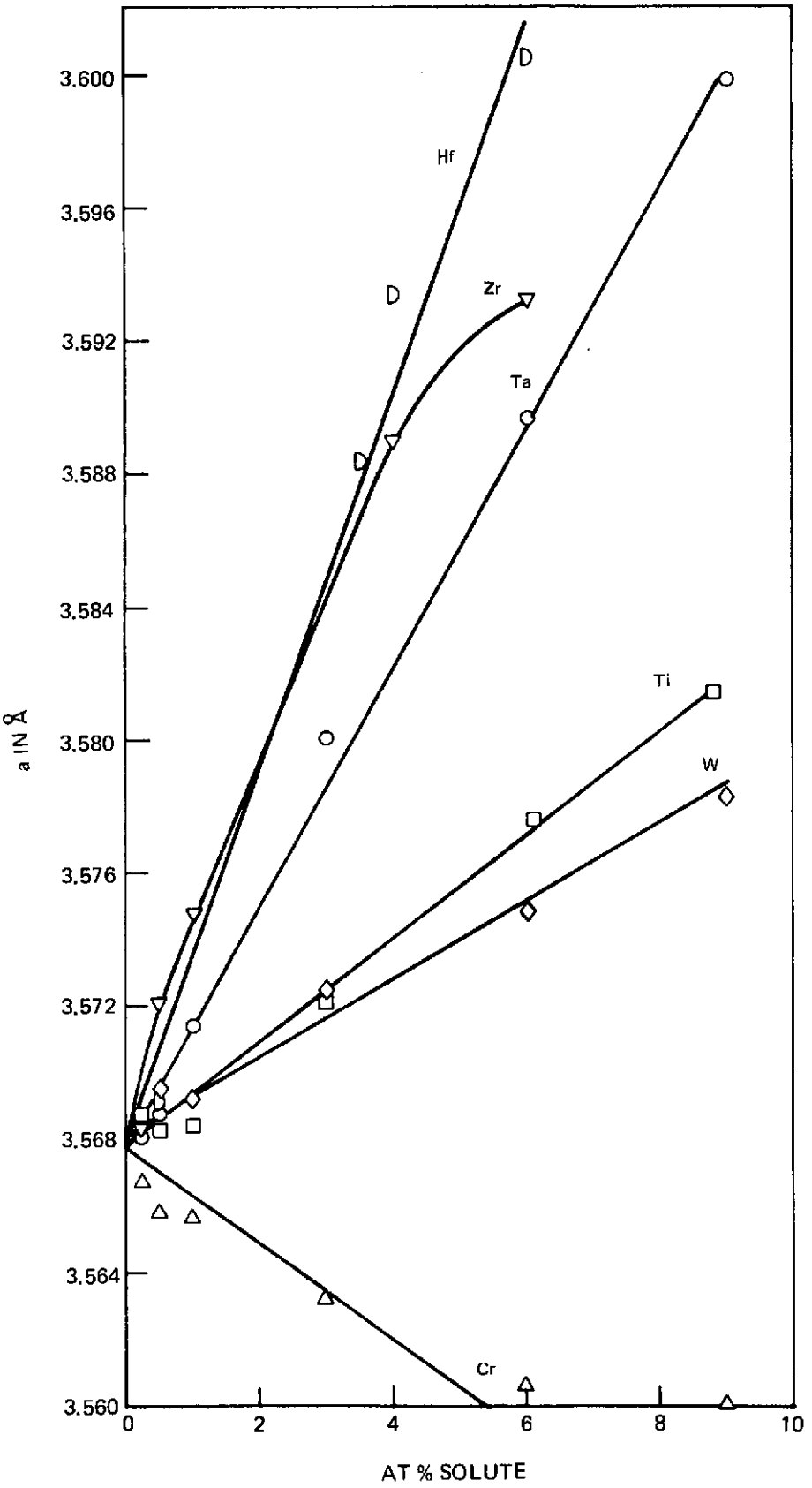

N03-260-2

These measures may permit the choice of an alloy composition which may minimize γ' ripening and improve long term creep resistance but did not permit the attainment of a zero misfit alloy composition due to uncertainties in the partitioning of alloyed elements in each phase and alloy base line constraints. Short of direct chemical analyses of isolated phases, as has been previously described (Ref. 36), quantitative information on the respective solubilities is unknown. Furthermore, the required presence of 6 w/o chromium which contracts the lattice parameter of γ' militates against the attainment of a zero misfit alloy as there is only one element known to correspondingly contract the lattice parameter of γ. As the solubility of niobium in gamma nickel is 9 a/o at 1200°C and ~4 a/o at 800°C and in gamma prime is ~7 a/o at 1200°C and below, this element expands, almost equally, both pure γ/γ' phases. Additions of Ti,Co,Ta,Mo,W, and Re, regardless of the amount and partitioning to the γ/γ' phases, did not permit the attainment of a zero misfit for γ/γ'-δ alloys containing 6 w/o Cr as the gamma phase lattice parameter will always be larger than the gamma prime phase lattice parameter. Chromium free γ/γ'-δ alloys on the other hand show promise for attainment of a zero misfit by alloying since the lattice parameter of the γ' phase is less than 0.5% larger than the γ phase (Ref. 14).

3.2 Microstructure

3.2.1 Quaternary Modifications

The quaternary base line γ/γ'-δ alloy, Ni-19.7 w/o Cb-6.0 w/o Cr-2.5 w/o Al, was modified as identified in Table II by composition and freezing conditions. To improve oxidation resistance first increases were made to both the chromium (0.5-3.0 w/o) and aluminum (0.2-0.3 w/o) content (specimens A72-1014, A73-603 and A73-777). The next modification consisted of increasing only the chromium content by 2 w/o (A73-604) and aluminum content by 0.3 w/o (A73-611). Further modifications were made by increasing chromium while lowering the aluminum (A73-712) and vice versa (A73-611). In all these experiments some slight adjustments to the columbium content were required to achieve directional phase alignment without primary phases. Because of the steepness of the liquidus surface in the region of high chromium content (Ref. 1), a processing advantage was derived by decreasing chromium from 9 to 4 percent by weight. Further decreases in the chromium level while improving processability, decrease the oxidation resistance so that some compromise among properties would be required.

An interesting microstructural effect was observed with chromium contents above and below the base level of 6.0 w/o. The lamellar interfaces were noted to be more jagged at chromium contents below the base line resembling, as shown in Fig. 12, the simple binary γ-δ microstructure (Ref. 33), and more smooth and

Table II

Composition and Growth Conditions of Modified γ/γ'-δ Alloys

D.S. Bar No.	Alloy Composition (w/o)	Freezing Rate (cm/hr)	Thermal Gradient (°C/cm)	Microstructure
A. Quaternary Alloys				
Al,Cr Modifications				
A73-097	Ni-19.7Cb-6.0Cr-2.5Al	3	~300	Lamellar
A73-706	Ni-20.0Cb-6.0Cr-2.5Al	3	~300	Lamellar, slightly δ dendritic
A73-717	Ni-19.7Cb-6.0Cr-2.5Al	3	~300	Lamellar
A72-1014	Ni-19.8Cb-6.5Cr-2.7Al	2	~300	Lamellar
A73-611	Ni-20.3Cb-4.0Cr-2.8Al	3	~300	Lamellar
A73-603	Ni-19.8Cb-6.0Cr-2.8Al	3	~300	Lamellar
A73-604	Ni-20.0Cb-8.0Cr-2.5Al	3	~300	Lamellar
A73-712	Ni-19.7Cb-9.0Cr-1.5Al	3	~300	Lamellar
A73-777	Ni-20.0Cb-9.0Cr-2.8Al	3	~300	Cellular shallow cusp
A74-168	Ni-20.0Cb-9.0Cr-2.8Al	3	~300	Cellular shallow cusp
A73-717	Ni-19.7Cb-6.0Cr-2.5Al	3	~300	Lamellar
A73-728	Ni-19.7Cb-6.0Cr-2.5Al	3	~300	Lamellar
A73-735	Ni-19.7Cb-6.0Cr-2.5Al	3	~300	Lamellar
A73-772	Ni-20.0Cb-6.0Cr-2.5Al	3	~300	Lamellar
A73-778	Ni-20.0Cb-6.0Cr-2.5Al	7	~300	Lamellar
A74-163	Ni-20.0Cb-6.0Cr-2.5Al	3	~300	Seeded growth
A74-201	Ni-20.0Cb-6.0Cr-2.5Al	5	~300	Seeded growth
A74-238	Ni-20.0Cb-6.0Cr-2.5Al	3	~300	Lamellar
A74-264	Ni-20.0Cb-6.0Cr-2.5Al	5	~ 80	Cellular
A74-269	Ni-20.1Cb-6.0Cr-2.5Al	10	~300	Cellular
A74-295	Ni-20.0Cb-6.0Cr-2.5Al	1	~ 80	Lamellar
A74-320	Ni-20.3Cb-4.0Cr-2.8Al	3	~300	Lamellar
B. Quinary Alloys				
Ti,Co,B,Si Additions				
A74-039B	Ni-7.9Cb-6.0Cr-1.2Al-8.2Ti	2	~ 80	Cellular
A74-101	Ni-18.6Cb-6.0Cr-2.5Al-.87Ti	3	~300	Lamellar
A74-103	Ni-18.6Cb-6.0Cr-2.5Al-.87Ti	3	~300	Lamellar
A73-142	Ni-18.6Cb-6.0Cr-2.5Al-0.8Ti	3	~300	Plane front, lamellar
A74-302	Ni-18.6Cb-6.0Cr-2.5Al-.87Ti	3	~300	Lamellar
A73-326	Ni-18.6Cb-6.0Cr-2.5Al-0.8Ti	3	~300	Plane front, lamellar
A73-598	Ni-18.6Cb-6.0Cr-2.5Al-0.87Ti	3	~300	Plane front, lamellar
A73-499	Ni-17.5Cb-6.0Cr-2.5Al-1.6Ti	2	~ 80	Very shallow cusp, one new phase
A74-083	Ni-20.1Cb-6.0Cr-2.5Al-1.0Co	3	~300	Lamellar
A74-281	Ni-20.1Cb-6.0Cr-2.5Al-1.0Co	3	~300	Lamellar
A74-142	Ni-20.3Cb-6.0Cr-2.5Al-2.0Co	3	~300	Lamellar
A74-143	Ni-20.3Cb-6.0Cr-2.5Al-2.0Co	3	~300	Lamellar
A74-073	Ni-20.2Cb-6.0Cr-2.5Al-2.0Co	3	~300	Lamellar
A74-091	Ni-20.2Cb-6.0Cr-2.5Al-2.0Co	3	~300	Lamellar
A74-260	Ni-20.1Cb-6.0Cr-2.5Al-2.0Co	3	~300	Lamellar
A74-262	Ni-20.1Cb-6.0Cr-2.5Al-2.0Co	3	~300	Lamellar
A74-263	Ni-20.1Cb-6.0Cr-2.5Al-2.0Co	3	~300	Lamellar
A74-237	Ni-20.1Cb-6.0Cr-2.5Al-2.0Co	3	~300	Lamellar (high purity elements)
A74-188	Ni-20.1Cb-6.0Cr-2.5Al-2.0Co	3	~300	Lamellar
A74-075	Ni-20.3Cb-6.0Cr-2.5Al-3.0Co	3	~300	Lamellar
A73-509	Ni-20.5Cb-6.0Cr-2.5Al-3.0Co	2	~ 80	Very shallow cusp, cellular
A73-632	Ni-20.5Cb-6.0Cr-2.5Al-3.0Co	3	~300	Plane front, slightly δ dendritic
A73-620	Ni-21.0Cb-6.0Cr-2.5Al-6.0Co	3	~300	Shallow cusp, cellular

Table II (Cont'd)

D.S. Bar No.	Alloy Composition (w/o)	Freezing Rate (cm/hr)	Thermal Gradient (°C/cm)	Microstructure
A72-1011	Ni-19.8Cb-6.0Cr-2.5Al-0.005B	2	~300	Plane front, lamellar
A73-485	Ni-19.7Cb-6.0Cr-2.5Al-0.1B	2	~ 80	Deep cells, two new phases
A74-045	Ni-19.7Cb-6.0Cr-2.5Al-1.0Si	2	~ 80	Cellular, third phase
Mo,W,Re,Ta Additions				
A73-076B	Ni-19.8Cb-6.0Cr-2.5Al-1.0Mo	2	~ 80	Shallow cusp, cellular
A73-114	Ni-19.7Cb-6.0Cr-2.5Al-1.0Mo	3	~300	Plane front, lamellar
A74-197	Ni-19.7Cb-6.0Cr-2.5Al-1.0Mo	3	~300	Lamellar
A74-311	Ni-19.7Cb-6.0Cr-2.5Al-1.0Mo	3	~300	Lamellar
A73-601	Ni-19.7Cb-6.0Cr-2.5Al-1.0Mo	3	~300	Plane front, lamellar
A73-330	Ni-19.7Cb-6.0Cr-2.5Al-1.0Mo	3	~300	Plane front, lamellar
A74-095	Ni-19.7Cb-6.0Cr-2.5Al-1.0Mo	3	~300	Lamellar
A73-504	Ni-20.5Cb-6.0Cr-2.5Al-3.0Mo	2	~ 80	Very deep cells, new phases
A73-491	Ni-19.7Cb-6.0Cr-2.5Al-1.0W	2	~ 80	Very shallow cusp, cellular
A73-634	Ni-19.7Cb-6.0Cr-2.5Al-1.0W	3	~300	Plane front, slightly δ dendritic
A74-097	Ni-19.7Cb-6.0Cr-2.5Al-1.0W	3	~300	Lamellar
A74-176	Ni-19.7Cb-6.0Cr-2.5Al-1.0W	3	~300	Lamellar
A74-304	Ni-19.7Cb-6.0Cr-2.5Al-1.0W	3	~300	Lamellar
A73-468	Ni-19.7Cb-6.0Cr-2.5Al-1.0Re	3	~300	Lamellar
A74-024	Ni-18.7Cb-6.0Cr-2.5Al-1.0Ta	2	~ 80	Primary γ
A74-029	Ni-18.9Cb-6.0Cr-2.5Al-1.0Ta	2	~ 80	Primary γ
A74-114	Ni-19.5Cb-6.0Cr-2.5Al-1.0Ta	3	~300	Primary δ
A74-140	Ni-19.3Cb-6.0Cr-2.5Al-1.0Ta	3	~300	Lamellar, slight primary δ
A74-301	Ni-19.5Cb-6.0Cr-2.5Al-1.0Ta	3	~300	Lamellar
A74-136	Ni-17.9Cb-6.0Cr-2.5Al-3.0Ta	2	~ 80	Shallow cusp, cellular
A74-177	Ni-17.9Cb-6.0Cr-2.5Al-3.0Ta	3	~300	Lamellar
A74-186	Ni-17.9Cb-6.0Cr-2.5Al-3.0Ta	3	~300	Lamellar
A74-187	Ni-17.9Cb-6.0Cr-2.5Al-3.0Ta	3	~300	Lamellar
A74-511	Ni-16.1Cb-6.0Cr-2.5Al-6.0Ta	2	~300	Lamellar, dendritic
A74-516	Ni-17.8Cb-6.0Cr-2.5Al-3.0Ta	3	~300	Lamellar
A74-519	Ni-17.9Cb-6.0Cr-2.5Al-.2C-5.0Ta	2	~300	Deeply cellular dendritic
A74-550	Ni-17.8Cb-6.0Cr-2.5Al-3.0Ta	3	~300	Lamellar
A74-563	Ni-17.8Cb-6.0Cr-2.5Al-3.0Ta	3	~300	Crucible run out
A74-575	Ni-17.8Cb-6.0Cr-2.5Al-3.0Ta	2	~300	Lamellar
A74-605	Ni-17.8Cb-6.0Cr-2.5Al-3.0Ta	3	~300	Lamellar
A74-610	Ni-17.8Cb-6.0Cr-2.5Al-3.0Ta	3	~300	Lamellar
A74-611	Ni-17.8Cb-6.0Cr-2.5Al-3.0Ta	2	~300	Crucible run out
A74-633	Ni-17.8Cb-6.0Cr-2.5Al-3.0Ta	2	~300	Lamellar
A74-639	Ni-17.8Cb-6.0Cr-2.5Al-3.0Ta	2	~300	Lamellar
A74-663	Ni-17.8Cb-6.0Cr-2.5Al-3.0Ta	2	~300	Lamellar
A74-670	Ni-17.8Cb-6.0Cr-2.5Al-3.0Ta	2	~300	Lamellar
A74-677	Ni-17.8Cb-6.0Cr-2.5Al-3.0Ta	3	~300	Lamellar (to NASA)
A74-686	Ni-17.8Cb-6.0Cr-2.5Al-3.0Ta	3	~300	Lamellar (to NASA)
A74-689	Ni-17.8Cb-6.0Cr-2.5Al-3.0Ta	3	~300	Lamellar (to NASA)
A74-694	Ni-17.8Cb-6.0Cr-2.5Al-3.0Ta	3	~300	Lamellar (to NASA)

TRANSVERSE MICROSTRUCTURE OF Ni–20.3 W/O Cb–4.0 W/O Cr–2.8 W/O Al
DIRECTIONALLY SOLIDIFIED @ R = 3 cm/hr, $G_L \sim 300^{\circ}$C/cm

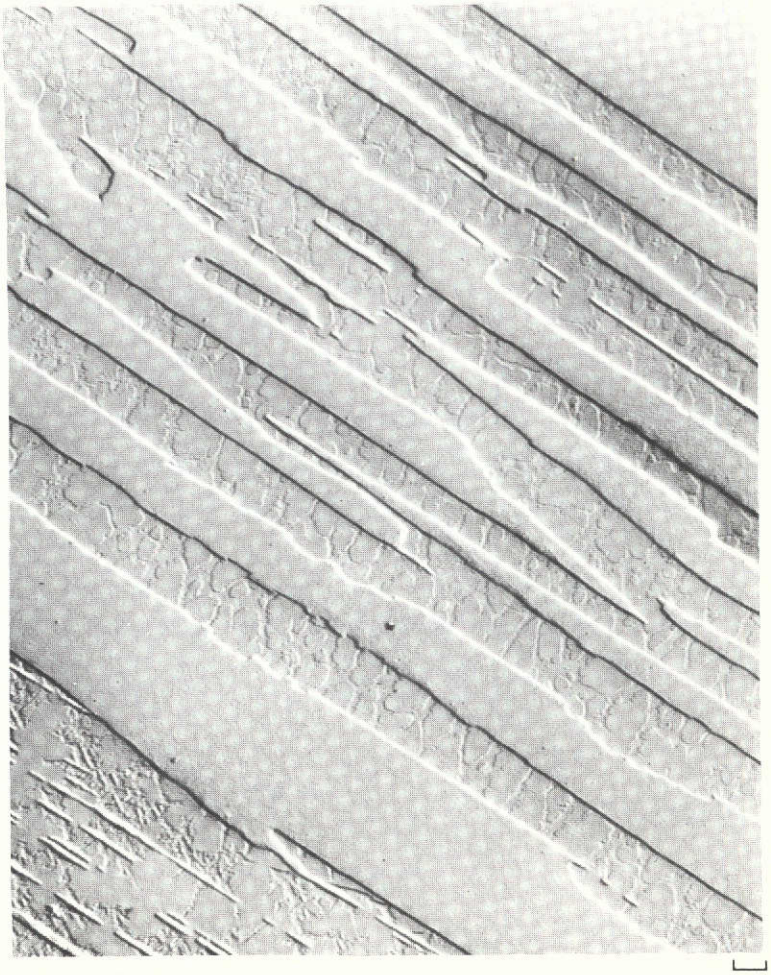

1μ

N02–18–6

straight at 9.0 w/o Cr as shown in Fig. 13. Transmission photomicrographs, Figs. 14 and 15, also illustrate this effect for the γ/γ'-δ compositions, Ni-20.3 w/o Cb-4.0 w/o Cr-2.8 w/o Al and Ni-20 w/o Cb-9.0 w/o Cr-1.5 w/o Al. The volume fraction of both δ and γ' phases decreases with decreases in Cr and Al content respectively with reference to the base line alloy as tabulated in Table III. However, the misfit in lattice parameter is minimized by decreasing chromium as shown in Table IV. As was previously discussed, if the chromium level in γ/γ'-δ were reduced, a zero γ/γ' lattice parameter misfit could be achieved.

3.2.2 Quinary Additions

The quinary additions to the base line γ/γ'-δ alloy are identified in Table II by composition, freezing conditions, and resulting microstructures. The alloying plan required that each new multivariant eutectic composition solidify within the equilibrium phase space wherein:

$$L \xrightarrow{\Delta T} \gamma + \delta.$$

Alloy additions, which exceeded the solid solubility limits of either phase and resulted in the formation of additional phases upon freezing, were not considered within the scope of subsequent property evaluation. Moreover, specimens exhibiting deeply cellular and unaligned lamellar microstructures resulting from processing in a low gradient furnace were not subsequently evaluated.

Cobalt was added first to increase the volume percentage of δ-Ni_3Cb. As quinary substitutions of cobalt for nickel were made to the base quaternary γ/γ'-δ alloy, adjustments in columbium content were required to retain biphase coupled growth free of γ dendrites. The areal quantitative metallographic technique of weighing tens of lamellae cut from electron micrographs of replicated transverse surfaces was used to arrive at the volume percent δ-Ni_3Cb values reported in Table III. As the weight percentage of cobalt increases from 1-3, the volume percentage δ increases from 40-45. The volume percentage δ is also influenced at 3 w/o cobalt, 6 w/o chromium, and 2.5 w/o aluminum by rather small (.2 w/o) increases in columbium content. The microstructure of the base quaternary alloy modified by 3 w/o Co is shown in Fig. 16. Cobalt could be extensively alloyed (>15 w/o) but three percent was considered optimum as the delta volume fraction was approaching 0.5. Cobalt substitutes for Ni atom sites in the $(NiCo)_3Cb$ for these dilute alloys. The crystal structure of Co_3Nb is hexagonal and thus not isotypic with δ-Ni_3Cb.

Molybdenum, tungsten, and rhenium were substituted for nickel to solid solution strengthen the gamma phase and lower the stacking fault energy to make cross slip more difficult in γ. Hardening had been previously (Refs. 23-24) related to the atomic diameter oversize as measured by γ lattice expansion.

TRANSVERSE MICROSTRUCTURE OF Ni–20 W/O Cb–9.0 W/O Cr–1.5 W/O Al
DIRECTIONALLY SOLIDIFIED @ R = 3 cm/hr, $G_L \backsim 300^{o}$C/cm

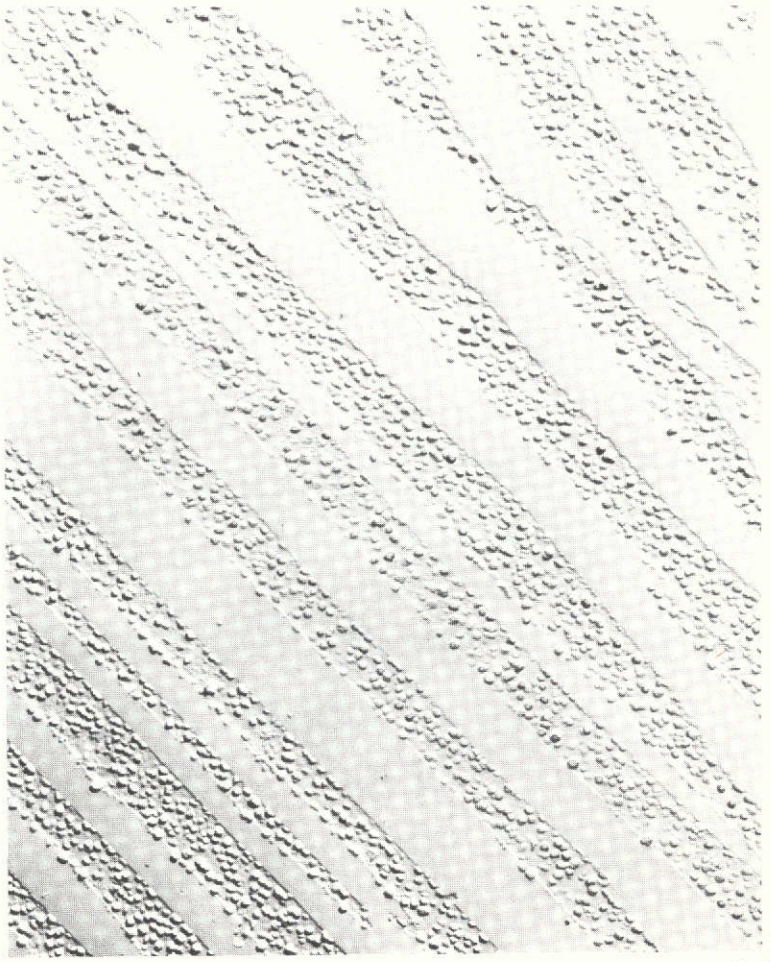

N02–18–2

TRANSMISSION ELECTRON MICROGRAPH
OF Ni–20.3 w/o Cb–4.0 w/o Cr–2.8 w/o Al (A73–611)

X12,600

1 μm

FIG. 14

TRANSMISSION ELECTRON MICROGRAPH
OF Ni–20.0 w/o Cb–9.0 w/o Cr–1.5 w/o Al (A73–712)

X16,300

1 μm

FIG. 15

N04–82–1

Table III

Volume Fraction Analysis of Various γ/γ'-δ Alloys

Specimen No.	Composition (w/o)	δ v/o (lineal)	δ v/o (areal)	γ/γ' v/o (lineal)	γ/γ' v/o (areal)
A73-083	Ni-20.1Cb-6.0Cr-2.5Al-1.0Co	-	40.1	-	-
A73-091	Ni-20.2Cb-6.0Cr-2.5Al-2.0Co	-	43.4	-	-
A73-075	Ni-20.3Cb-6.0Cr-2.5Al-3.0Co	-	45.0	-	-
A73-632 T	Ni-20.5Cb-6.0Cr-2.5Al-3.0Co	49	50	51	50
A73-611 T	Ni-20.3Cb-4.0Cr-2.8Al	40	33	60	67
A73-712 T	Ni-20.0Cb-9.0Cr-1.5Al	49	49	51	51
A73-634 T	Ni-19.7Cb-6.0Cr-2.5Al-1.0W	35	36	65	64
A73-601 T	Ni-19.7Cb-6.0Cr-2.5Al-1.0Mo	33	33	67	67
A73-598 T	Ni-18.6Cb-6.0Cr-2.5Al-0.87Ti	35	36	65	64
A74-177	Ni-17.8Cb-6.0Cr-3.0Ta-2.5Al	40	39	52	55

Table IV

γ/γ' Misfit for Compositional Modifications to γ/γ'-δ

D.S. Bar	Composition (w/o)	$d(220)_\gamma - d(220)_{\gamma'}$	Percent Misfit
A73-598	Ni-18.6Cb-6Cr-2.5Al-.87Ti	1.308-1.284	1.83
A73-634	Ni-19.7Cb-6Cr-2.5Al-1W	1.285-1.265	1.55
A71-639	Ni-20.0Cb-5.5Cr-2.5Al	1.315-1.280	1.91
A73-712	Ni-20.0Cb-9Cr-1.5Al	1.287-1.265	1.69
A73-611	Ni-20.3Cb-4Cr-2.8Al	1.292-1.280	0.93
A73-735	Ni-19.7Cb-6Cr-2.5Al	1.290-1.268	1.71
A74-177	Ni-17.8Cb-3Ta-6Cr-2.5Al	1.305-1.279	1.89

TRANSVERSE MICROSTRUCTURE OF
Ni–20.5 W/O Cb–6.0 W/O Cr–2.5 W/O Al–3.0 W/O Co
DIRECTIONALLY SOLIDIFIED @ R = 3 cm/hr, $G_L \sim 300^{\circ}C/cm$

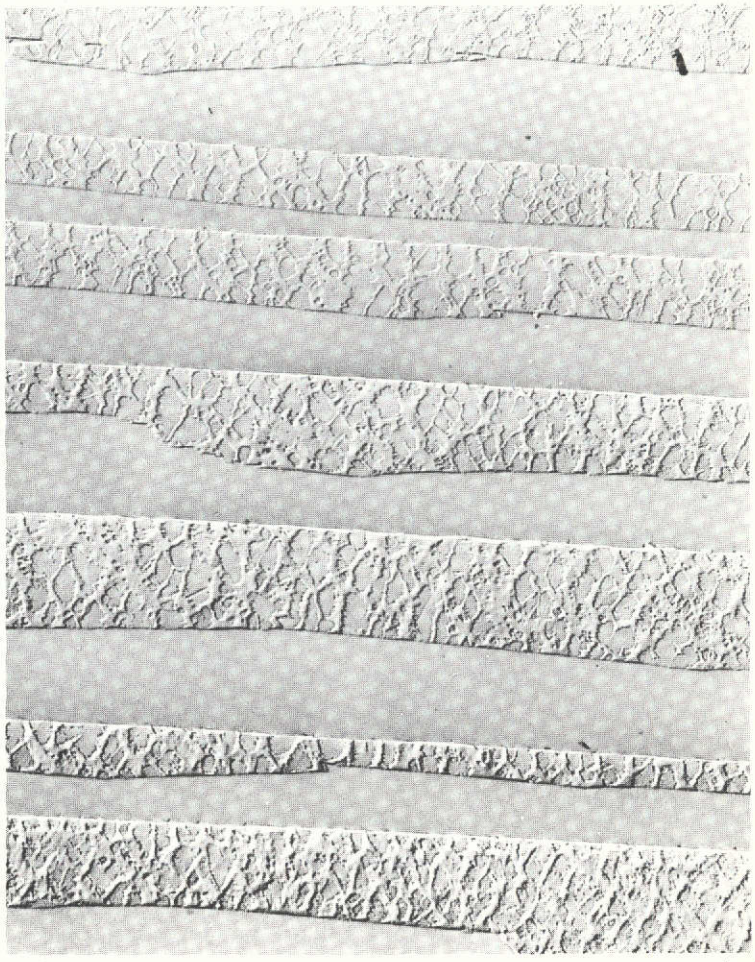

Above 0.6 T_m, within the range of high temperature creep, γ strengthening is diffusion dependent. Thus, the slowly diffusing elements, molybdenum, tungsten and rhenium,would be expected to be most potent hardeners.

Addition of more than 1 w/o of these elements, however, brought about the presence of new phases and thus only a low level of solute could be evaluated. All three elemental additions had little effect on the volume fraction of γ' and δ as indicated in Table III. The microstructures, photographed after replication and electron transmission, are presented in Figs. 17-19 for the molybdenum and tungsten modifications.

Substitution of Ti was made because of its rather extensive solubility in γ and γ' and its more limited solubility in δ-Ni_3Cb as reported by Pryakhina, et al (Ref. 29). These Russians disclosed an absence of continuous series of solid solution between Ni_3Ti and Ni_3Nb as well as the formation of two ternary intermetallic compounds for alloys within the Ni_3Ti-Ni_3Nb section. The solubility of titanium in Ni_3Nb was found by Pyrakhina, et al to be about 5 atomic percent. Levels of 0.87, 1.6 and 8.2 w/o Ti were examined and both the 0.87 w/o and 8.2 w/o addition resulted in an aligned two lamellar composite. A noteworthy effect of adding Ti was the increased amount of γ/γ'' precipitation that took place within the matrix lamellae as shown in Figs. 20 and 21. Although it is reported in equilibrium diagrams otherwise, almost all the aluminum in Ni_3Al can be replaced by Ti. Thus, introducing Ti influences the properties of all three phases γ, γ' and δ. The addition of titanium at the 0.87 w/o level did not affect the volume fraction of either δ or γ' found for the base line composition as shown in Table III.

Tantalum extensively substitutes for columbium within the δ phase to apparently form a continuous solid solution phase (Ref. 28). This $Ni_3(Cb,Ta)$ phase possesses the β-Cu_3Ti orthorhombic crystal structure (Ref. 34). Therefore, Ta will partition in both δ and γ phases, as the reported solubility of Ta in γ nickel at 1300°C is 33 w/o decreasing to ~5 w/o at room temperature (Ref. 28). Because of its relatively high density compared to columbium (16.6 vs 8.5 gm/cc), small additions (less than 10 w/o) were considered. An undesirable slight increase in overall γ/γ'-δ density from small Ta additions were compensated in part by an increase in the melting point. The liquidus and solidus temperature of the Ni-17.8 w/o Cb-3.0 w/o Ta-6.0 w/o Cr-2.5 w/o Al alloy, for example, was determined from differential thermal analysis (Ref. 37). The differential thermal trace shown in Fig. 22 indicates liquidus and solidus temperatures of 1264 and 1247°C respectively. A detailed summary of the alloy compositions consolidated and directionally solidified within this report period is presented in Table II. Thin foils of the γ/γ'-δ alloy containing 3 w/o Ta were prepared from discs cut normal to the growth direction. The transverse microstructure is presented in Fig. 23 as viewed in electron transmission. The γ/γ' lattice parameter misfit was computed from measurements of respective (220) diffraction

TRANSVERSE MICROSTRUCTURE OF Ni–19.7 W/O Cb–6.0 W/O Cr–2.5 W/O Al–1.0 W/O Mo
DIRECTIONALLY SOLIDIFIED @ R = 3 cm/hr, $G_L \sim 300^{\circ}$C/cm

TRANSVERSE MICROSTRUCTURE OF
Ni–19.7 W/O Cb–6.0 W/O Cr–2.5 W/O Al–1.0 W/O W
DIRECTIONALLY SOLIDIFIED @ R = 3 cm/hr, $G_L \sim 300^{\circ}$ C/cm

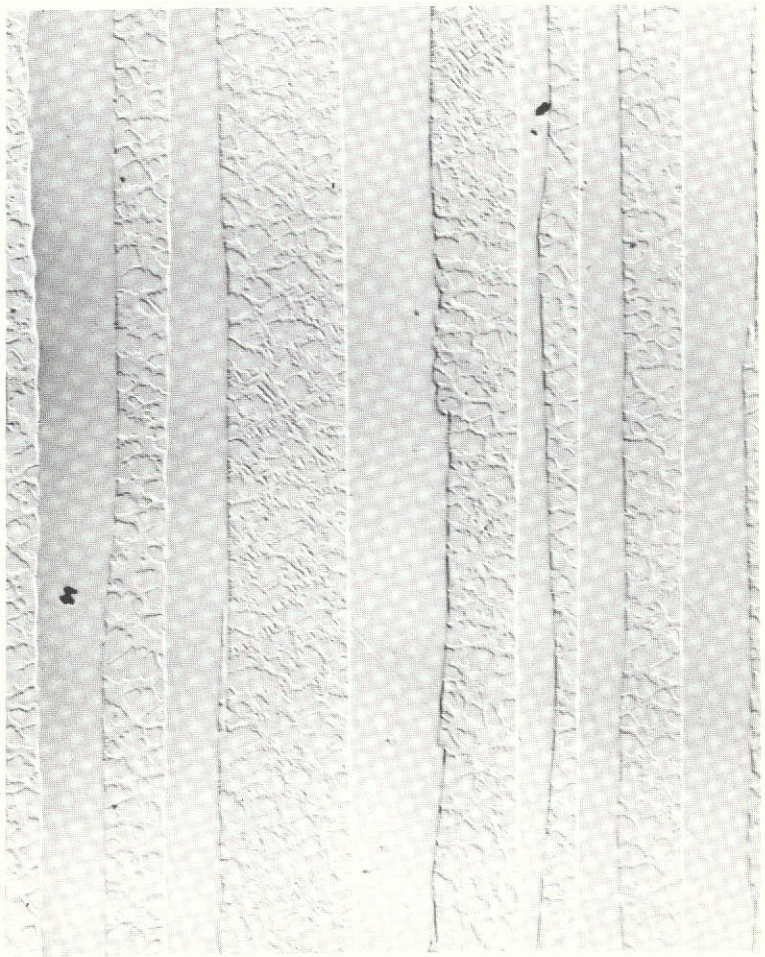

TRANSMISSION ELECTRON MICROGRAPH
OF Ni–19.7 w/o Cb–6.0 w/o Cr–2.5 w/oAl–1.0 w/o W (A73–634)

X12,600

1 μm

FIG. 19

N04–82–3

TRANSVERSE MICROSTRUCTURE OF
Ni–18.6 W/O Cb–6.0 W/O Cr–2.5 W/O Al–0.87 W/O Ti
DIRECTIONALLY SOLIDIFIED @ R = 3 cm/hr, $G_L \sim 300^{\circ}C/cm$

TRANSMISSION ELECTRON MICROGRAPH
OF Ni–18.6 w/o Cb–6.0 w/o Cr–2.5 w/o Al–0.87 w/o Ti (A73–598)

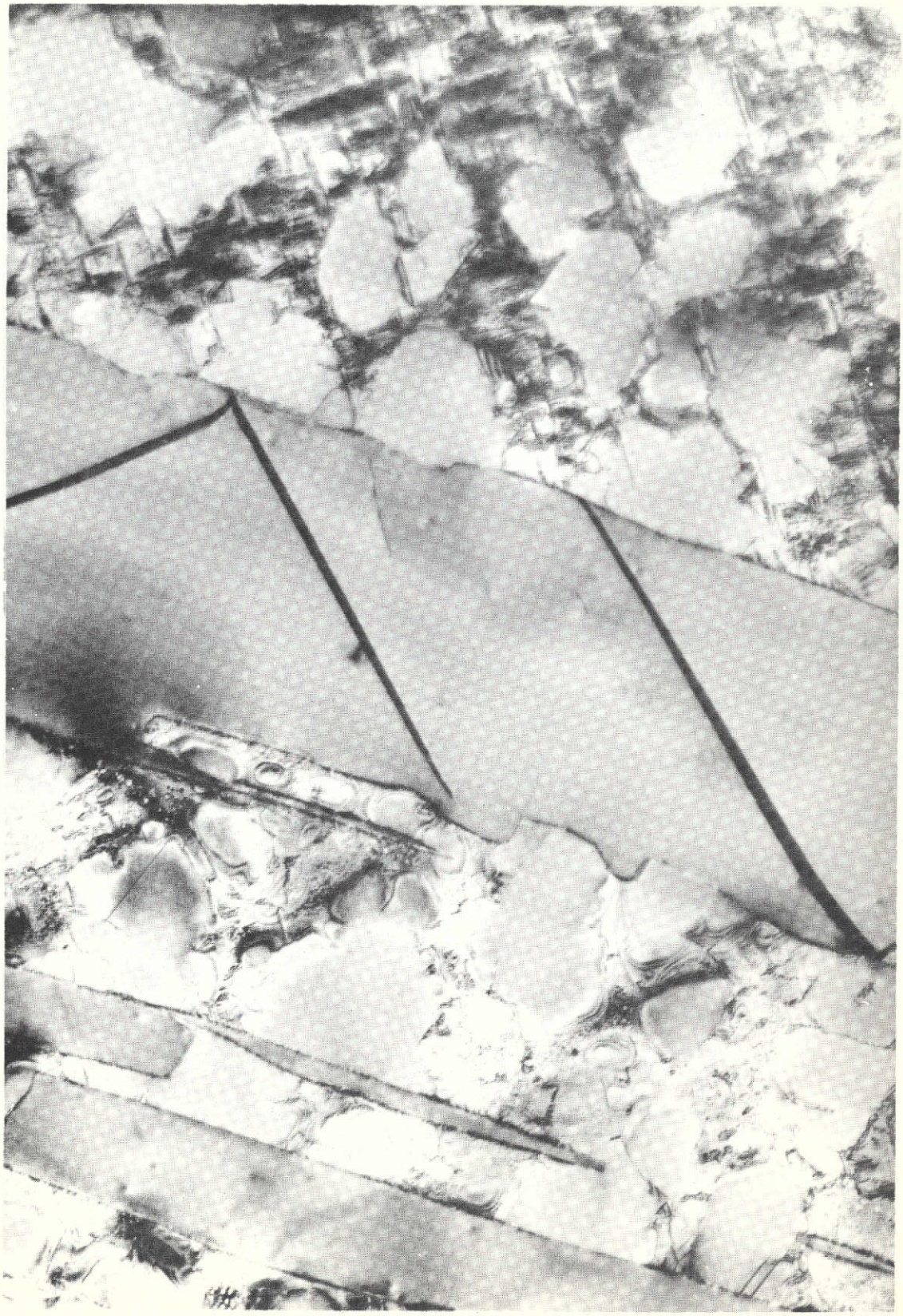

DIFFERENTIAL THERMAL ANALYSIS TRACE OF 70.6 w/o Ni, 17.9 w/o Cb 6.0 w/o Cr 3.0 w/o Ta 2.5 w/o Al (HEATING RATE 3°C/min)

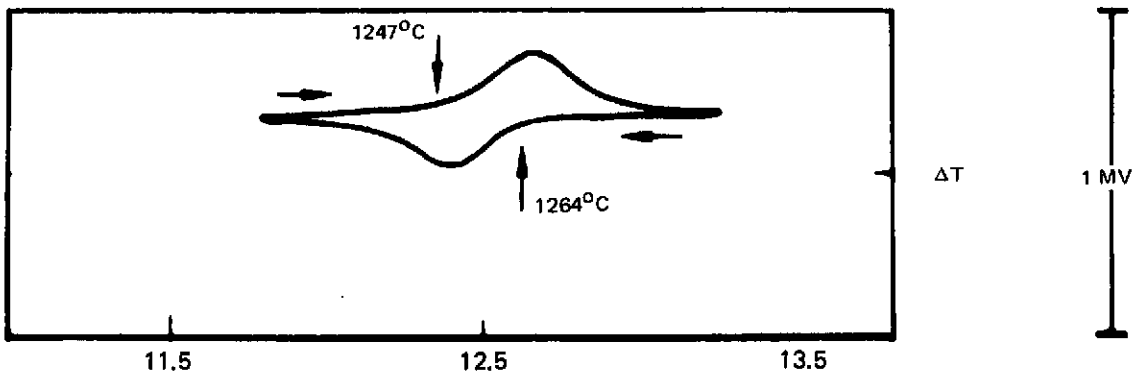

TRANSMISSION ELECTRON MICROGRAPH OF Ni–17.8 w/o Cb–3.0 w/o Ta–6.0 w/o Cr–2.5 w/o Al (A74–177)

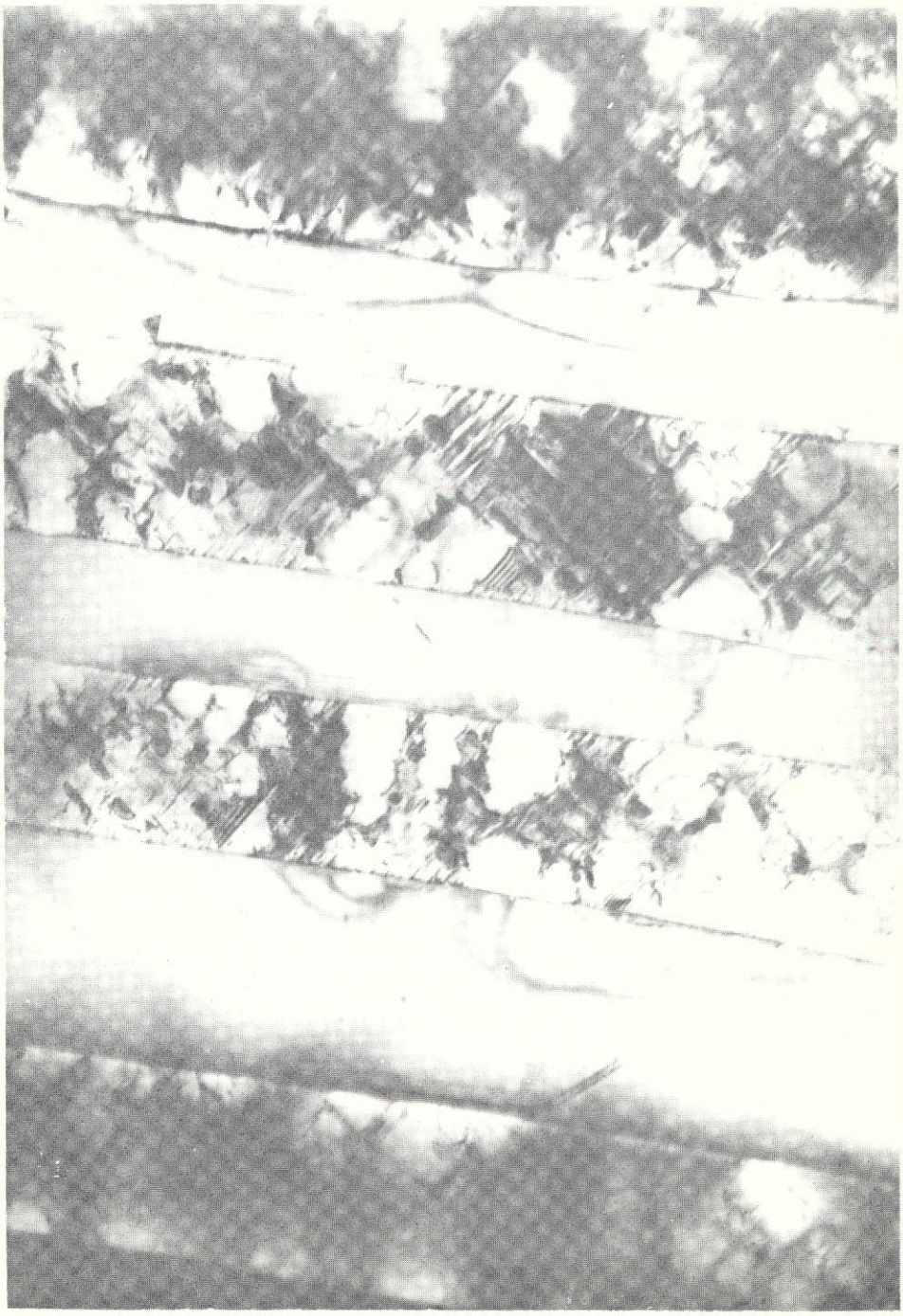

N07–43–1

spots of γ and γ' and found to be 1.89 percent. The volume fraction of δ $Ni_3(CbTa)$ was determined by lineal analysis and found to be ~40% (Table III). The size and distribution of the γ' precipitates as shown in Fig. 24 closely resembled that of the base line γ/γ'-δ quaternary eutectic.

In the search for an alloy with improved grain boundary strength and resistance to oxidation, the base quaternary γ/γ'-δ alloy was modified by small additions of B and Si (i.e. .005-.1, and 1.0 w/o respectively). All but the 0.005 w/o B alloy resulted in cellular microstructure when processed at G_L = 300°C/cm and R = 3 cm/hr. The alloys both exhibited additional boride and silicide phases within grain/cell boundaries indicating the formation of unidentified, undesirable, low melting and rather brittle phases. The microstructure of one γ/γ'-δ alloy, Ni-19.8 w/o Cb-6.0 w/o Cr-2.5 w/o Al-0.1 w/o B, displaying nickel boride and coarsened γ' particles in the cell boundaries, is shown in Fig. 25.

3.3 Solidification Behavior

There are macrosegregation effects during polyphase solidification which result from the application of directional normal freezing of off eutectic (monovariant, bivariant, ... polyvariant) alloys. The freezing range ΔT of these alloys is responsible for segregation.

3.3.1 Longitudinal Macrosegregation

During this investigation certain base line quaternary specimens were directionally solidified under a thermal gradient in the liquid measured at the liquid/solid interface of ~400°C/cm. This gradient was achieved by empirical changes in the induction coil shape, coolant position and flow, and the level of superheat in the liquid. A feedback loop was further introduced in the plate current circuit of the 20 Kw Lepel apparatus to minimize input power fluctuations to the heating coil. Two ingots, produced in this apparatus and another similar high gradient withdrawal unit employing a 35 Kw Westinghouse power supply (without a feedback loop) were examined for variations in composition along their lengths. Positions approximately 1.2 cm apart were examined by X-ray fluorescence along the entire length of each ingot. The results of the XRF analyses are presented in Tables V and VI. A slight but continuous increase in chromium and aluminum content was observed with distance from the initiation of freezing as was previously observed (Ref. 1). The results of our previous XRF analysis (Ref. 1) of an ingot directionally solidified in the prototype high gradient apparatus employing a 50 Kw Lepel power supply are presented in Table VII. From comparing the changes in the maximum and minimum values of Cb, Cr and Al content, Figs. 26-28, it is apparent that a more uniform compositional distribution has been produced for the γ/γ'-δ quaternary alloy of nominal composition Ni-20.0 w/o Cb-6.0 w/o Cr-2.5 w/o Al using the newer apparatuses.

TRANSVERSE MICROSTURCTURE OF Ni–17.9 W/O Cb–6.0 W/O Cr–2.5 W/O Al–3.0 W/O Ta DIRECTIONALLY SOLIDIFIED @ R=3 cm/hr, $G_L \sim 300\ ^oC/cm$

(AFTER ROOM TEMPERATURE TENSILE TEST)

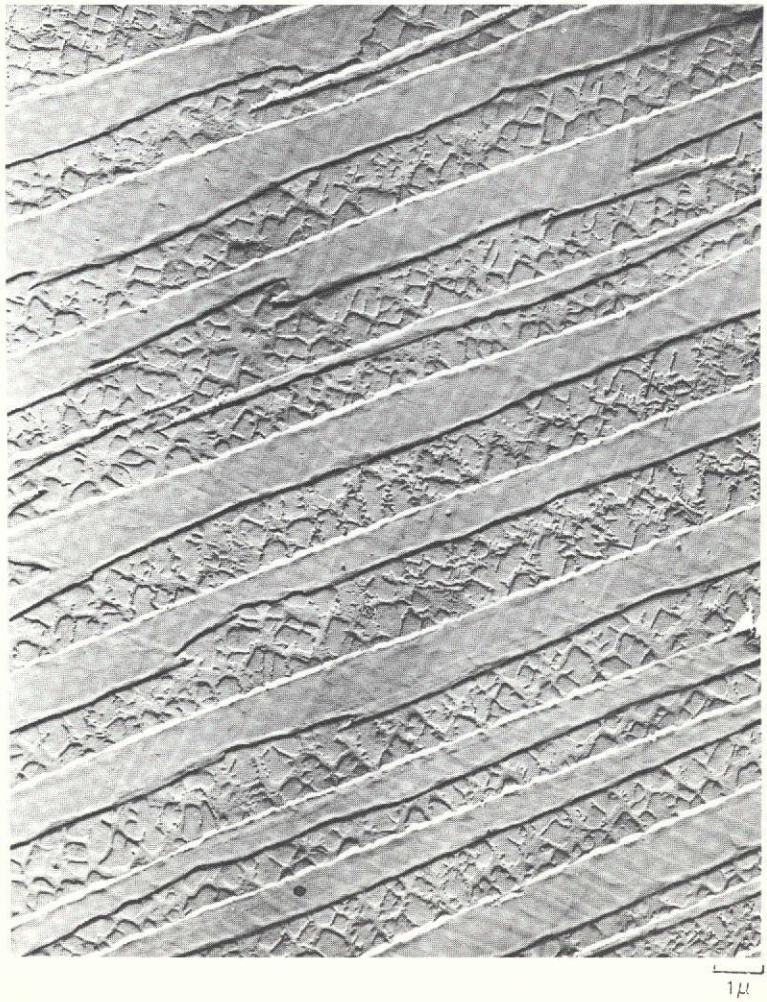

LONGITUDINAL MICROSTRUCTURE OF $\gamma/\gamma'-\delta$ (A73–485)
Ni–19.8 w/o Cb–6.0 w/o Cr–2.5 w/o Al–0.1 w/o B

R = 2 cm/hr $G_L \sim 80^{o}C/cm$

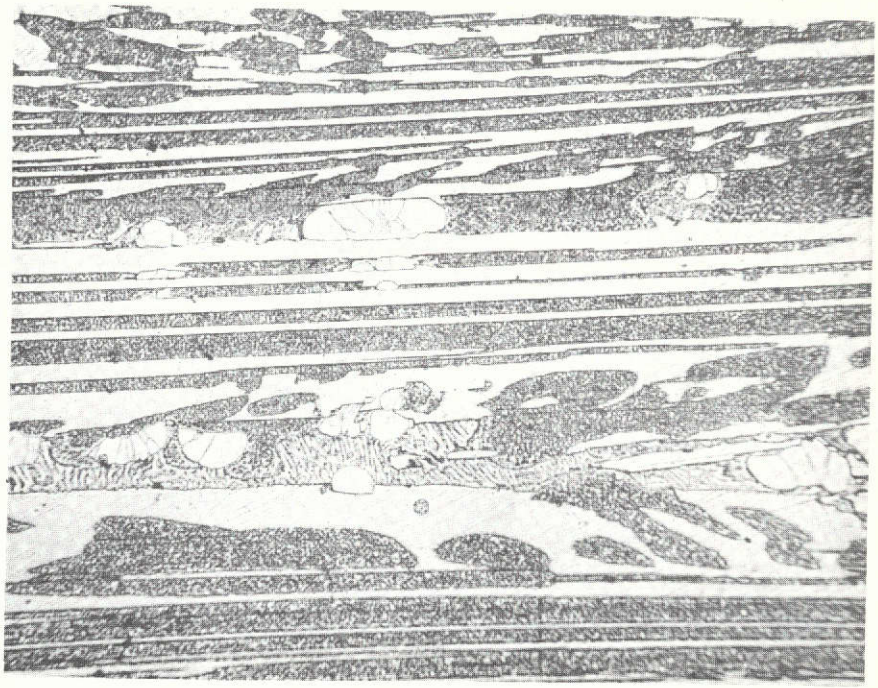

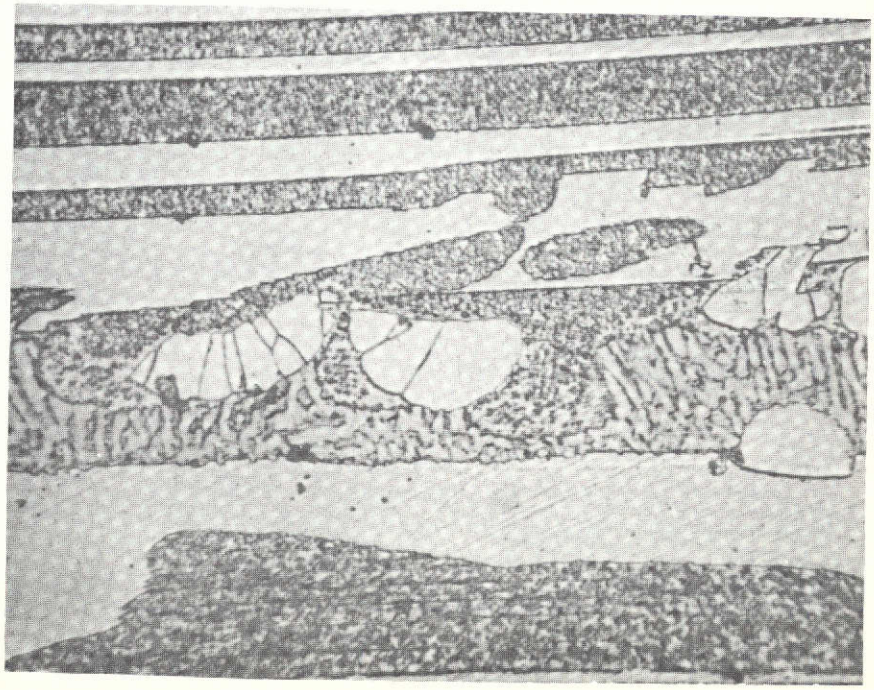

N04–28–1

Table V

X-ray Fluorescence Analysis of A74-730
Nominal Composition Ni-20.0 w/o Cb-6.0 w/o Cr-2.5 w/o Al
Processed at 3 cm/hr in 35 kW Westinghouse High Gradient Apparatus

Solidification Position Identification	w/o Ni min max	w/o Cb min max	w/o Cr min max	w/o Al min max
A74-370-A*	71.83-71.42	20.16-20.16	6.15-6.21	1.86-2.21
-B	71.71-71.60	20.04-20.15	6.10-6.14	2.15-2.26
-C	71.75-71.59	20.11-20.15	6.07-6.11	2.07-2.15
-D	71.71-71.52	20.18-20.18	6.06-6.06	2.05-2.23
-E	72.06-71.65	20.13-20.24	6.10-6.10	1.71-2.01
-F	71.98-71.72	20.15-20.33	6.10-6.10	1.77-1.85
-G	71.74-71.54	20.26-20.26	6.05-6.10	1.95-2.10
-H	71.56-71.34	20.25-20.25	6.15-6.19	2.04-2.22
-I	71.66-71.25	20.18-20.29	6.14-6.18	2.02-2.28
-J	71.48-71.22	20.35-20.45	6.17-6.17	2.00-2.16
-K	71.48-71.35	20.31-20.35	6.14-6.23	2.07-2.07
-L	71.35-71.13	20.41-20.41	6.33-6.33	1.91-2.13
-M	71.13-70.86	20.30-20.42	6.35-6.38	2.22-2.34
-N**	70.98-70.61	20.11-20.28	6.39-6.50	2.52-2.61

*First Solidified
**Last Solidified

Table VI

X-ray Fluorescence Analysis of A74-376
Nominal Composition Ni-20.0 w/o Cb-6.0 w/o Cr-2.5 w/o Al
Processed at 3 cm/hr in 20 kW Lepel High Gradient Apparatus

Solidification Position Identification	w/o Ni		w/o Cb		w/o Cr		w/o Al	
	min	max	min	max	min	max	min	max
A74-376-A*	71.08	70.62	20.12	20.21	6.18	6.23	2.62	2.94
-B	71.31	7.15	20.25	20.33	6.14	6.14	2.30	2.38
-C	71.43	71.20	20.05	20.16	6.14	6.14	2.38	2.50
-D	71.53	71.30	20.07	20.12	6.06	6.12	2.34	2.46
-E	71.75	71.48	20.09	20.12	6.02	6.06	2.14	2.34
-F	71.65	71.23	20.10	20.16	6.13	6.19	2.34	2.42
-G	71.17	71.05	20.21	20.22	6.18	6.23	2.44	2.50
-H	71.39	71.10	20.10	20.28	6.19	6.24	2.32	2.38
-I	71.22	70.72	20.26	20.43	6.10	6.29	2.42	2.56
-J	71.18	71.04	20.18	20.20	6.30	6.34	2.34	2.42
-K	71.01	70.79	20.35	20.37	6.31	6.40	2.33	2.44
-L	71.03	70.60	20.31	20.44	6.32	6.37	2.34	2.59
-M	70.81	70.63	20.33	20.42	6.44	6.50	2.42	2.45
-N**	70.29	69.92	20.42	20.51	6.55	6.63	2.74	2.94

* First Solidified
**Last Solidified

Table VII

X-ray Fluorescence Analysis of A72-627
Nominal Composition Ni-19.7 w/o Cb-6.0 w/o Cr-2.5 w/o Al

Solidification Position Identification	w/o Ni min max	w/o Cb min max	w/o Cr min max	w/o Al min max
A72-627-A*	71.35-71.43	19.49-19.55	5.46-5.68	3.40-3.80
-B	72.07-72.13	19.25-19.75	5.82-5.86	2.56-2.64
-C	71.51-72.15	19.61-19.81	5.68-5.72	2.74-2.76
-D	72.44-72.58	19.66-19.88	5.67-5.81	2.40-2.64
-E	72.02-72.10	19.60-19.72	5.77-5.77	2.53-2.67
-F	70.66-70.74	19.44-19.62	5.80-5.96	2.50-2.54
-G	71.33-71.73	19.43-19.77	5.80-5.90	2.96-2.50
-H	72.01-72.31	19.00-19.82	5.91-6.63	2.41-2.65
-I	70.66-71.74	19.66-19.80	5.94-6.06	2.47-2.81
-J	71.85-72.07	20.02-20.14	5.96-5.98	2.49-2.65
-K	71.55-71.95	19.26-20.06	6.00-6.00	2.62-2.68
-L	70.44-71.12	19.90-20.04	5.99-6.09	2.76-2.82
-M**	68.83-70.17	19.43-19.93	6.23-6.27	2.78-3.12

* First Solidified
**Last Solidified

COMPOSITIONAL VARIATION ALONG LENGTH OF $\gamma/\gamma'\delta$(Ni–20.0 w/o Cb–6.0 w/o Cr–2.5 w/o Al)
1/2 IN. BAR SPECIMEN DIRECTIONALLY SOLIDIFIED AT 3cm/hr (35kw WESTINGHOUSE)

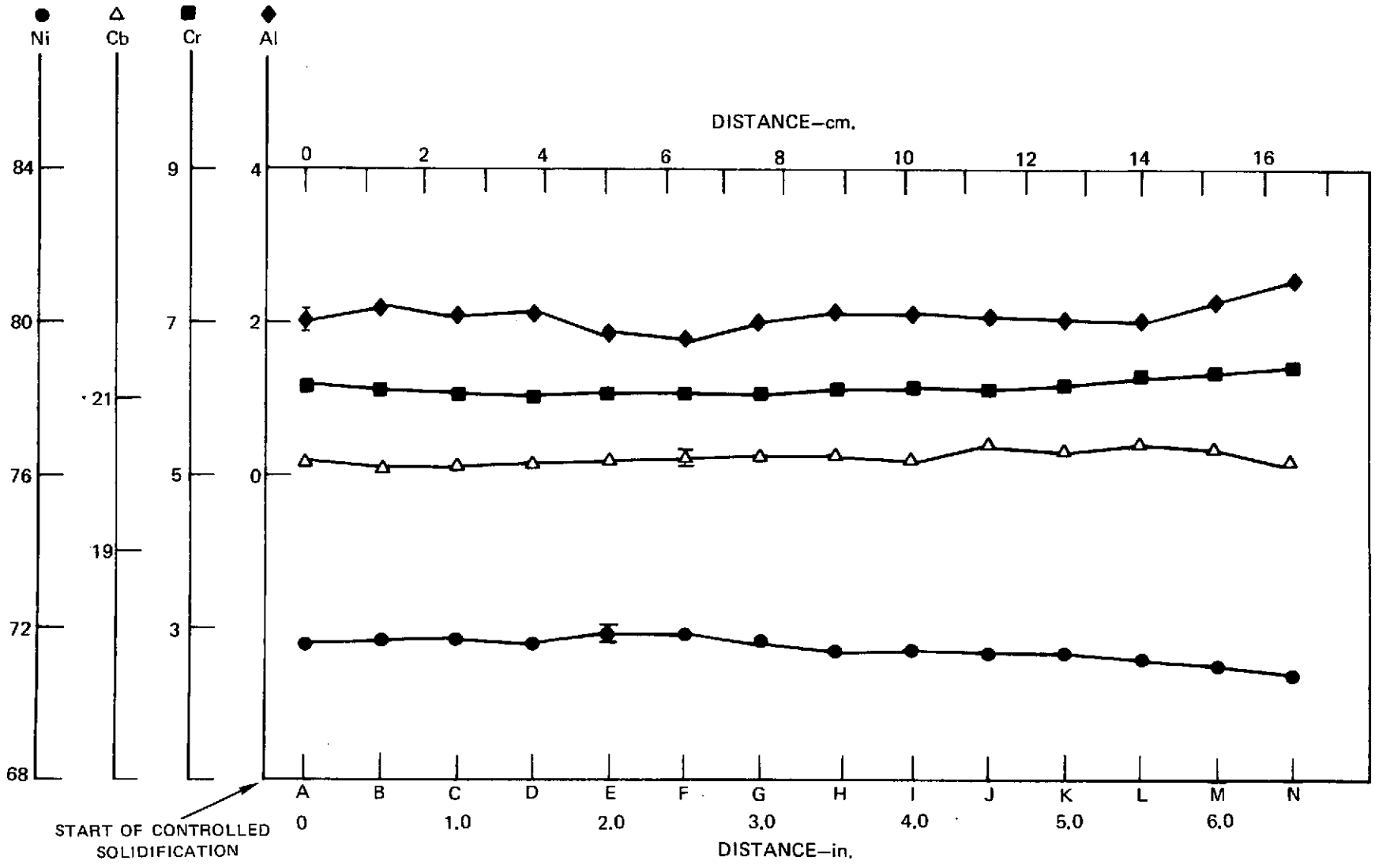

N06–27–1

FIG. 26

COMPOSITIONAL VARIATION ALONG LENGTH OF γ/γ'-δ (Ni–20.0 w/o Cb–6.0 w/o Cr–2.5 w/o Al)
1/2 IN. BAR SPECIMEN DIRECTIONALLY SOLIDIFIED AT 3cm/hr (20kw LEPEL)

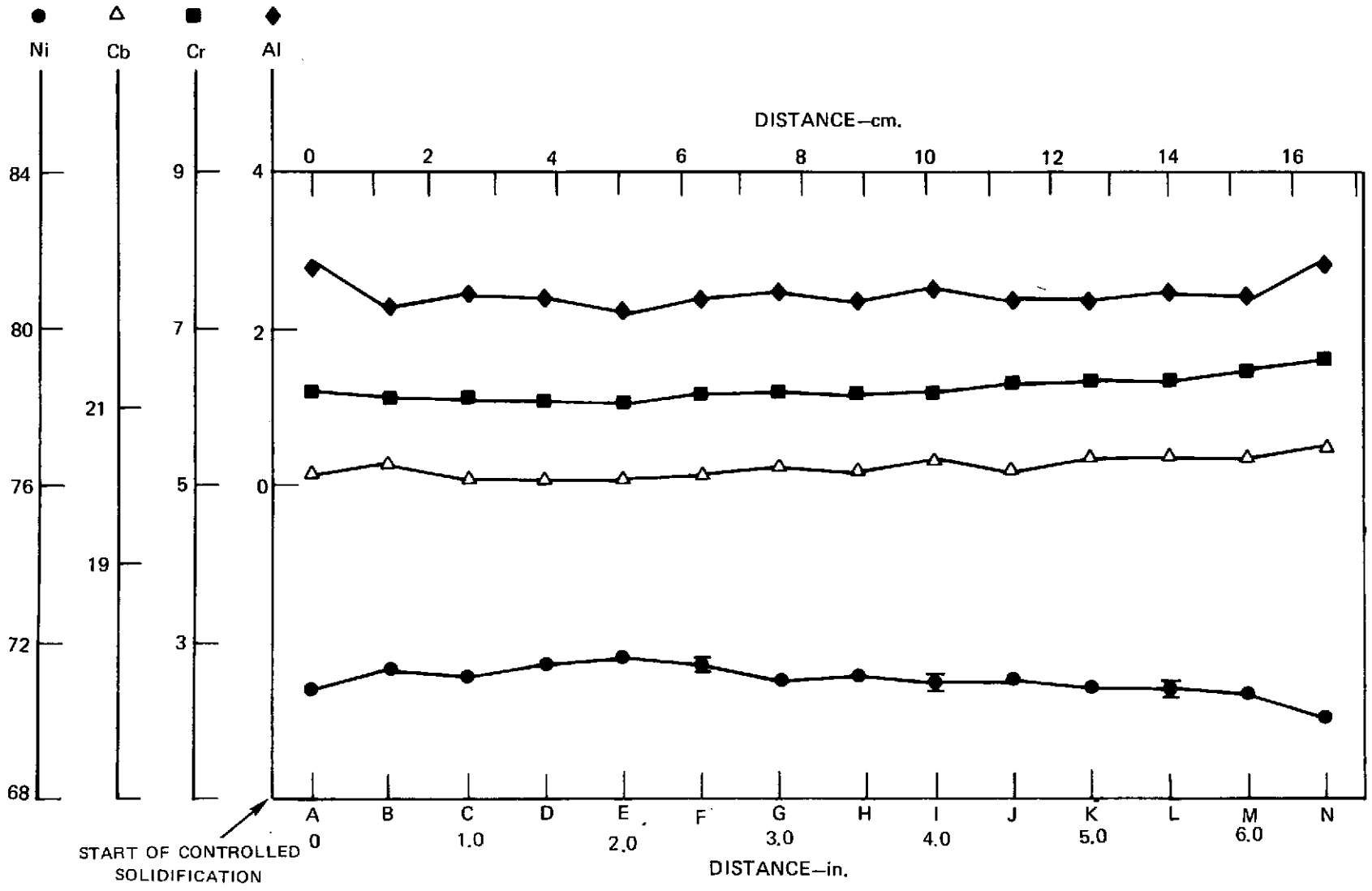

N06-27-2

FIG. 27

COMPOSITIONAL VARIATION ALONG LENGTH OF $\gamma/\gamma' - \delta$ (Ni–19.7 w/o Cb–6.0 w/o Cr–2.5 w/o Al)
1.2 CM BAR SPECIMEN DIRECTIONALLY SOLIDIFIED AT 3 cm/hr (50 kw LEPEL)

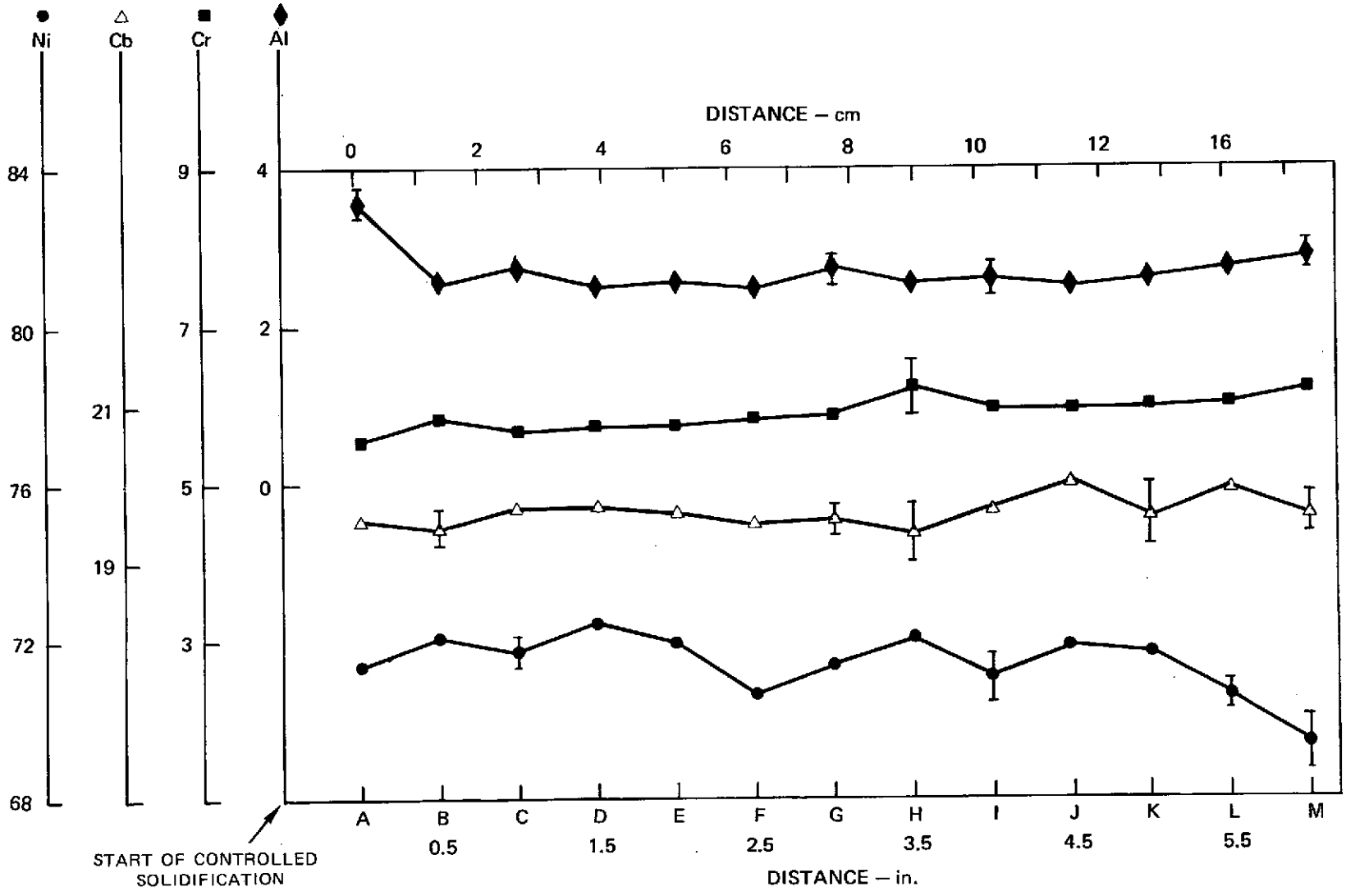

FIG. 28

N06–27–1

3.3.2 Metal/Mold and Metal/Gas Reactions

At liquid temperatures exceeding 1700°C metal mold reactions were observed, as previously reported (Ref. 1), from the prolonged contact of γ/γ'-δ melt with Al_2O_3. This reaction was manifested by an included dendritic phase distributed predominantly in the last one third of longitudinal growth. The composition of this phase was determined by electron microbeam probe as: Al 38.7 w/o, Cb 4.0 w/o, Ni 4.7 w/o, Cr 8.4 w/o and O 44.3 w/o (by difference). The morphology of this reaction product phase is shown in Fig. 29, wherein also is presented the X-ray spectral response for the principal components, Al, Ni, Nb, and Cr. The presence of this third phase did not break down the advancing planar liquid/solid interface. However, its presence was shown to be detrimental to the mechanical properties of the system (Ref. 1). Moreover, a very small script-like grain boundary phase was observed after high gradient solidification. This phase was identified by electron microbeam probe as NbC and the relevant elemental distribution scans are shown in Fig. 30. This phase is thought to form from carbon diffusion into the melt from the H_2O-graphite water gas reaction products diffusing through cracks in the oxide crucible. The carbides which form at grain boundaries and are occasionally aligned with same are not considered at this time to be desirable from a reinforcement standpoint. Carbon pickup could be minimized if not entirely eliminated by wrapping the susceptor and baffle in tantalum foil reducing the availability of carbon sites for water gas reaction.

3.3.3 Growth from Eutectic Seeds

To examine the possibility of creating eutectic specimens without grain boundaries, attempts were made to seed and, by selective growth processes, to produce a single eutectic grain. Using large grain seeds of γ/γ'-δ base line quaternary, produced by slow growth in a low temperature gradient furnace, several eutectic ingots were prepared from these seeds by directional solidification in a high gradient crystal growth apparatus. It was surprising to note that no significant change in grain size was observed after 10 cm (~4 in.) of growth from the seed interface. Specimens grown from a chill cast eutectic polycrystal seed and a directionally solidified eutectic seed are presented in Fig. 31. Further analysis of certain aspects of the 'fine' structure or fault substructure including size and distribution of cell wells is required to better characterize any subtle changes in microstructures which may have been produced.

3.4 Heat Treatment

3.4.1 Base Line Alloy

A major contribution to the strength of most precipitation hardened nickel base superalloys and in particular to the γ/γ'-δ family of eutectic superalloys is the most fortunate precipitate phenomenon of stable coherent FCC compound γ', [Ni_3,(Al,Cb)]. The compatibility (~1% mismatch of lattice parameters) of the γ' phase with γ permits homogeneous nucleation of the precipitate with low surface energy and good long-time stability. Significant changes in creep rate

X–RAY SPECTRAL SCAN ACROSS METAL MOLD REACTION PHASE OBSERVED FROM HIGH GRADIENT D.S. $\gamma/\gamma'-\delta$ IN Al_2O_3 CRUCIBLE

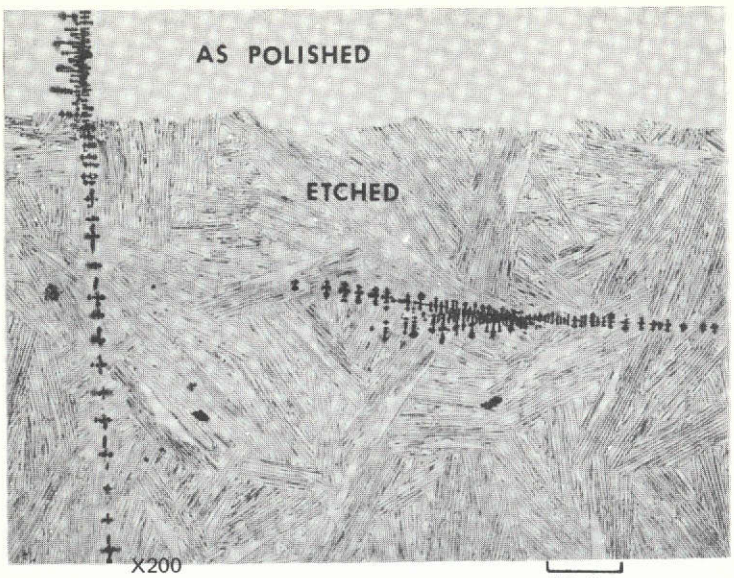

DARK DENDRITIC PHASE:

Al: 38.7 w/o
Nb: 4.0 w/o
Ni: 4.7 w/o
Cr: 8.4 w/o
O: 44.3 w/o BY DIFF.

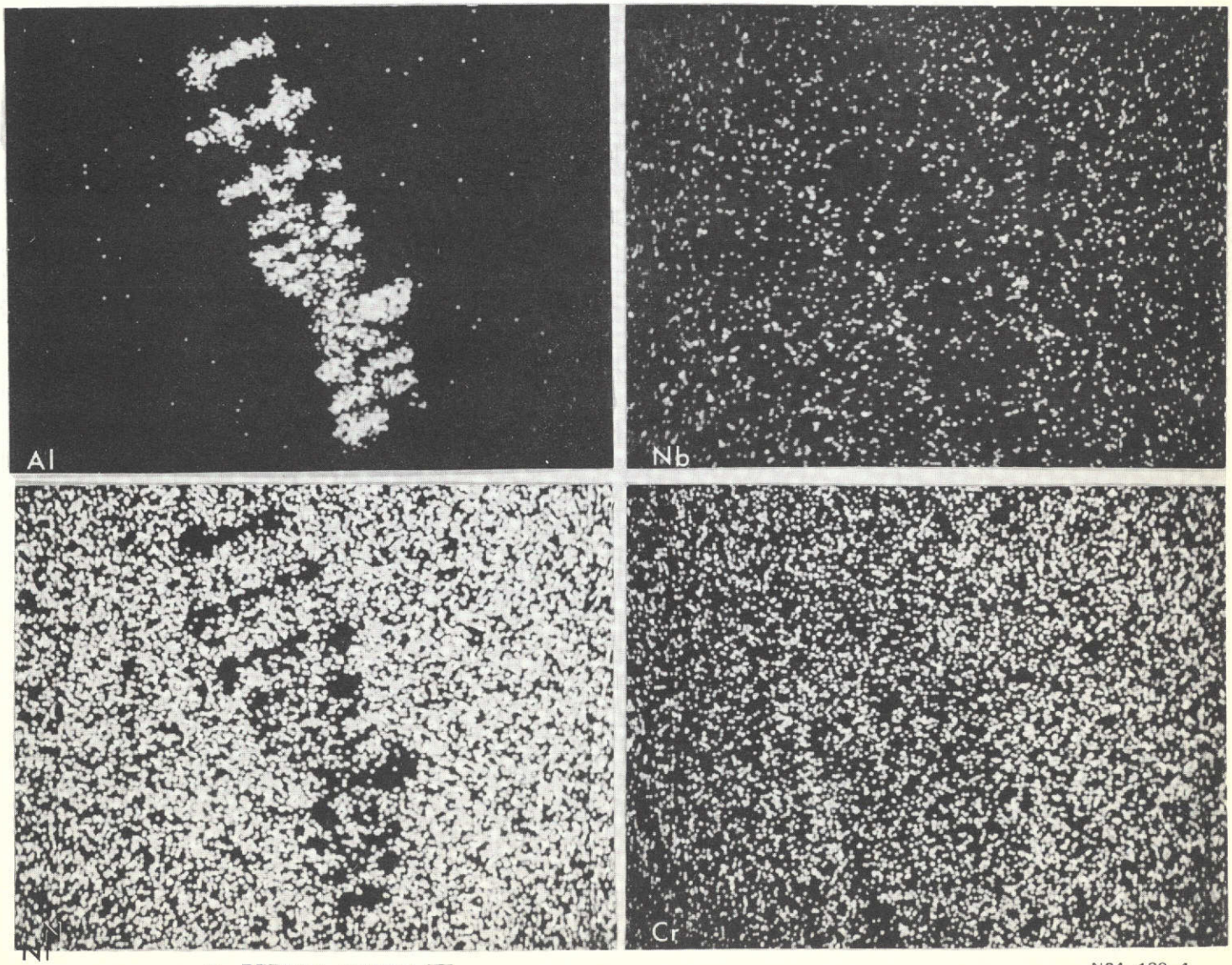

N04–139–1

ELECTRON MICROBEAM PROBE SCANS ACROSS GRAIN BOUNDARY PHASE IN $\gamma/\gamma'-\delta$

(Ni – 20.0 w/o Cb – 6.0 w/o Cr – 2.5 w/o Al) A74–327

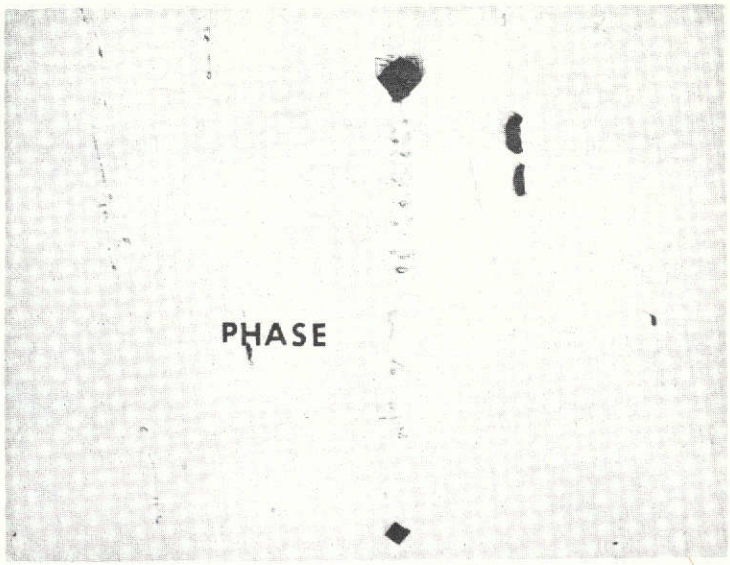

a) SCRIPT–LIKE PHASE ALIGNED IN GRAIN BOUNDARIES

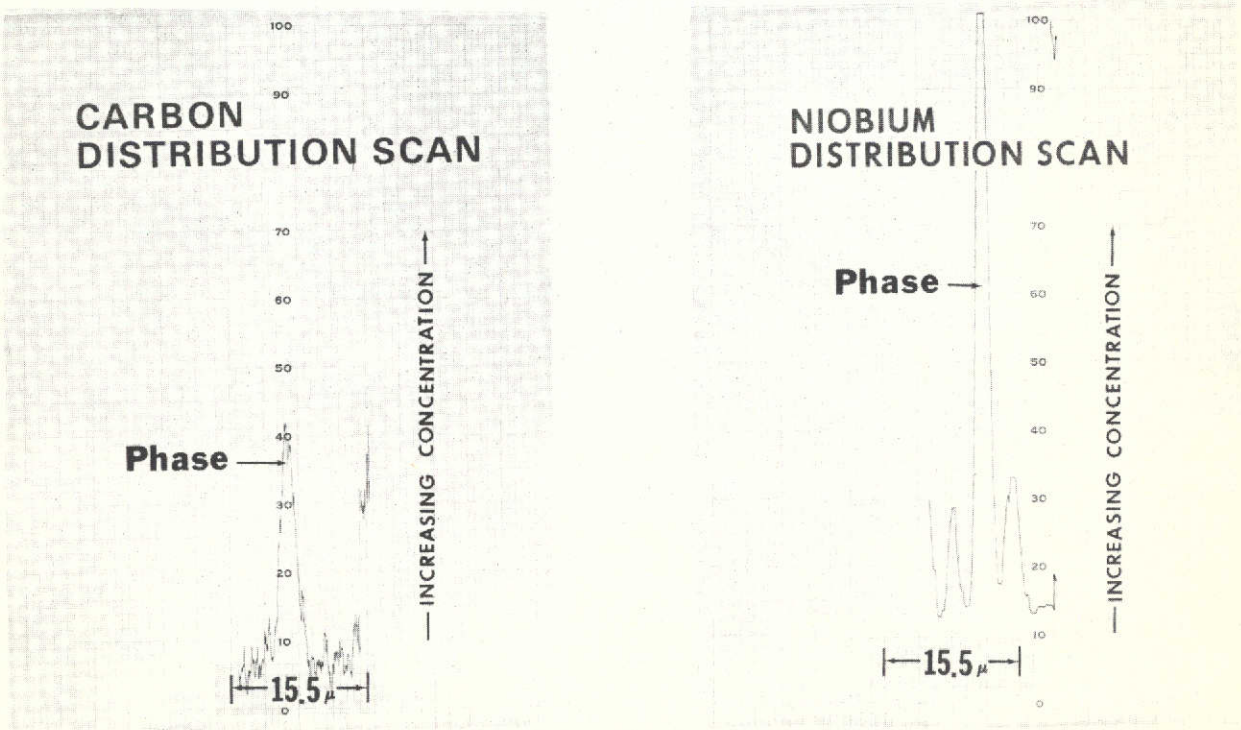

b) DISTRIBUTION SCANS INDICATE PHASE TO BE A NIOBIUM RICH CARBIDE

EFFECT OF SEEDING GROWTH ON THE MICROSTRUCTURE OF $\gamma/\gamma'-\delta$ (Ni–20.0 w/o Cb–6.0 w/o Cr–2.5 w/o Al) AFTER 10 cm OF DIRECTIONAL SOLIDIFICATION

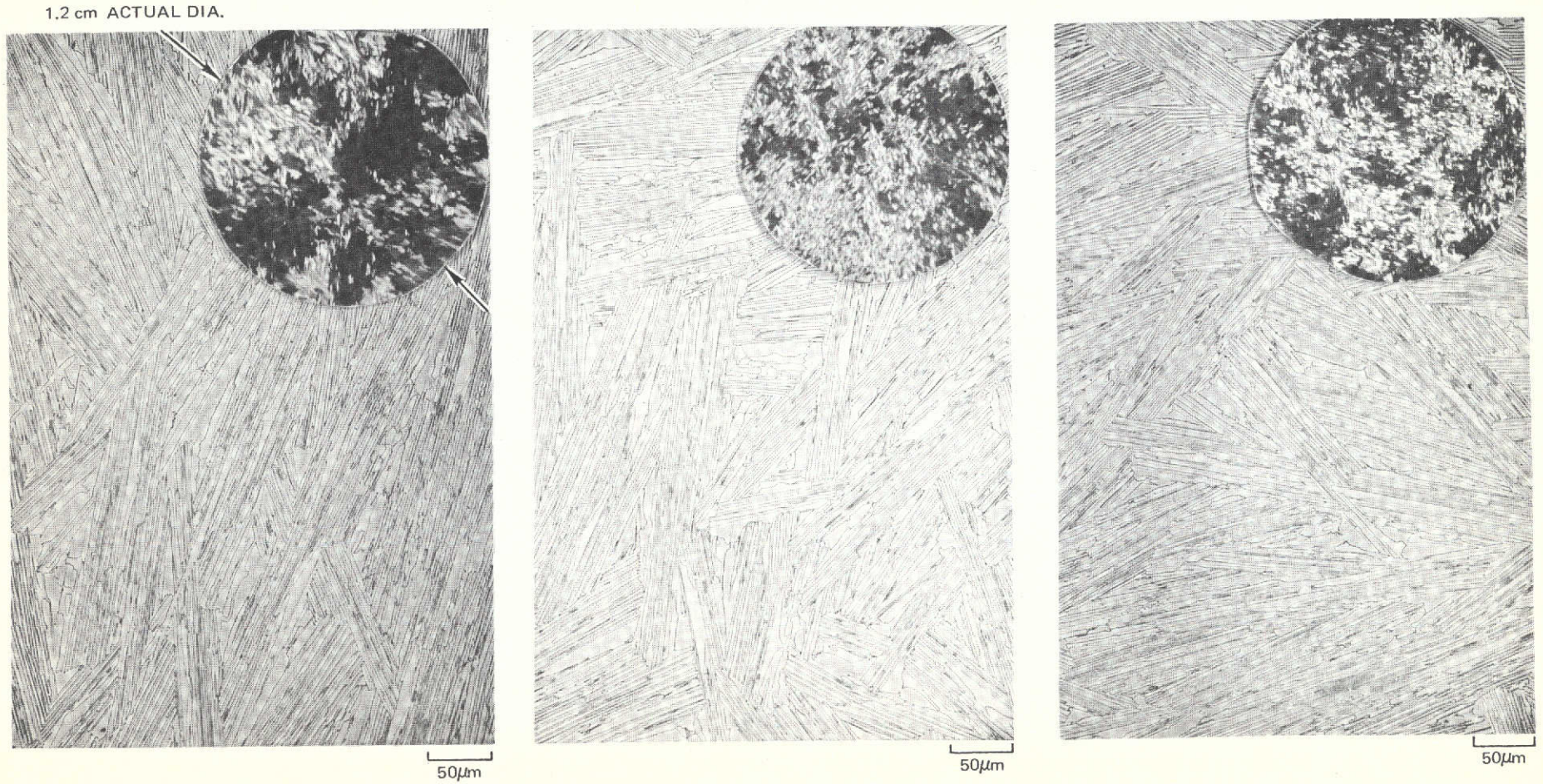

a) CHILL CAST SEED AND R = 3 cm/hr, G_L~300°C/cm

b) D.S. EUTECTIC SEED AND R = 3 cm/hr, G_L~ 300° C/cm

c) D.S. EUTECTIC SEED AND R = 5 cm/hr, G_L~ 300° C/cm

N04–28–2

FIG. 31

and rupture life of superalloy have previously been obtained through knowledge of the structure-property relationships which were obtained through empirical thermal treatments. However, our knowledge of the interdependence of constitution, phase transformation, morphology control, and properties is taxed to optimally heat treat these multicomponent alloys. Therefore, rather straightforward solutionizing and aging heat treatment were selected to evaluate their effects on the tensile properties of $\gamma/\gamma'-\delta$ (Ni-19.7 w/o Cb-6.0 w/o Cr-2.5 w/o Al). Previous results of Barkalow and Donachie (Ref. 38) have indicated that the creep rupture properties of $\gamma/\gamma'-\delta$ are unaffected by long term exposures at elevated temperature, i.e. 2500 and 1500 hrs at 871°C (1600°F) and 982°C (1800°F) respectively. The heat treatments investigated were the following:

Treatment A	Treatment B
Solutionize @ 1200°C (2192°F) 4 hrs	Solutionize @ 1200°C (2192°F) 4 hrs
Air cool to room temperature	Air cool to room temperature
Age @ 871°C (1600°F) 40 hrs	Age @ 1079°C (1975°F) 40 hrs

The γ' solutioning temperature selected was based on a previous metallographic determination of the γ' solvus temperature of between 1149-1177°C (Ref. 1). Heat treatment A was selected to produce fine γ'/γ'' precipitates for maximizing strength at intermediate temperatures and heat treatment B was chosen to represent a thermal history given the alloy during vapor coating (Ref. 39).

The effects of these heat treatments on the microstructure of $\gamma/\gamma'-\delta$ are shown in Fig. 32. Areal analysis techniques were performed on representative micrographs of each heat treated specimen and the original directionally solidified specimen to determine the volume percentage of γ' present in each condition. As the fine precipitates could not be accurately cut out and weighed they were estimated by point count and added to that determined by the direct separation technique. The average volume percentage of solid state precipitates in the 'as directionally solidified' samples was 63 (50.5 percent massive and 12.5 percent fine γ'). The volume percentage precipitates after heat treatment A was 72.1 (60.2 percent massive γ' and 11.9 percent disc shaped γ'' and fine γ') and after heat treatment B was 43.1 (all massive γ'). Some Widmanstätten precipitates of the δ phase were observed to further decorate the octahedral planes of the matrix γ phase on eutectic grain boundaries of specimens aged for 40 hrs at 871°C (1600°F) as indicated on virgin d.s. $\gamma/\gamma'-\delta$ bars. It is interesting to note that all three precipitate phases observed during these aging experiments (namely face centered cubic γ'-Ni_3Al, body centered tetragonal γ''-Ni_3Cb, and orthorhombic δ-Ni_3Cb) permit removal of Cb (Nb) atoms from the γ supersaturated nickel solid solution. Neither heat treatment produced observable γ' precipitates in the δ phase as was previously noted in aging studies of the quasi-binary $\gamma'-\delta$ and ternary $\gamma-\gamma'-\delta$ eutectic (Ref. 40).

EFFECT OF HEAT TREATMENT ON THE MICROSTRUCTURE OF $\gamma/\gamma' - \delta$

Ni - 19.7 w/o Cb - 6.0 w/o Cr - 2.5w/o Al

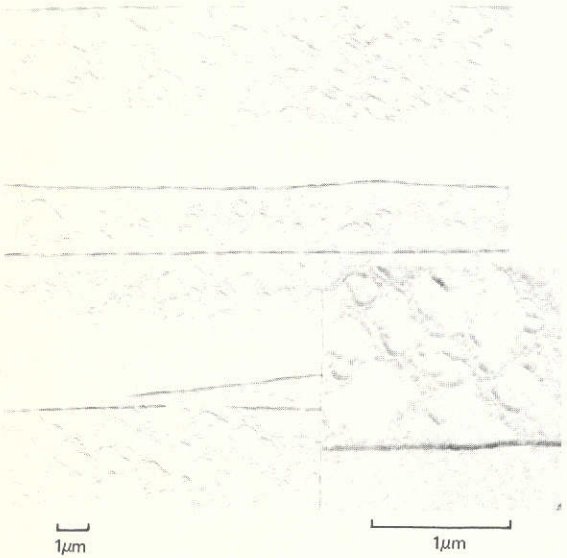

a) AS DIRECTIONALLY SOLIDIFIED,
R = 3cm/hr, $G_L \sim 300^o$ C/cm

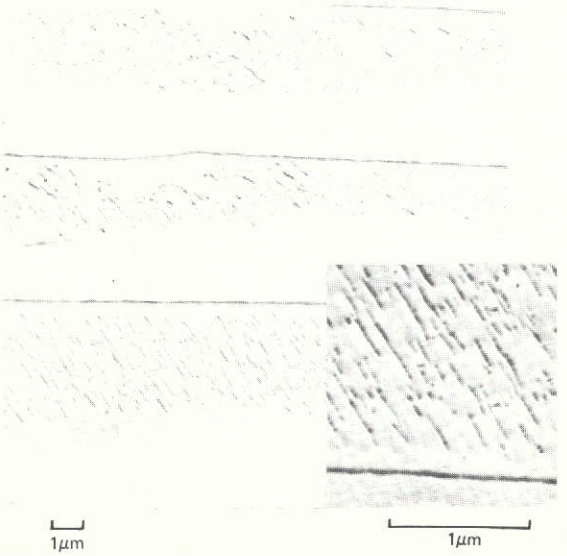

b) SOLUTIONIZED AT 1200° FOR 4 hrs,
AIR COOLED AND AGED AT 872°C FOR 40 hrs.

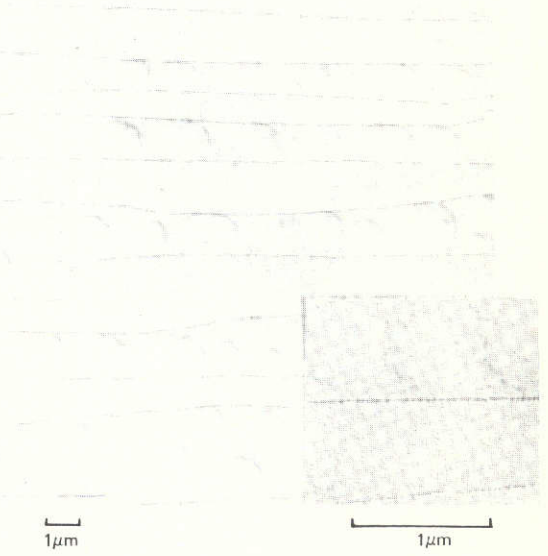

c) SOLUTIONIZED AT 1200°C FOR 4 hrs,
AIR COOLED AND AGED AT 1079°C FOR 40 hrs.

N04-30-1

FIG. 32

The longitudinal tensile properties from 20-1100°C of γ/γ'-δ specimens after heat treatments A and B are presented in Table VIII and graphically in Fig. 33. From a comparison with the base line 'as directionally solidified' γ/γ'-δ alloy shown in Fig. 34 (Ref. 1) one observes an improvement in ultimate tensile strength at low to intermediate temperatures for specimens receiving heat treatment A with no change observed at elevated temperature. Specimens receiving heat treatment B displayed greater ductility in general but were slightly weaker in tension than the 'as directionally solidified' specimens which contain fine γ' precipitates as well. With certain quinary modified alloys, a wider variance may be achieved for those additions which permit precipitation reactions in both lamellar phases, γ and δ. The optimum heat treatment cycle for any modified γ/γ'-δ alloy will depend upon the property requiring optimization.

3.4.2 Ternary γ/γ'-δ

During the course of microstructural examination of γ/γ'-δ alloys containing quinary additions a lenticular precipitate was frequently observed within the δ-Ni_3Cb lamellae which is not seen in un-heat treated bars. The controlled precipitation of such a phase during heat treatment was thought to provide a path for alloy property improvement depending on the character of the precipitate and its orientation. No direct identification had previously been made (Refs. 37,40) of this type of precipitate in studies of the γ'-δ system, for example, and the possibility exists that it may be gamma, gamma prime, or a new intermetallic phase depending on γ/γ'-δ composition. The reported solubility of aluminum in δ-Ni_3Cb is only 0.16 a/o at 1000°C (Ref. 14).

Copious amounts of this precipitate were found after 30 hrs at 1000°C during heat treatment studies of the less complex ternary monovariant eutectic (Ni-21.5 w/o Cb-2.8 w/o Al). This microstructural condition, achieved through furnace cool, provided precipitates large enough for direct identification by transmission electron metallography. From analysis of selected area diffraction patterns from thin foils, like that of γ/γ'-δ shown in Fig. 35, the precipitate within δ-Ni_3Cb was positively identified as γ' from the presence of ordered superlattice diffraction spots. These elongated lenticular precipitates were found to be oriented parallel to the lamellae interface and to the (001) plane of δ-Ni_3Cb. Occasionally lenticular precipitates were observed normal to the lamellar interface. Although not positively identified by diffraction patterns because of their size, they too are believed to be γ', on the basis of identical contrast changes which occur with the massive γ' within adjacent γ/γ' lamellae when the specimen is tilted.

Table VIII

Tensile Properties of γ/γ'-δ (Ni-19.7 w/o Cb-6.0 w/o Cr-2.5 w/o Al)
After Heat Treatments A and B

Specimen No.	Temp °F	Temp °C	~.2% Y.S. 10^7 N/m^2	~.2% Y.S. ksi	UTS 10^7 N/m^2	UTS ksi	E 10^{10} N/m^2	E msi	Elong. %	R.A. %	$\dot{\epsilon}$ min^{-1}
HEAT TREATMENT A:											
Solutionized at 1200°C (4 hrs) and aged at 872°C (40 hrs)											
A74-728-04	68	20	135.9	197.0	138.3	200.5	236.0	34.2	2.6	2.9	.01
A74-728-03	1472	800	109.0	158.0	109.7	159.0	154.6	22.4	9.3	14.2	.05
A74-728-01	2012	1100	50.5	73.2	51.9	75.2	82.1	11.9	18.6	31.2	.05
HEAT TREATMENT B:											
Solutionized at 1200°C (4 hrs) and aged at 1079°C (40 hrs)											
A74-717-04	68	20	112.9	163.6	118.3	171.5	229.8	33.3	3.1	4.6	.01
A74-717-03	1472	800	90.1	130.6	93.4	135.4	139.4	20.2	13.0	26.6	.05
A74-717-01	2012	1100	46.8	67.8	50.0	72.5	91.1	13.2	16.2	35.0	.05

TEMPERATURE DEPENDENCE OF ULTIMATE STRENGTH, ELONGATION AND REDUCTION OF AREA FOR 3 CM/HR D.S. EUTECTIC SUPERALLOY Ni–19.7 w/o Cb–6.0 w/o Cr–2.5 w/o Al AFTER HEAT TREATMENTS OF:

△ ◇ SOLUTIONIZED @ 1200°C (4 hrs) AND AGED @ 872°C (40 hrs), HEAT TREATMENT A

□ ○ SOLUTIONIZED @ 1200°C (4 hrs) AND AGED @ 1079°C (40 hrs), HEAT TREATMENT B

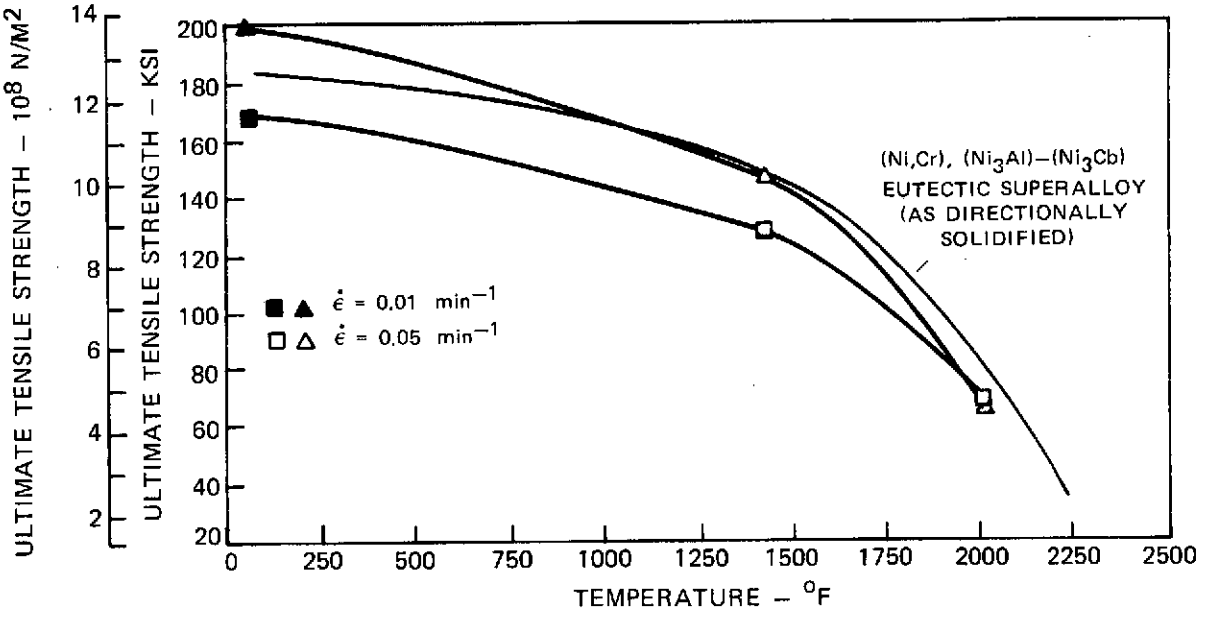

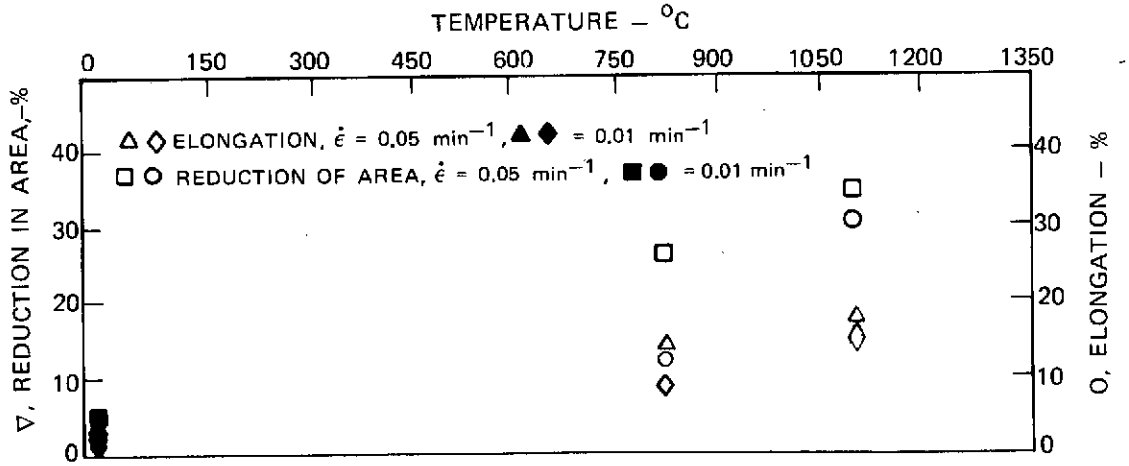

N03–294–1

TEMPERATURE DEPENDENCE OF ULTIMATE STRENGTH, ELONGATION AND REDUCTION OF AREA FOR 3 CM/HR D.S. EUTECTIC SUPERALLOY, Ni–19.7w/o Cb–6.0 w/o Cr–2.5 w/o Al

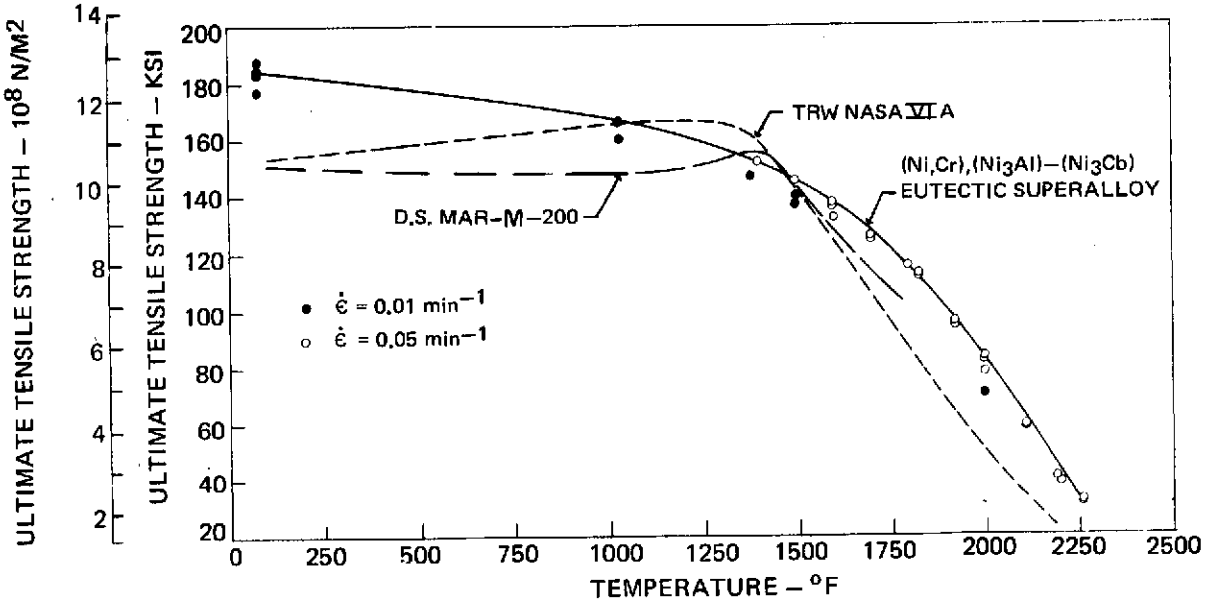

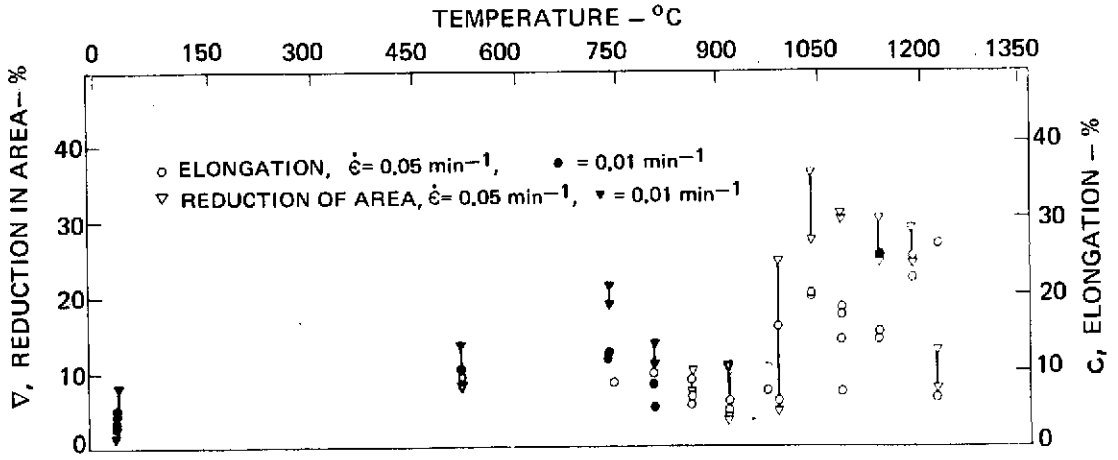

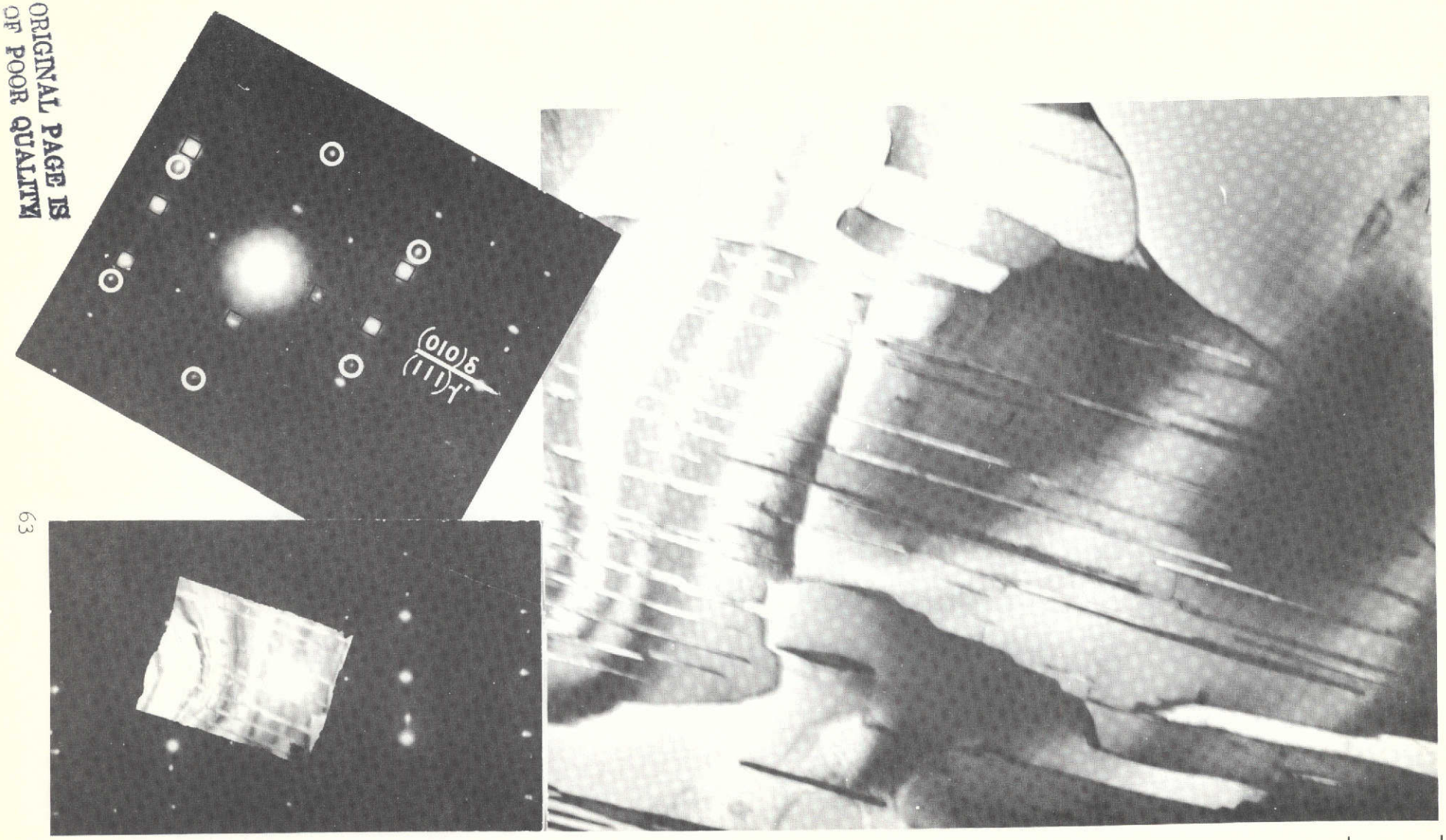

SUPERIMPOSED SELECTED AREA AND ELECTRON DIFFRACTION PATTERN

ELECTRON MICROGRAPH AND ASSOCIATED DIFFRACTION PATTERN IDENTIFYING PRECIPITATE PHASE IN δ–Ni_3Cb OF $\gamma/\gamma'-\delta$ (Ni–21.5 w/o Cb–2.8 w/o Al) AS γ'

FIG. 35

3.5 Mechanical Properties of Base Line γ/γ'-δ and Modifications

3.5.1 Background

One alloy (Ni-19.7 w/o Cb-6.0 w/o Cr-2.5 w/o Al) from the γ-δ 'lamellar eutectic family' was found to be superior to all advanced nickel-base superalloys in tension and creep under the previous contract NAS3-15562 (Ref. 1). Although the longitudinal mechanical properties of this alloy are outstanding, further improvements in creep, shear, and transverse strength are deemed necessary prior to its application as advanced air cooled turbine blading. The object of this program was to improve these mechanical properties while maintaining an acceptable balance between the existing rupture strength, ductility, oxidation resistance, and phase stability. One alloy modification was to be chosen for more detailed mechanical property characterization from screening tests on five candidate alloys identified below:

1) Ni-19.7 w/o Cb-6.0 w/o Cr-2.5 w/o Al-1.0 w/o W
2) Ni-19.7 w/o Cb-6.0 w/o Cr-2.5 w/o Al-1.0 w/o Mo
3) Ni-18.6 w/o Cb-6.0 w/o Cr-2.5 w/o Al-0.87 w/o Ti
4) Ni-20.2 w/o Cb-6.0 w/o Cr-2.5 w/o Al-2.0 w/o Co
5) Ni-17.9 w/o Cb-6.0 w/o Cr-2.5 w/o Al-3.0 w/o Ta

3.5.2 Tension Testing

Tensile tests were conducted on the five candidate γ/γ'-δ alloy modifications in accordance with ASTM specification E21-69 from room temperature to 1100°C (2012°F). The results are presented in Table IX and graphically shown in Fig. 36.

The room temperature strength, elongation, and reduction in area values of all the quinary modified alloys compare very closely with the base line quaternary γ/γ'-δ results, Fig. 34 (Ref. 1). Microstructural examination of the fracture surface, as revealed by longitudinal sectioning, indicated that extensive twinning and microcleavage of the δ-Ni_3Cb phase occurred throughout the gage section but that it was more concentrated at the fracture surface. A single surface trace analysis (Ref. 41) was performed on the cobalt modified γ/γ'-δ alloy normal to the deformation axis to determine if the geometry of the observed twin planes and microcracks were consistent with that reported previously for the base line γ/γ'-δ alloy (Ref. 1). Assuming the preferred growth direction remains unchanged at $[1\bar{1}0]_\gamma \,||\, [100]_\delta$, twin traces corresponding to the intersection of $(2\bar{1}1)$ and (211) planes are again observed, confirming that previously reported (Ref. 42).

Table IX

Tensile Properties of Quinary Modified γ/γ'-δ Specimens Directionally Solidified at 3 cm/hr and Tested in Air

Specimen No.	Composition w/o	Temp. °C	0.2% Y.S. 10^7 N/m^2	0.2% Y.S. ksi	UTS 10^7 N/m^2	UTS ksi	E 10^{10} N/m^2	E msi	Elong. %	R.A. %	$\dot{\varepsilon}$ min^{-1}
A73-634-03	Ni-19.7Cb-6Cr-2.5Al-1W	20	118.2	171.3	122.8	178.0	251.9	36.5	4.1	1.4	.01
A73-634-02	"	800	94.53	137.0	97.3	141.0	148.4	21.5	9.0	9.8	.05
A73-634-01	"	1100	44.9	65.0	46.2	67.0	*	*	16.2	27.6	.05
A73-601-03	Ni-19.7Cb-6Cr-2.5Al-1Mo	20	121.9	176.7	124.2	180.0	254.6	36.9	2.4	1.3	.01
A73-601-02	"	800	-	-	97.1	140.7	*	*	10.3	18.6	.05
A73-601-01	"	1100	48.3	70.0	49.5	71.8	*	*	37.6	29.2	.05
A73-598-03	Ni-18.6Cb-6Cr-2.5Al-.87Ti	20	125.6	182.0	127.1	184.2	242.9	35.2	2.2	2.5	.01
A73-598-02	"	800	98.7	143.0	100.7	146.0	142.1	20.6	11.7	17.5	.05
A73-598-01	"	1100	49.0	71.0	50.8	73.6	*	*	19.9	19.6	.05
A74-091-04	Ni-20.2Cb-6Cr-2.5Al-2Co	20	121.4	176.0	127.4	184.7	229.1	33.2	2.7	2.3	.01
A74-091-03		800	100.1	145.0	103.1	149.4	137.3	19.9	11.3	16.5	.05
A74-091-01		1100	50.4	73.0	51.8	75.0	*	*	20.1	15.1	.05
A74-186-03	Ni-17.9Cb-6Cr-2.5Al-3Ta	20	121.2	175.7	124.2	180.0	254.6	36.9	2.6	-	.01
A74-186-02		800	97.3	141.0	101.4	147.0	190.4	27.6	**	**	.05
A74-186-01		1100	44.9	65.0	46.6	67.5	*	*	27.4	28.1	.05

*Insufficient strain magnification

**Specimen failed outside of gage

TEMPERATURE DEPENDENCE OF ULTIMATE STRENGTH AND ELONGATION OF QUINARY MODIFIED γ/γ' δ SPECIMENS

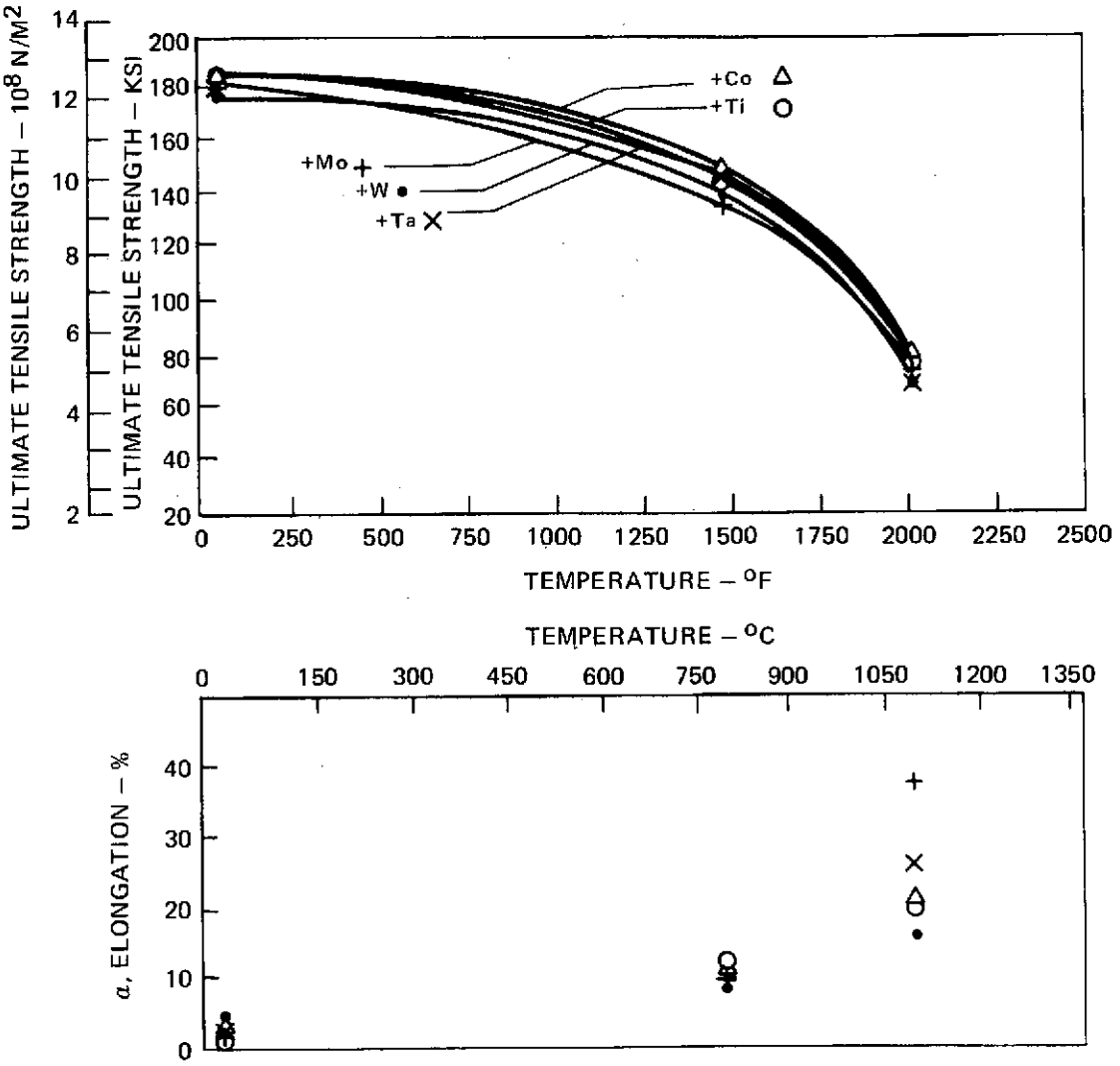

N11–160–1

An anomalously lower (~10%) elastic modulus was measured for the cobalt modified alloy at room temperature. This low value (i.e. 229.1 x 10^{10} N/m^2) was surprising in that this alloy modification indicated the largest volume fraction of δ-Ni_3Cb from lineal analyses (Table III). Cobalt substitution on the nickel atomic sites of δ-Ni_3Cb may lower the binding energy and consequently the elastic modulus. The crystal structure of delta appears unchanged.

At elevated temperature the strength and elongation values of all the quinary modified alloys again compare favorably with the base line quaternary γ/γ'-δ results, Fig. 34 (Ref. 1). In fact all tension results for the modified alloys are so close to those of the base line quaternary eutectic they might be considered as coming from the same statistical population. Because of similarity in tensile behavior, greater emphasis was placed on stress rupture life measurements as the final arbiter on alloy strength.

3.5.3 Shear Tests

Bolt designed shear specimens (Ref. 43), which appeared satisfactory in yielding reproducible shear strength values for eutectic composites, were used to study the effect of alloying on the temperature dependence of the eutectic strength in shear parallel (longitudinal) to the growth direction. The shear strength of the modified alloys compared with the base line γ/γ'-δ quaternary are presented in Table X and graphically displayed in Fig. 37. In general, there was an initial increase in longitudinal shear strength with an increase in temperature. This increase was partly due to the increase in the flow stress of the γ/γ' phases with temperature. This behavior was also observed in a $Ni_3(Al,Cb)$ single phase alloy (Ref. 44). Each longitudinal shear strength value was determined using the diameter of the bolt shank in calculating the shear area. This approximation was employed since the actual sheared area was not perfectly cylindrical, especially at low temperatures, which reflects the effect of different orientations of the various lamellar grains sheared. Of the alloy modifications tested, both tantalum and tungsten show improvement over the base line quaternary γ/γ'-δ alloy. Additions of cobalt and titanium appear to lower the room temperature shear strength appreciably.

Metallographic examinations, Figs. 38-43, indicated that at all three temperatures studied the principal deformation mechanism was one of intergranular sliding. However, evidence was obtained that irregular cleavage of the δ-Ni_3Cb phase and interlamellar decohesion contributed to shear strength values which are approximately 50% of those measured on typical cast superalloys (Ref. 2).

Table X

Longitudinal Shear Strength* of Various
γ/γ'-δ Alloy Modifications

Specimen No.	Composition (w/o)	Temp. (°C)	Temp. (°F)	Effective Shear Strength (MN/m^2)	Effective Shear Strength (10^3 psi)	Failure Mode
A72-287-02	Ni-19.7Cb-6Cr-2.5Al	20	68	311.9	45.2	Tensile
A72-344-02	"	20	68	291.2	42.2	Tensile
A72-274-02	"	815	1500	302.9	43.9	Shear
A72-279-02	"	815	1500	280.1	40.6	Shear
A74-097-01	Ni-19.7Cb-6Cr-2.5Al-1W	20	68	309.0	44.8	Tension
A73-491-04	"	400	752	306.9	44.5	Tension
A74-097-03	"	800	1472	327.5	47.5	Shear
A74-097-04	"	1100	2012	87.6	12.7	Shear
A74-197-01	Ni-19.7Cb-6Cr-2.5Al-1Mo	20	68	252.4	36.6	50-50
A74-095-01	"	800	1472	304.1	44.1	50-50
A74-095-02	"	1100	2012	89.1	12.9	Shear
A74-187-04	Ni-17.9Cb-6Cr-2.5Al-3Ta	20	68	324.7	47.1	50-50
A74-187-03	"	800	1472	348.2	50.5	Shear
A74-187-02	"	1100	2012	83.4	12.1	Shear
A74-101-04	Ni-18.6Cb-6Cr-2.5Al-.87Ti	20	68	199.9	29.0	Shear
A74-103-02	"	800	1472	339.2	49.2	Shear
A74-103-03	"	1100	2012	94.8	13.7	Shear
A74-237-01	Ni-20.1Cb-6Cr-2.5Al-2.0Co	20	68	228.9	33.2	Shear
A74-237-02	"	800	1472	297.2	43.1	Shear
A74-263	"	1100	2012	86.9	12.6	Shear

*Loading rate = 0.025 cm/hr (0.01 in./min)
Shearing span = 0.025 cm (0.010 in.)
Diam of bolt = 0.635 cm (0.250 in.)
Specimen head height ≈ 0.32 cm (~0.125 in.)

TEMPERATURE DEPENDENCE OF LONGITUDINAL SHEAR STRENGTH OF VARIOUS δ REINFORCED ALLOYS

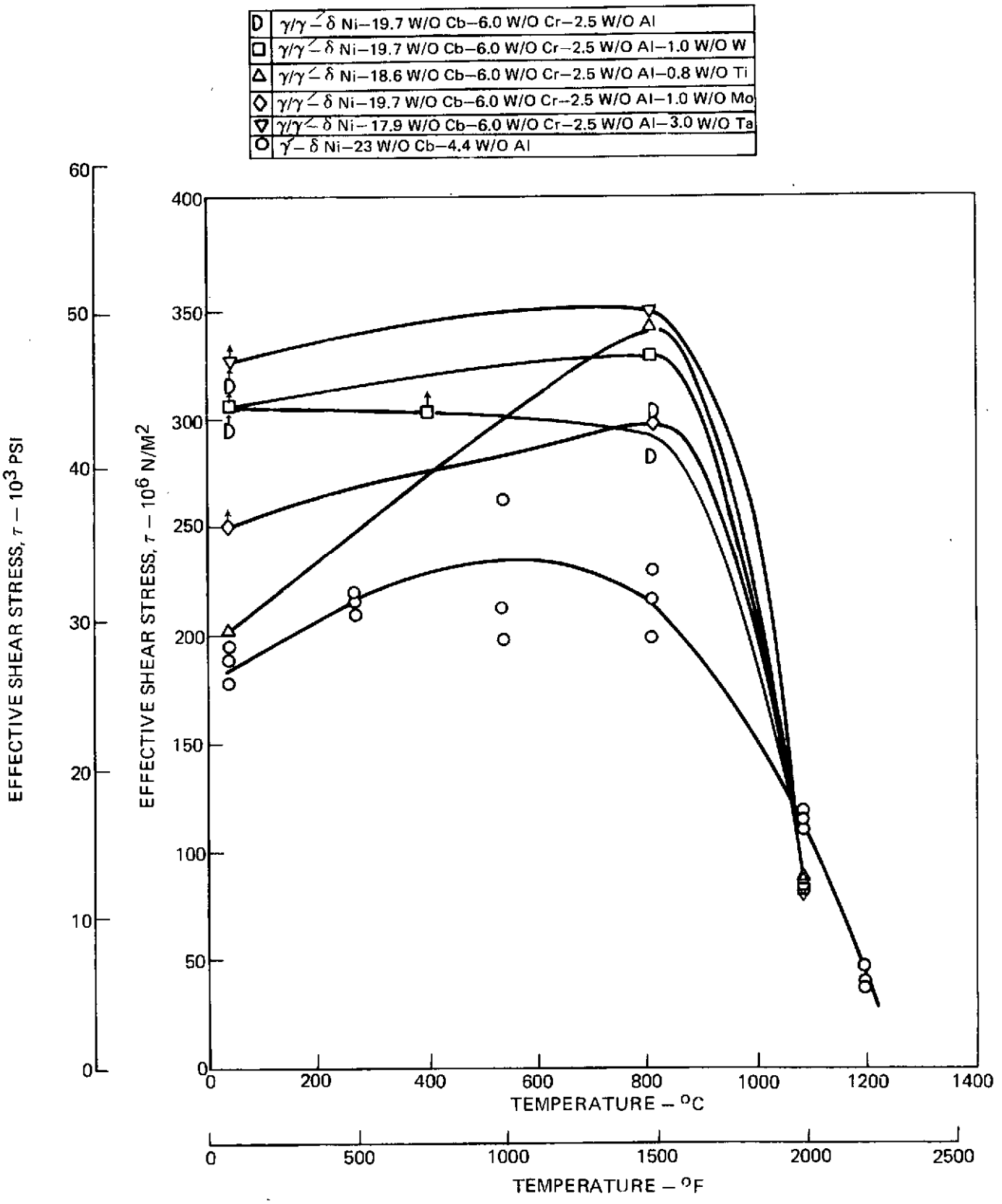

N03–57–1

TRANSVERSE SECTIONS THROUGH FRACTURE OF SHEAR SPECIMEN

(Ni–20.0 w/o Cb–6.0 w/o Cr–2.5 w/o Al)

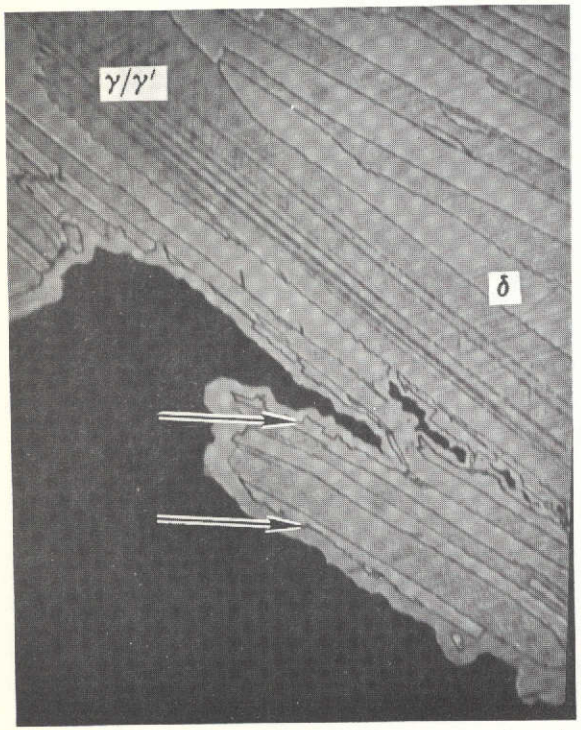

a) ROOM TEMPERATURE

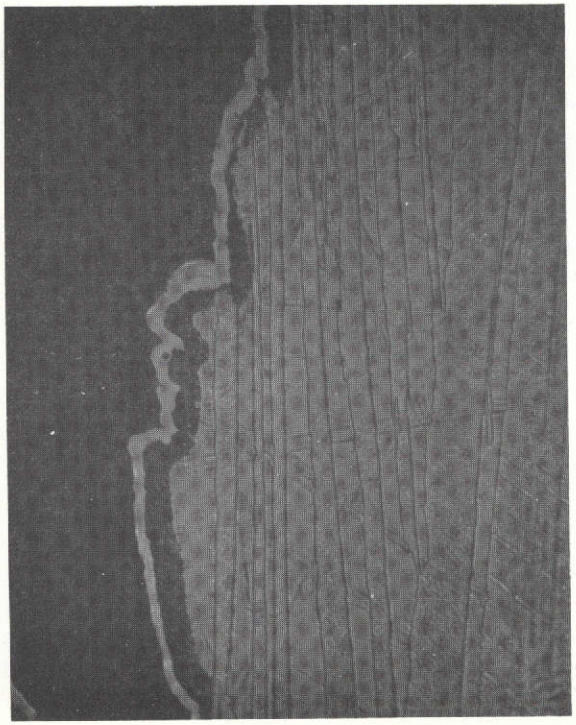

b) 800°C

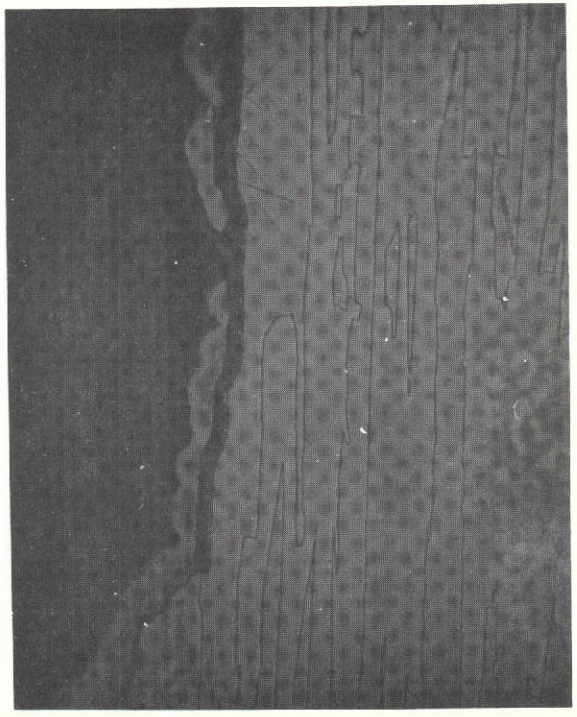

c) 1100°C

FIG. 38

TRANSVERSE SECTIONS THROUGH FRACTURE OF SHEAR SPECIMENS

(Ni–19.7 w/o Cb–6.0 w/o Cr–2.5 w/o Al–1.0 w/o W)

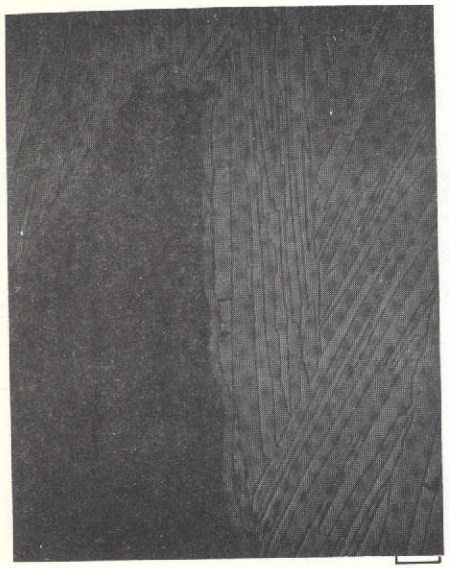

a) ROOM TEMPERATURE

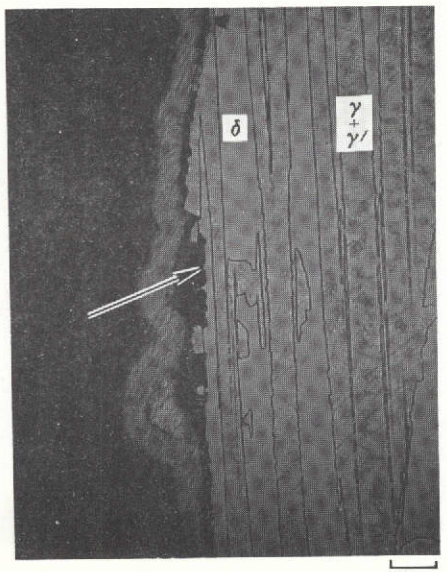

b) 400°C

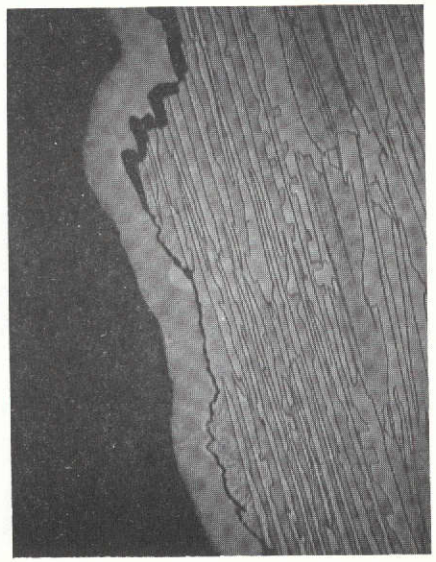

c) 800°C

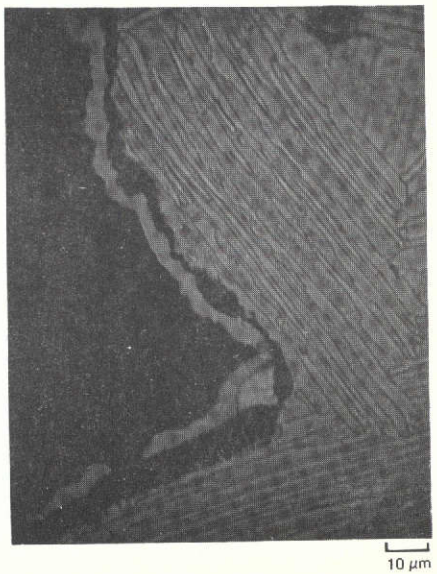

d) 1100°C

FIG. 39

TRANSVERSE SECTIONS THROUGH FRACTURE OF SHEAR SPECIMEN

(Ni–19.7 w/o Cb–6.0 w/o Cr–2.5 w/o Al–1.0 w/o Mo)

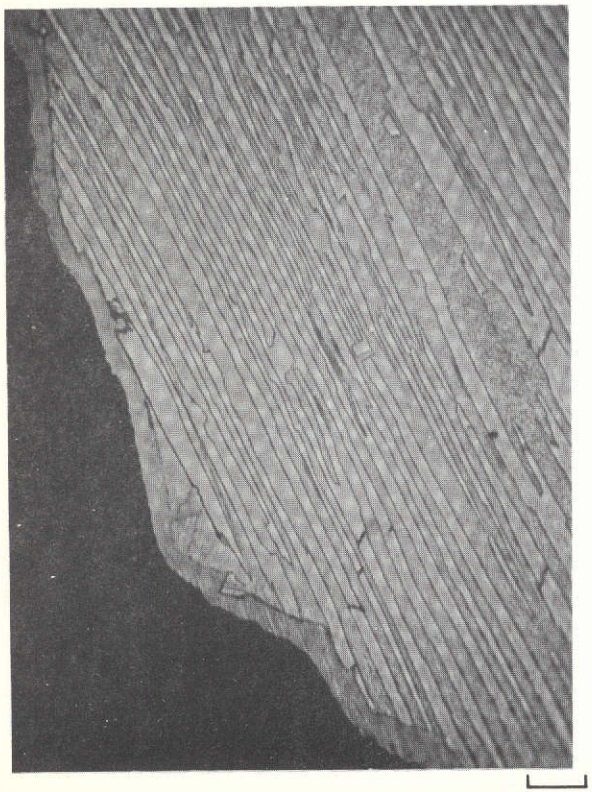

10 μm

a) ROOM TEMPERATURE

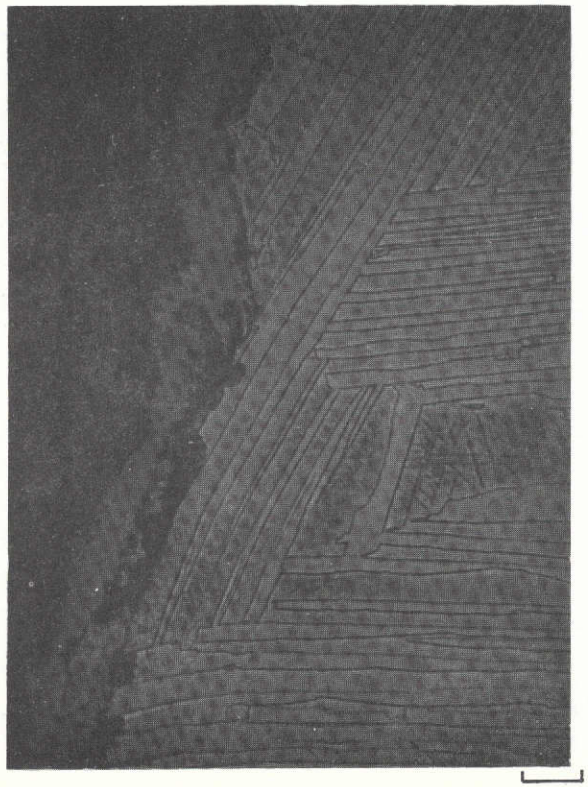

10 μm

b) 800°C

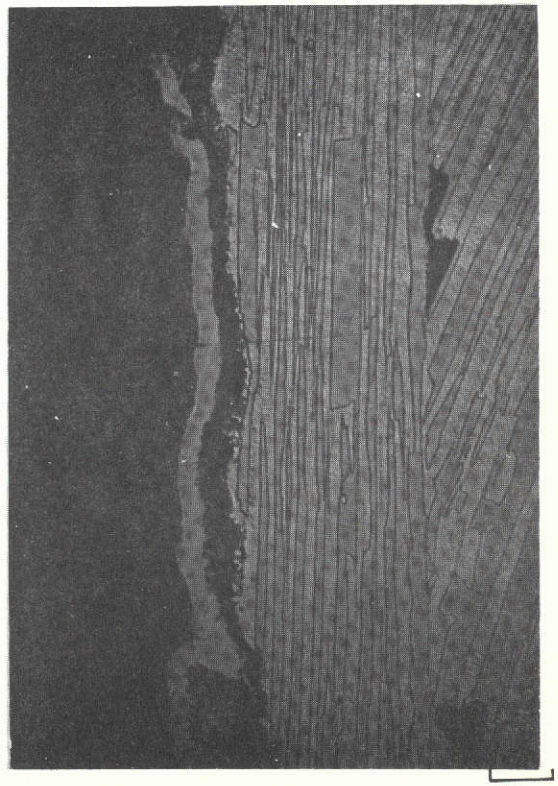

10 μm

c) 1100°C

FIG. 40

TRANSVERSE SECTIONS THROUGH FRACTURE OF SHEAR SPECIMENS

(Ni–17.9 Cb–6.0 Cr–2.5 Al–3.0 Ta)

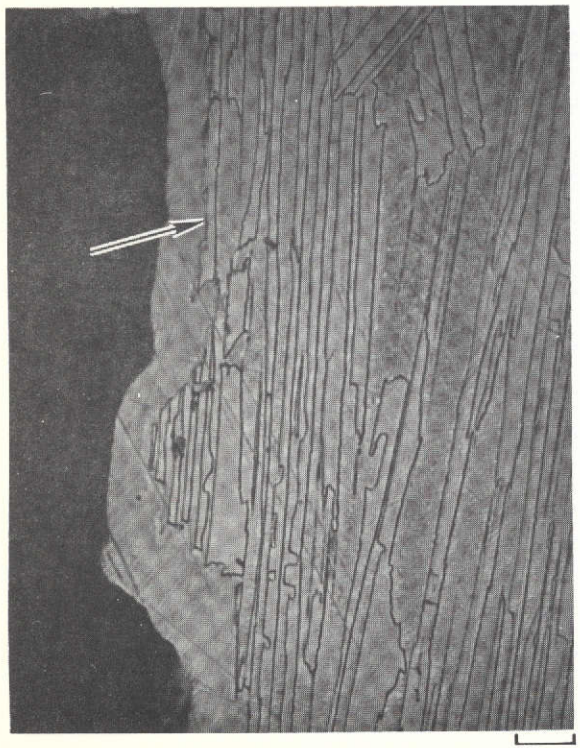

a) ROOM TEMPERATURE

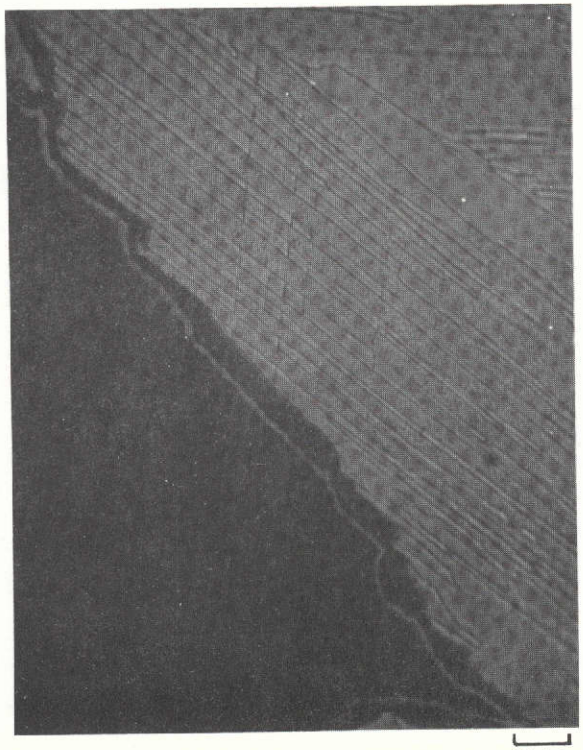

b) 800°C

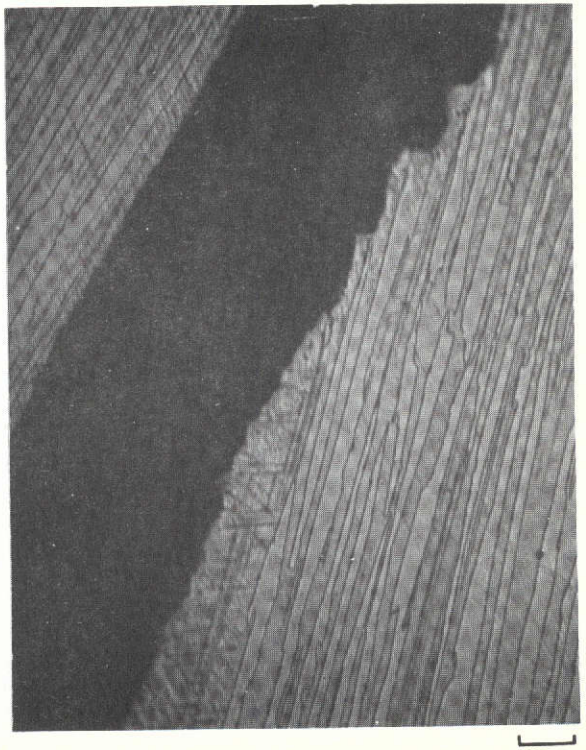

c) 1100°C

FIG. 41

TRANSVERSE SECTIONS THROUGH FRACTURE OF SHEAR SPECIMENS

(Ni–18.6w/o Cb–6.0 w/o Cr–2.5 w/o Al–0.87 w/o Ti)

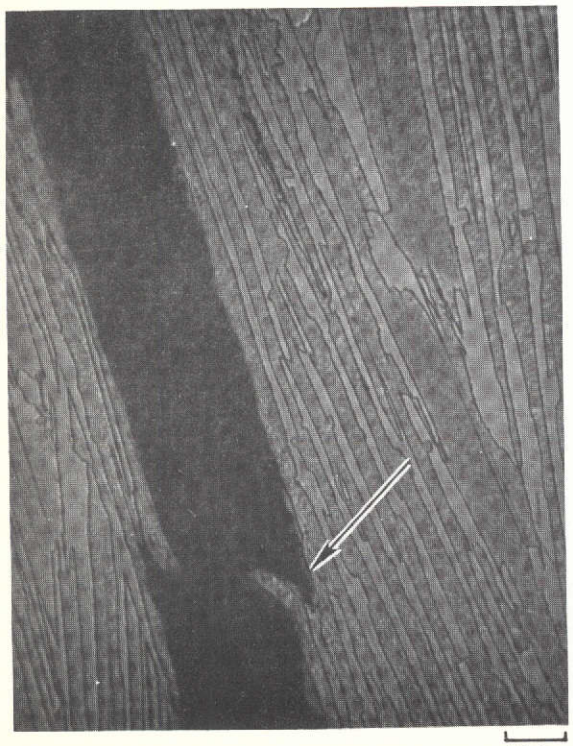

a) ROOM TEMPERATURE

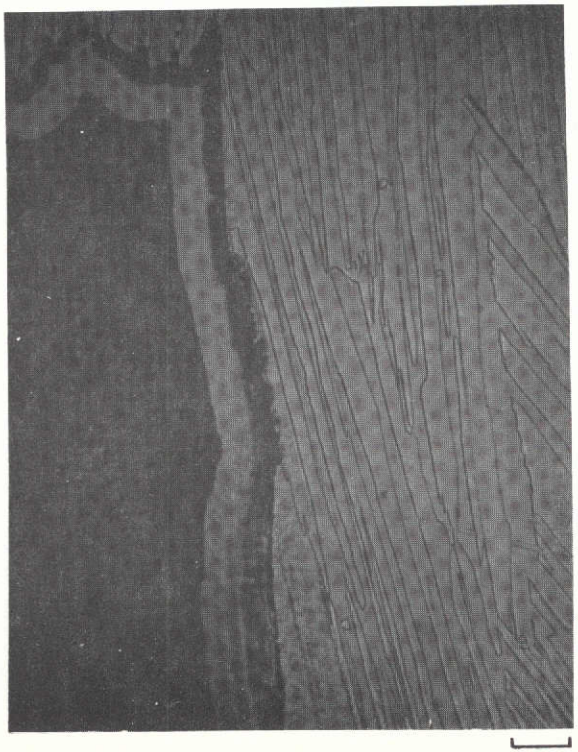

b) 800°C

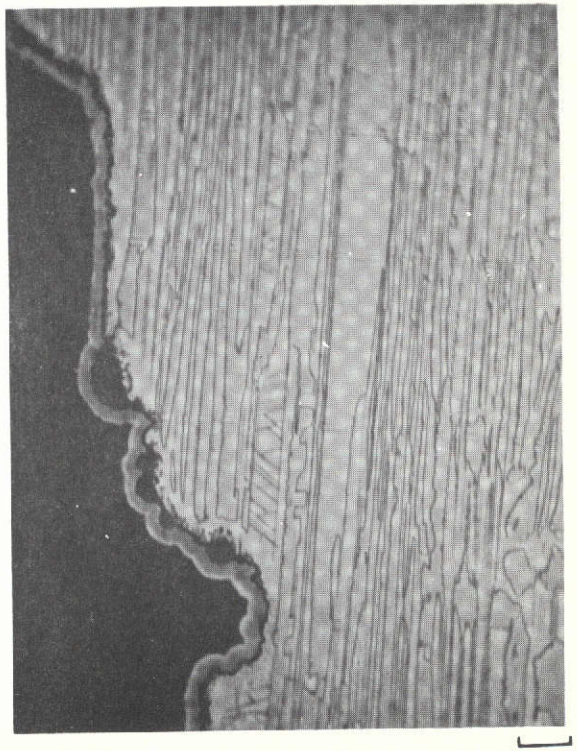

c) 1100°C

FIG. 42

TRANSVERSE SECTIONS THROUGH FRACTURE OF SHEAR SPECIMENS

(Ni–20.1 w/o Cb–6.0 w/o Cr–2.5 w/o Al–2.0 w/o Co)

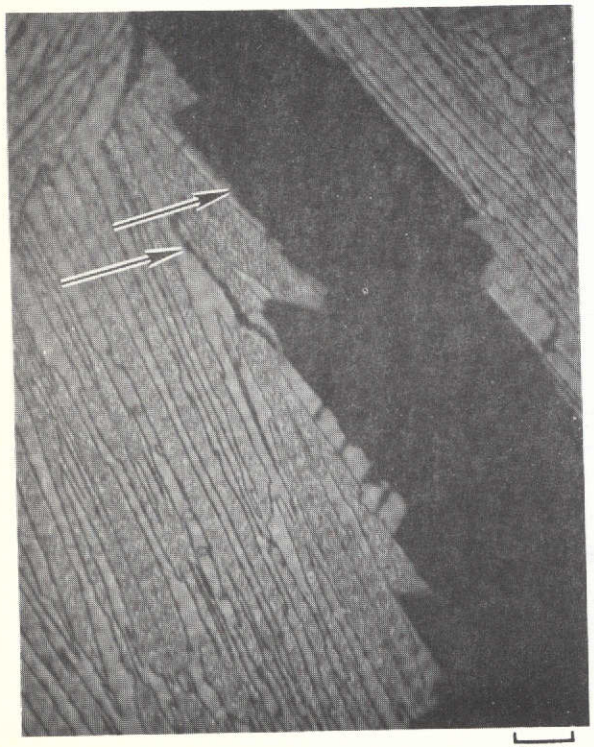

a) ROOM TEMPERATURE

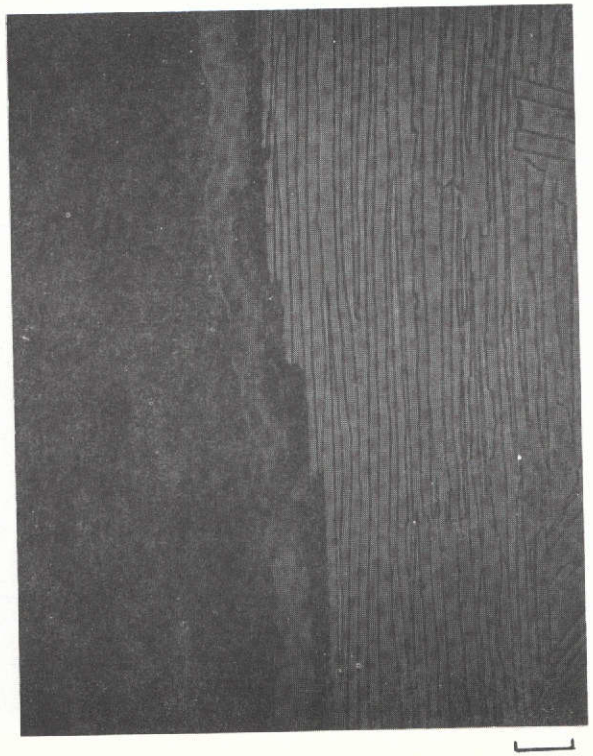

b) 800°C

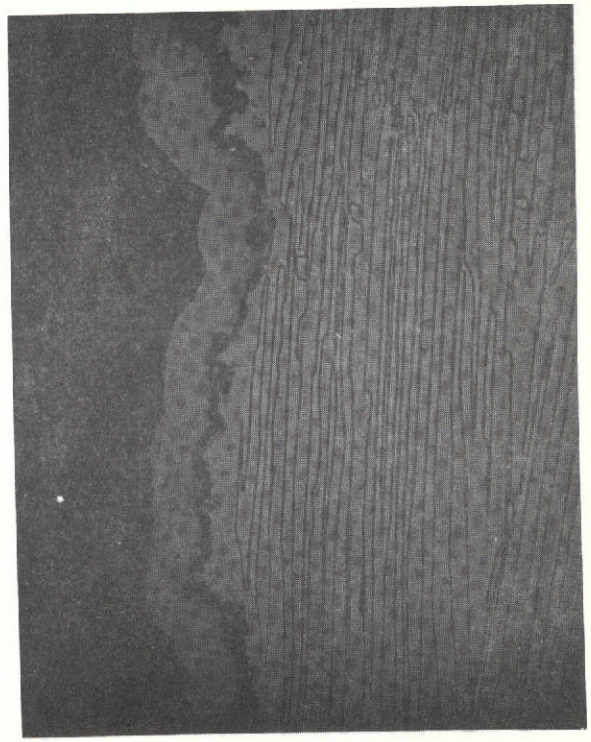

c) 1100°C

FIG. 43

Irregular δ cleavage is captured by the nickel electroplate layer in Figs. 38a, 39b, 41a, 42a and 43a and interlamellar decohesion in Figs. 39a, 40a, and 43a.

Only the tantalum and tungsten γ/γ'-δ modifications met the goal of the program which was to achieve a longitudinal shear yield strength in excess of 40% of the longitudinal yield strength (0.2% offset) at 800°C (1472°F). All the alloy modifications fell short of this goal at 1100°C (2012°F).

3.5.4 Stress Rupture

Stress rupture tests were performed at various temperatures in air at United Aircraft Research Laboratories and creep-rupture testing was performed principally in vacuum at the Materials Engineering and Research Laboratories of Pratt and Whitney Aircraft. These tests were performed in accordance with ASTM E139-69, as applicable. Elongation and reduction of area were measured on the fracture halves. The results of these tests are presented in Table XI.

3.5.4.1 Quaternary Modifications

Increasing the chromium content alone to 8 and 9 percent by weight (specimens A73-604 and A74-168, Table XI) led to shorter rupture lives compared to the base line alloy, A73-097-03. However, increasing the aluminum content only (and thereby the volume percent γ') to 2.8 w/o, resulted in longer times to rupture. Finally increases in both the aluminum and chromium content to promote more α-Al_2O_3 in the oxide scale led to the shortest rupture lives. Decreasing the chromium content however resulted in longer rupture lives but of course at the sacrifice of oxidation resistance. The solidification velocity was held constant at 3 cm/hr to attempt to eliminate interlamellar spacing effects on rupture life.

3.5.4.2 Velocity Effects

Stress rupture tests on γ/γ'-δ (Ni-20.0 w/o Cb-6.0 w/o Cr-2.5 w/o Al) directionally solidified at five and seven centimeters per hour under an estimated thermal gradient in the liquid of 300°C/cm were performed to reinvestigate the effect of solidification velocity (Ref. 45). Times to rupture of 77.3 hrs (A73-097-03), 42.7 hrs (A73-772-01) and 27.7 hrs (A73-778-02) for respectively 3, 5, and 7 cm/hr specimens creep tested at 1093°C (2000°F) and 138 MN/m^2 (20 ksi) indicate a gradual decrease in rupture life with increasing freezing velocity (decreasing interlamellar spacing λ). As these specimens also exhibited near plane front growth modes, as determined from longitudinal

Table XI

Stress Rupture Properties of Various γ/γ'-δ Alloys

D.S. Bar Identification No.	Composition (w/o)		Stress (ksi)	Stress (MN/m^2)	Temp (°C)	Rupture Life (hrs)	Elong. (%)	Area Reduction (%)	Environment
Quaternary Modifications									
A73-611-03	Ni-20.3Cb-4.0Cr-2.8Al		20	138	1100	48.2	11.9	20.7	air
A73-611-02	Ni-20.3Cb-4.0Cr-2.8Al		20	138	1100	46.1	6.7	13.9	vacuum
A73-603-03	Ni-19.8Cb-6.0Cr-2.8Al		20	138	1100	24.2	6.1	19.1	air
A73-603-02	Ni-19.8Cb-6.0Cr-2.8Al		20	138	1100	18.0	10.6	12.9	vacuum
A74-295-02	Ni-20.0Cb-6.0Cr-2.5Al		20	138	1100	16.8	18.0	51.0	air
A72-1014	Ni-19.8Cb-6.5Cr-2.5Al		20	138	1093	32.9	6.6	-	air
A73-604-02	Ni-20.0Cb-8.0Cr-2.5Al		20	138	1100	13.2	10.9	23.8	air
A74-168-02	Ni-20.0Cb-9.0Cr-2.8Al		20	138	1100	9.4	8.9	14.9	air
A74-168-01	Ni-20.0Cb-9.0Cr-2.8Al		20	138	1100	4.2	8.0	10.1	vacuum
Velocity Effects		-R-							
A73-772-03	Ni-20.0Cb-6.0Cr-2.5Al	(5 cm/hr)	125	864	760	300 disc	1.0 disc	-	vacuum
A73-772-02	Ni-20.0Cb-6.0Cr-2.5Al	(5 cm/hr)	40	276	982	76.0	5.7	-	vacuum
A73-772-01	Ni-20.0Cb-6.0Cr-2.5Al	(5 cm/hr)	20	138	1093	42.7	6.8	-	vacuum
A73-778-03	Ni-20.0Cb-6.0Cr-2.5Al	(7 cm/hr)	40	276	982	61.4	12.7	-	vacuum
A73-778-02	Ni-20.0Cb-6.0Cr-2.5Al	(7 cm/hr)	20	138	1093	27.7	9.3	-	vacuum
A74-269-02	Ni-20.0Cb-6.0Cr-2.5Al	(10 cm/hr)	20	138	1100	28.3	9.1	16.1	air
Quinary Modifications									
A73-491-02	Ni-19.7Cb-6.0Cr-2.5Al-1.0W		20	138	1100	20.6	7.6	14.1	air
A74-176-03	Ni-19.7Cb-6.0Cr-2.5Al-1.0W		20	138	1100	30.7	7.6	23.8	air
A73-330-02	Ni-19.7Cb-6.0Cr-2.5Al-1.0Mo		20	138	1100	18.9	9.2	15.8	air
A73-076B-01	Ni-19.7Cb-6.0Cr-2.5Al-1.0Mo		20	138	1093	11.7	14.4	-	air
A73-076B-02	Ni-19.7Cb-6.0Cr-2.5Al-1.0Mo		35	242	1000	34.9	11.9	-	air
A73-114-01	Ni-19.7Cb-6.0Cr-2.5Al-1.0Mo		20	138	1093	37.2	9.6	-	vacuum
A73-114-02	Ni-19.7Cb-6.0Cr-2.5Al-1.0Mo		110	759	815	26.4	2.3	-	vacuum

Table XI (Cont'd)

D.S. Bar Identification No.	Composition (w/o)	Stress (ksi)	Stress (MN/m^2)	Temp (°C)	Rupture Life (hrs)	Elong. (%)	Area Reduction (%)	Environment
A74-101-01	Ni-18.6Cb-6.0Cr-2.5Al-0.87Ti	20	138	1100	36.0	5.9	17.4	air
A74-142-01	Ni-18.6Cb-6.0Cr-2.5Al-0.8Ti	20	138	1093	36.1	8.3	-	vacuum
A74-142-02	Ni-18.6Cb-6.0Cr-2.5Al-0.8Ti	110	759	815	107.7	4.3	-	vacuum
A74-281-02	Ni-20.1Cb-6.0Cr-2.5Al-1.0Co	20	138	1100	26.1	8.8	29.5	air
A74-260-01	Ni-20.1Cb-6.0Cr-2.5Al-2.0Co	20	138	1100	20.6	4.4	22.1	air
A74-075-01	Ni-20.3Cb-6.0Cr-2.5Al-3.0Co	20	138	1100	10.4	5.4	17.4	air
A74-301-02	Ni-19.5Cb-6.0Cr-2.5Al-1.0Ta	20	138	1100	51.3	18.0	36.8	air
A74-177-01	Ni-17.9Cb-6.0Cr-2.5Al-3.0Ta	20	138	1100	71.5	14.8	>20	air
A72-1011	Ni-19.8Cb-6.0Cr-2.5Al-0.005B	20	138	1093	38.7	9.2	-	air
Post Thermal Cycling								
A73-682-03[1]	Ni-19.7Cb-6.0Cr-2.5Al	20	138	1093	71.4	9.2	-	vacuum
A73-097-03[2]	Ni-19.7Cb-6.0Cr-2.5Al	20	138	1093	77.3	6.8	-	vacuum
A73-097-03[1]	Ni-19.7Cb-6.0Cr-2.5Al	20	138	1093	83.2	4.8	-	vacuum
A73-735-02[2]	Ni-19.7Cb-6.0Cr-2.5Al	110	759	815	119.9	10.1	-	vacuum
A73-734-01[2]	Ni-19.7Cb-6.0Cr-2.5Al	110	759	815	22.9	10.1	-	vacuum
A73-097-04[1]	Ni-19.7Cb-6.0Cr-2.5Al	110	759	815	62.1	1.6*	-	vacuum
A73-326[1]	Ni-18.6Cb-6.0Cr-2.5Al-0.87Ti	20	138	1100	13.0	5.8	-	vacuum
A73-324[1]	Ni-19.7Cb-6.0Cr-2.5Al-1.0Mo	20	138	1100	**	2.4	-	vacuum
A73-468[1]	Ni-19.7Cb-6.0Cr-2.5Al-1.0Re	20	138	1100	***	-	-	vacuum

[1]Post 3000 cycles: 1121°C (2050°F) max/399°C (750°F) min
[2]After Ref. 1

*failure at extensometer ridge
**broke on loading
***malfunction of equipment producing temperature overheat which resulted in local melting

sections, this creep behavior was unexpected in view of the previous experiments concerning the effect of decreasing λ on the rupture life of aligned γ'-δ specimens (Ref. 46). However, these results confirm the marked decrease in rupture life accompanying small departure from plane front growth conditions at rates up to 50 cm/hr (Ref. 45), and are now believed to be associated with solid/liquid interface shape changes due to velocity increases.

3.5.4.3 Quinary Modifications

Additions of W, Mo, Ti and B to the base line γ/γ'-δ quaternary alloy had unexpectedly little effect on the longitudinal rupture lives measured at various temperatures and stresses as indicated in Table XI. Rupture ductilities were also relatively unaffected. Cobalt additions to γ/γ'-δ were particularly disappointing in view of the fact that this addition increased the volume fraction of δ-Ni_3Cb as indicated in Table III. However, as was previously suggested cobalt may have a deleterious effect on the intrinsic strength of Ni_3Cb when it substitutes for nickel atoms in the orthorhombic lattice, as inferred from the elastic modulus decrease of over 10%.

Tantalum, substituted for columbium on an atom for atom basis, alone appeared to be beneficial to rupture life at 1100°C. Specimen A74-177-01 (Ni-17.9 w/o Cb-6.0 w/o Cr-2.5 w/o Al-3.0 w/o Ta), identified in Table XI, had the longest rupture life of all the alloys screened at 1100°C and 138 MN/m^2. Greater additions of Ta may result in further improvements in rupture life but it must be related to the increase it brings to density to give a true picture of its worth.

One noteworthy observation can further be derived from comparing the air and vacuum tests at 1100°C of three different γ/γ'-δ alloys listed in Table XI (Ni-20.3Cb-4.0Cr-2.8Al, Ni-19.8Cb-6.0Cr-2.8Al and Ni-20.0Cb-9.0Cr-2.5Al) which were tested under similar conditions of stress and temperature but in vacuum and air environments. Their small differences in rupture lives, i.e. 46.1 vs 48.2, 18.0 vs 24.2 and 4.2 vs 9.4, indicate not only good correlation between two laboratories performing the tests, but, more importantly, little atmospheric environmental effects on rupture life.

3.5.5 Thermal Cyclic Testing

The effect of three thousand (3000) thermal cycles on the physico-chemical stability of the aligned microstructure of γ/γ'-δ, Ni-19.7 w/o Cb-6.0 w/o Cr-2.5 w/o Al, is shown in Fig. 44. The interfaces of the δ-Ni_3Cb lamellae displayed no signs of coarsening or decohesion resulting from thermally induced stresses. However, both the size and distribution of the γ' precipitates within

THE EFFECT OF 3000 THERMAL CYCLES (2min) ON THE PHYSICO-CHEMICAL STABILITY OF $\gamma/\gamma'-\delta$

(Ni-19.7 w/o Cb-6.0 w/o Cr-2.5 w/o Al)

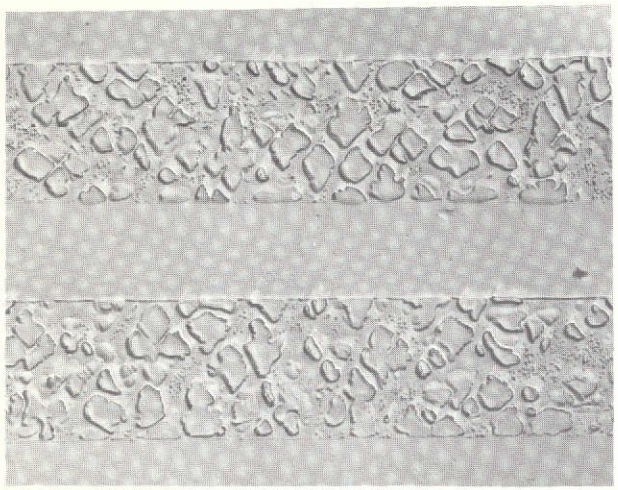

a) AS DIRECTIONALLY SOLIDIFIED:
R = 3 cm/hr, G_L = 300°C/cm

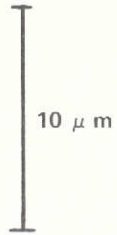

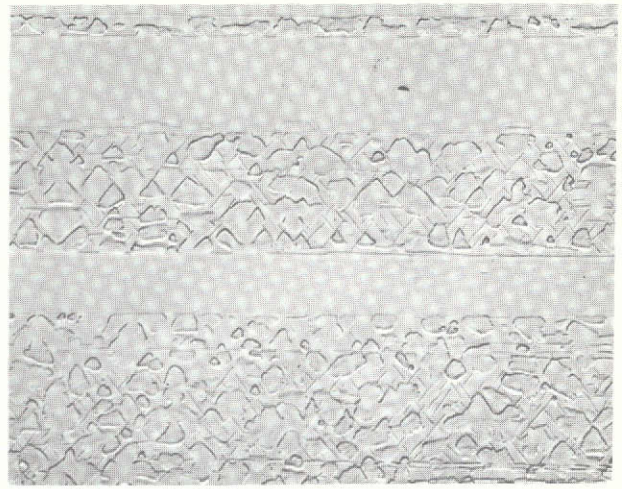

b) 716° C max/254° C min
(1320° F) (490° F)

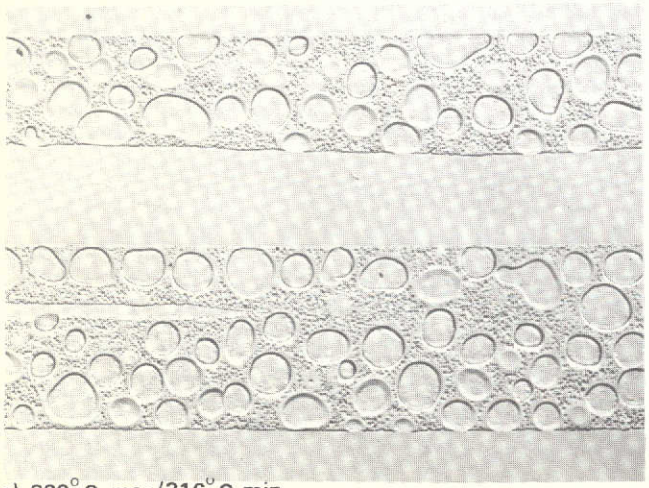

c) 899° C max/316° C min
(1650° F) (600° F)

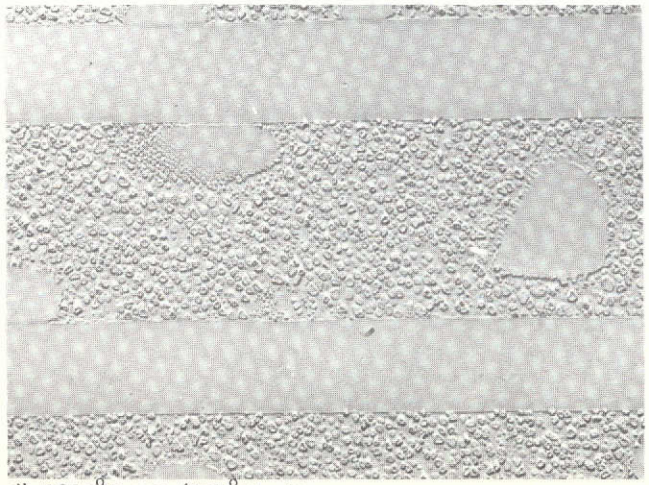

d) 1016° C max/360° C min
(1860° F) (680° F)

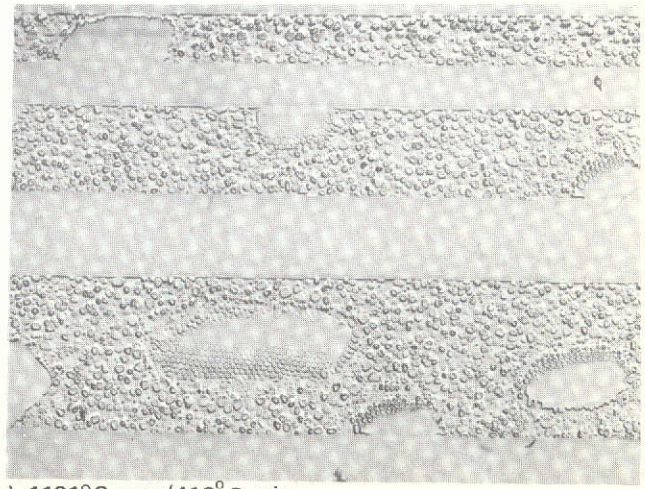

e) 1121°C max/416° C min
(2050° F) (780° F)

FIG. 44

the gamma phase were observed to undergo marked changes from cyclic heat treatment. Quantitative analyses of the microstructures at various positions along the bar were performed on electron photomicrographs of replicas. Each replicated position received a different thermal history due to the parabolic axial gradient along the test bar. The results of the analyses of size and distribution of γ' between various temperatures are presented in Fig. 45. The 'as directionally solidified' γ' size distribution was also analyzed and is presented in Fig. 46 for comparison purposes. For this γ/γ'-δ composition the cast γ' distribution was found to be bimodal. Cyclic heat treatment to the maximum temperature 1121°C (2050°F) resulted in some solutioning and reprecipitation of finer γ' as evidenced around the larger γ' island areas in Fig. 44c. However, it is difficult to distinguish between the 'cooling' γ' and the agglomerating γ'. A bimodal distribution of principally spherical γ' was observed to exist at each temperature interval except the lowest, i.e. 716°C (1320°F) max/254°C (490°F) min. At this lower temperature interval, fine Widmanstätten δ-Ni_3Cb precipitate was observed especially near eutectic 'grain boundaries' in the 899°C (1650°F) max/316°C (600°F) min heat affected zones. The Widmanstätten precipitate can be easily differentiated from the γ'' precipitates, observed but not counted in the analysis of the 'as-directionally solidified' γ/γ'-δ microstructure (Figs. 45 and 46), by trace symmetry. The δ-Ni_3Cb lath-like precipitates decorate the octahedral planes while the γ'' disc-shaped precipitates decorate the cuboidal planes of gamma nickel.

Creep specimens of the base line composition were ground from the above thermally cycled bars and tested in vacuum at 815 and 1093°C under stresses of 759 and 138 MN/m^2 respectively. The results presented in Table XI, indicated no change in rupture life from 3000 exposures to 1121°C/416°C.

The quinary alloys, Ni-19.7 w/o Cb-6.0 w/o Cr-2.5 w/o Al-1.0 w/o Mo and Ni-18.6 w/o Cb-6.0 w/o Cr-2.5 w/o Al-0.8 w/o Ti, were also cycled 3000 times between 416°C (780°F) and 1121°C (2050°F) in the thermal cycling apparatus. Each specimen displayed dimensional stability after cycling as was previously observed for the quaternary base line alloy and current nickel base superalloys. The as directionally solidified size distribution of γ' precipitates in γ were measured and are presented in Figs. 47 and 48. The absence of a marked bimodal size distribution is the most striking microstructural feature of these modified alloys compared with that measured on the base line quaternary γ/γ'-δ alloy, Fig. 46.

SIZE DISTRIBUTION OF γ' PRECIPITATES IN γ AFTER 3000 CYCLES BETWEEN VARIOUS TEMPERATURES

(Ni–19.7 w/o Cb–6.0 w/o Cr–2.5 w/o Al)

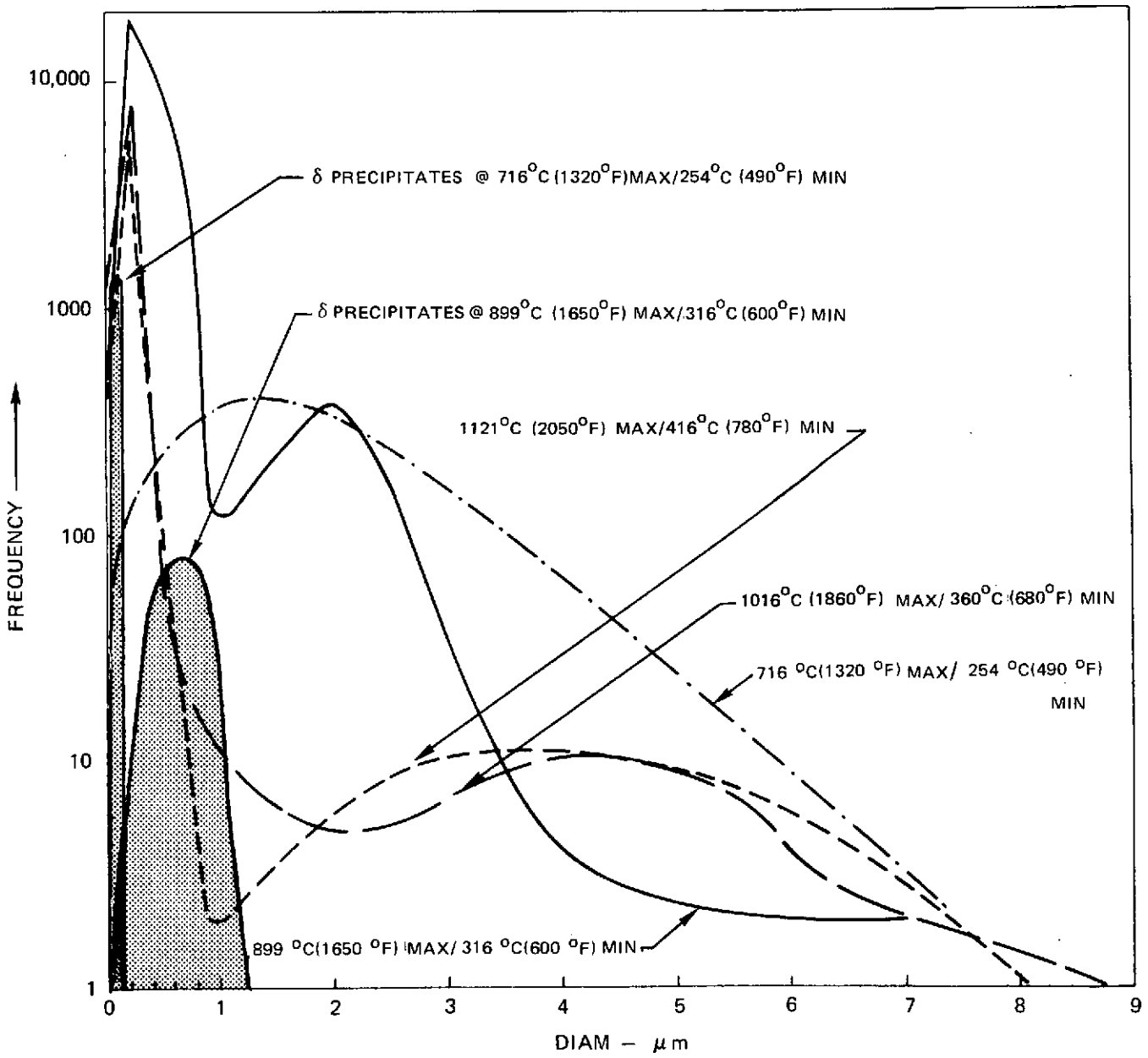

FIG. 46

SIZE DISTRIBUTION OF γ' PRECIPITATES IN γ AFTER DIRECTIONAL SOLIDIFICATION

(Ni–19.7 w/o Cb–6.0 w/o Cr–2.5 w/o Al)

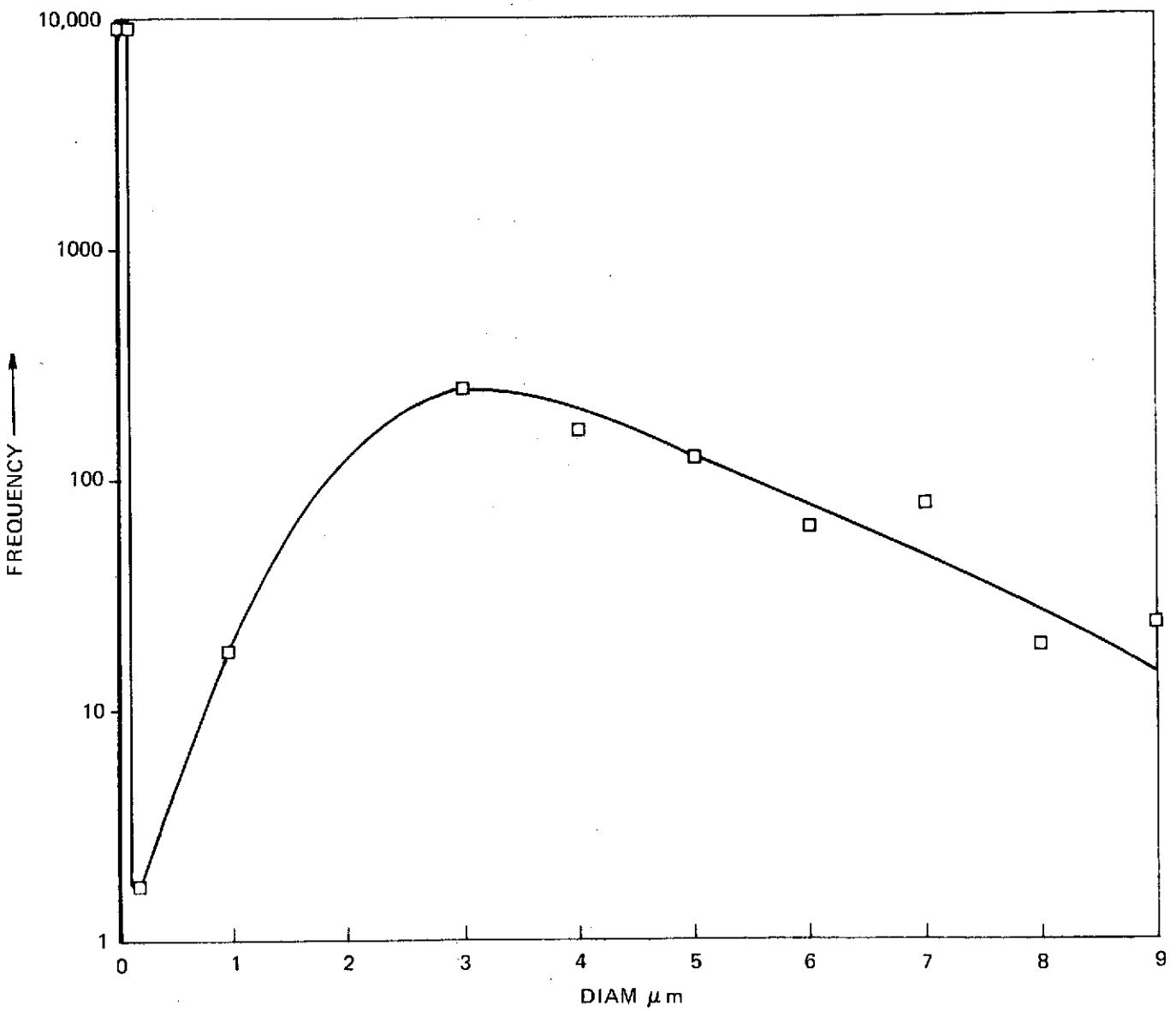

FIG. 47

SIZE DISTRIBUTION OF γ' PRECIPITATES IN γ AFTER DIRECTIONAL SOLIDIFICATION

(Ni–19.7 w/o Cb–6.0 w/o Cr–2.5 w/o Al–1.0 w/o Mo)

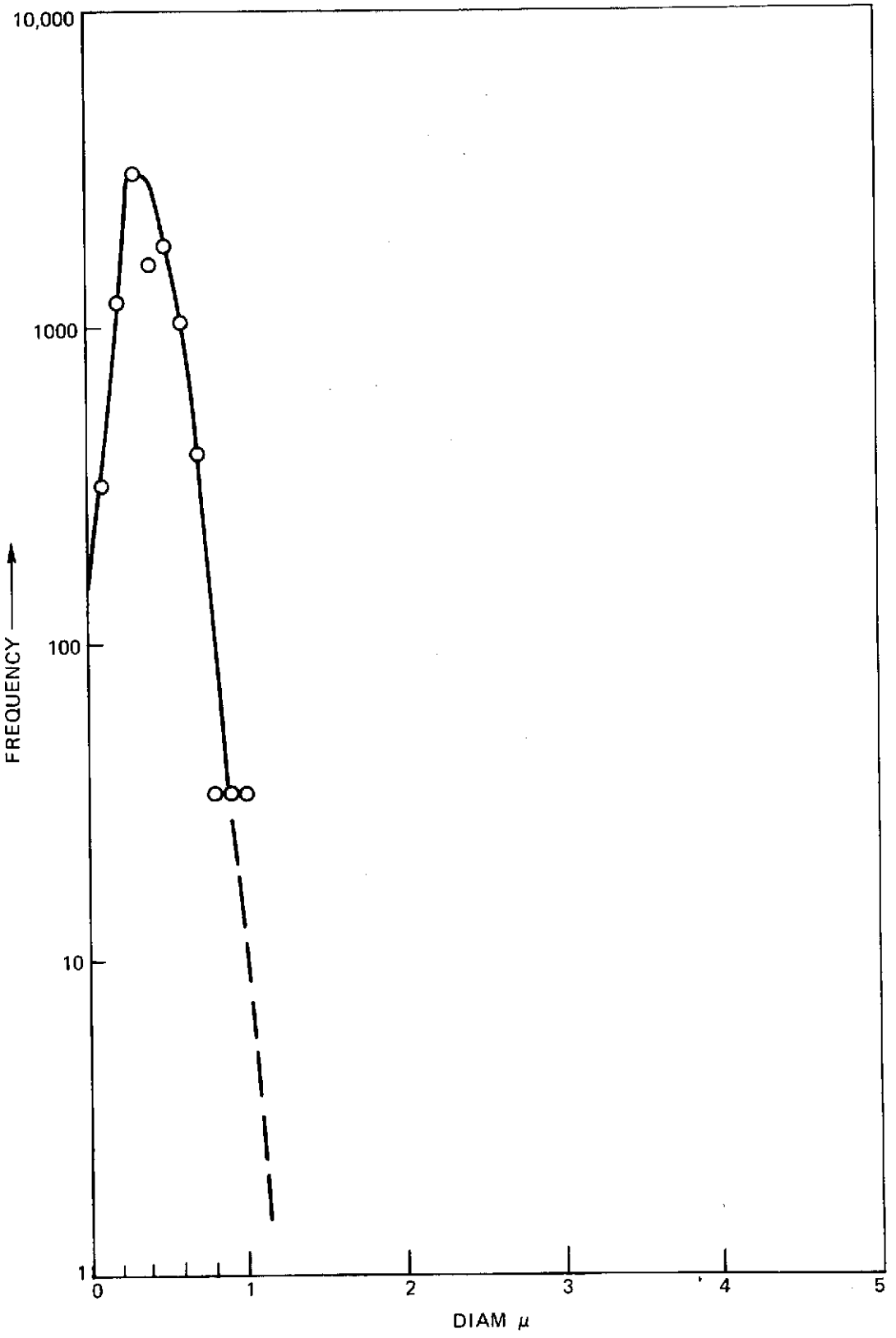

SIZE DISTRIBUTION OF γ' PRECIPITATES IN γ AFTER DIRECTIONAL SOLIDIFICATION

(Ni–18.6 w/o Cb–6.0 w/o Cr–2.5 w/o Al–0.8 w/o Ti)

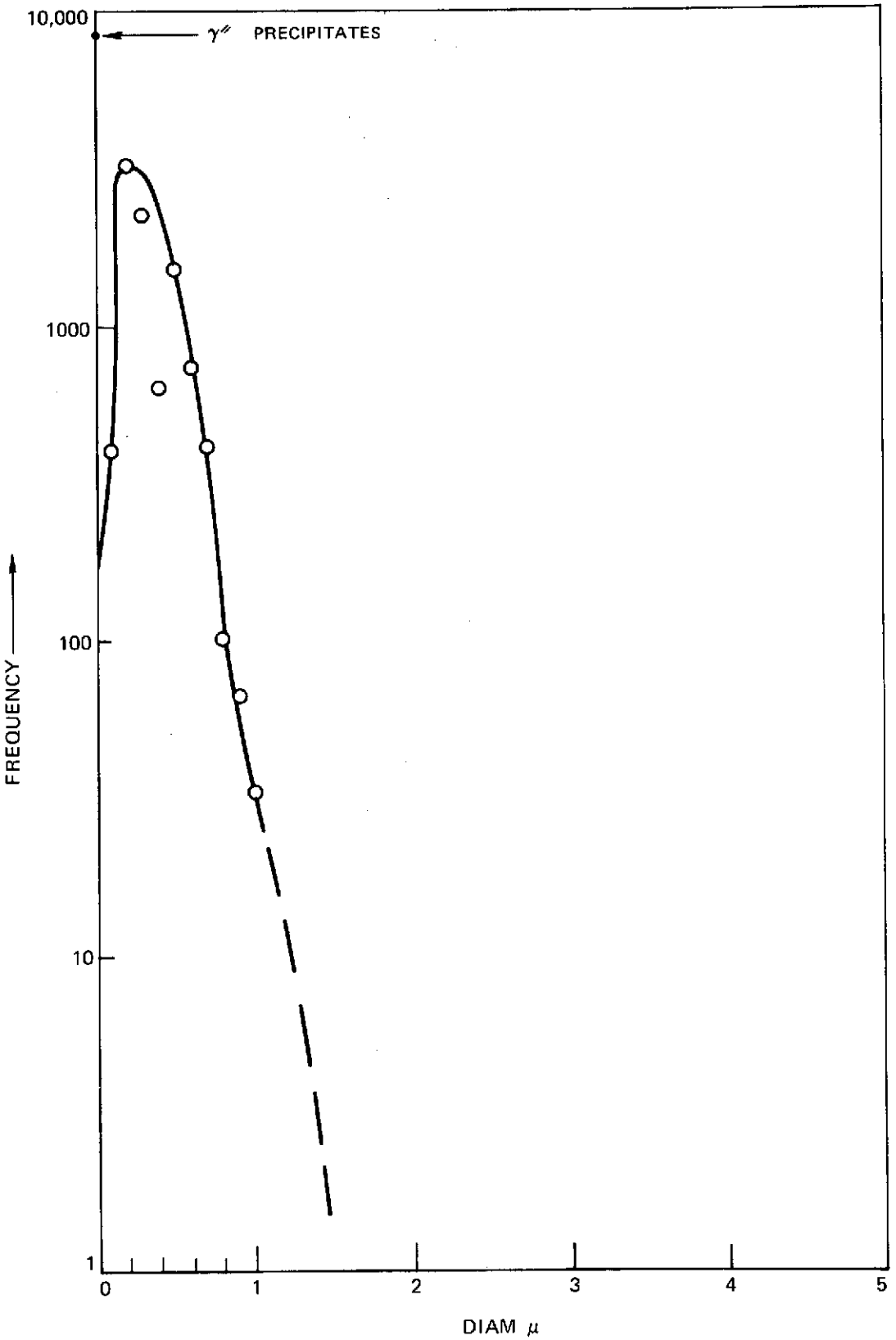

The effect of three thousand (3000) thermal cycles on the physico-chemical stability of the above two aligned quinary $\gamma/\gamma'-\delta$ alloys are shown in the longitudinal microstructure, Figs. 49 and 50. The interfaces between δ-Ni_3Cb and γ/γ' (Fig. 50e) showed some signs of coarsening for the Mo containing alloy which may result in reduced rupture properties. Furthermore, the γ' solvus temperature appears to have been lowered by this 1 w/o addition of Mo as may be seen by comparing Fig. 50d with Fig. 44d. The titanium modification resulted in the precipitation of a new phase after thermal cycling as seen in Figs. 49d and 49c. This intermetallic phase grew normal to the δ lamellae and sometimes perforated the aligned lamellar interfaces.

Creep specimens were ground from both the titanium and molybdenum containing thermal fatigue specimens and subjected to a stress of 138 MN/m^2 at 1100°C. The results, presented in Table XI, indicated that the rupture life for the titanium modified $\gamma/\gamma'-\delta$ decreased after 3000 cycles between 1121/399°C. The thermally cycled molybdenum modified specimen failed on loading so that no conclusion could be drawn. On subsequent inspection this specimen appeared to have melted perhaps during the cyclic exposures. These tests demonstrate the importance of phase stability during thermal cyclic exposures.

3.5.6 Transverse Tension

Tests were conducted to characterize the transverse strength of the base line quaternary $\gamma/\gamma'-\delta$ alloy and various quaternary modifications. Tests were performed on right cylindrical slugs which were electron discharge machined from an ~3.5 cm diameter ingot directionally solidified in the 50 kW high gradient apparatus and ground into standard Hounsfield tensile specimens. The results of triplicate specimens for the base line quaternary $\gamma/\gamma'-\delta$ alloy and other $\gamma/\gamma'-\delta$ alloys are presented in Table XII. Examination of base line $\gamma/\gamma'-\delta$ specimens at room temperature and 760°C indicate little evidence of plastic deformation within the gage. Fracture is primarily intergranular with secondary cracking clearly marking the path of propagation as illustrated in Fig. 51b. The fracture path primarily winds around eutectic grain boundaries occasionally propagating along lamellar interface or within δ-Ni_3Cb. Extensive plasticity (>3%) was exhibited at 1093°C although a similar fracture path was noted.

A less than expected improvement in the transverse ductility was observed after removing the chromium from the base line composition. Tests on $\gamma/\gamma'-\delta$ (Ni-21.0 w/o Cb-2.5 w/o Al) at 760°C (1400°F) revealed an approximately one percent reduction in area. Microscopic examination of the fracture surface

THE EFFECT OF 3000 THERMAL CYCLES (2 min) ON THE PHYSICO-CHEMICAL STABILITY OF γ/γ'-δ

(Ni–18.6 Cb–6.0 Cr–2.5 Al–0.8 Ti)

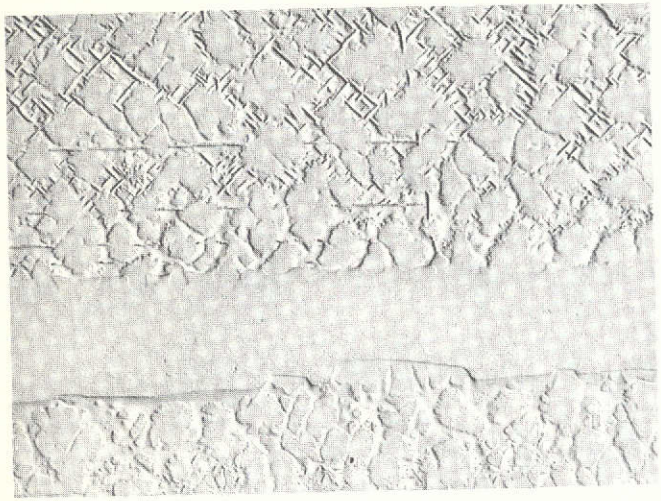

a) AS DIRECTIONALLY SOLIDIFIED:
R = 3 cm/hr, G_L = 300° C/cm

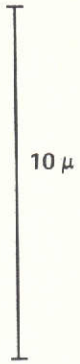

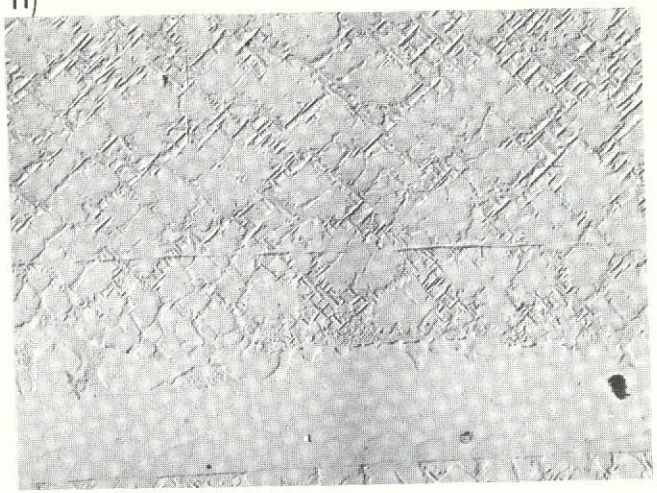

b) 716° C max/254° C min
(1320° F) (490° F)

c) 899° C max/316° C min
(1650° F) (600° F)

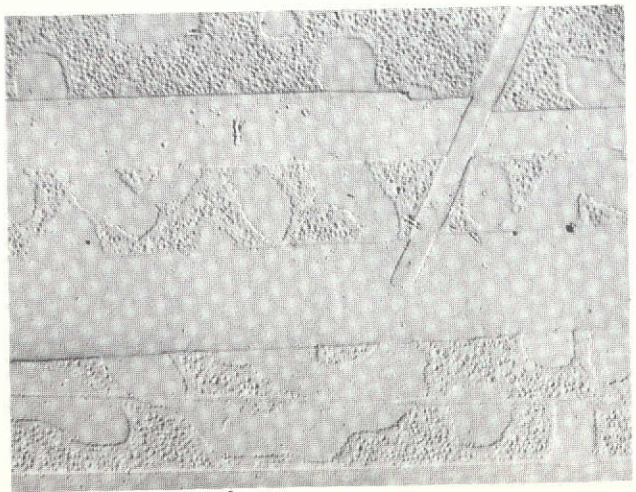

d) 1016° C max/360° C min
(1860° F) (680° F)

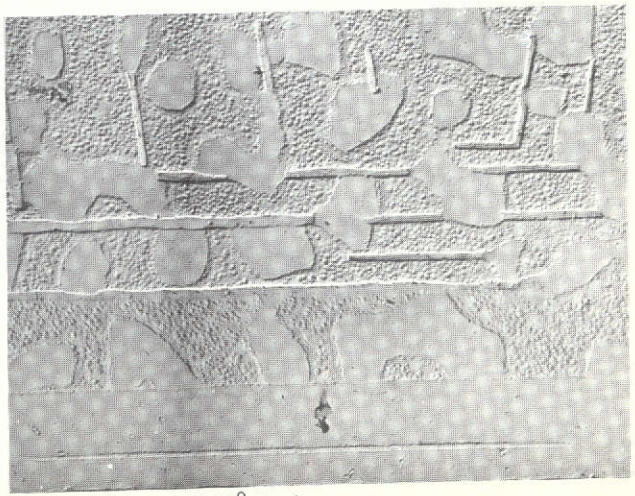

e) 1121° C max/416° C min
(2050° F) (780° F)

FIG. 49

THE EFFECT OF 3000 THERMAL CYCLES (2 min) ON THE PHYSICO-CHEMICAL STABILITY OF $\gamma/\gamma'-\delta$

(Ni–19.7Cb–6.0Cr–2.5Al–1.0Mo)

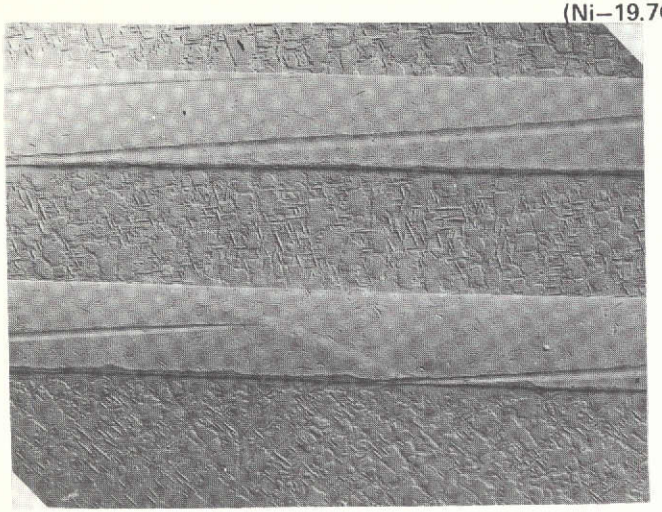

a) AS DIRECTIONALLY SOLIDIFIED:
R = 3 cm/hr, G_L = 300° C/cm

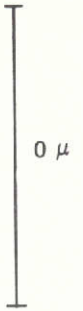

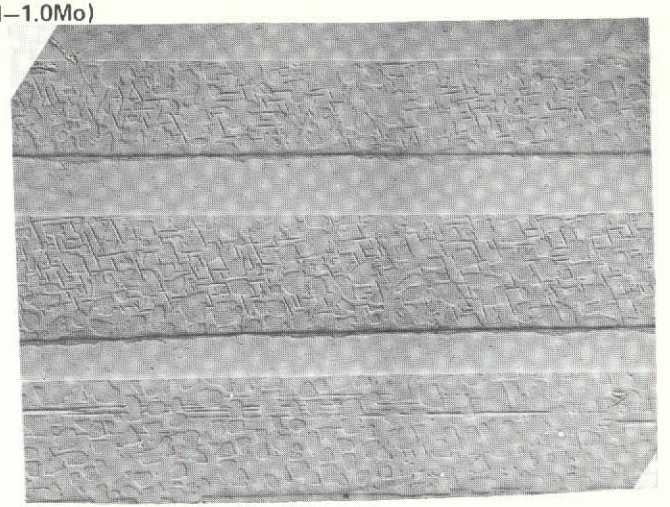

b) 716° C max/254° C min
(1320° F) (490° F)

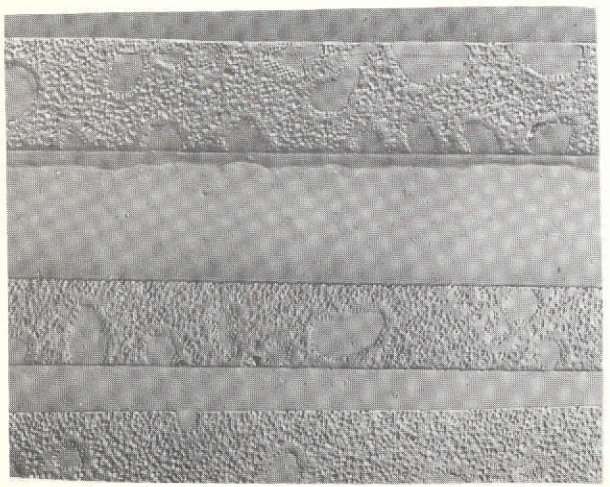

899° C max/316° C min
(1650° F) (600° F)

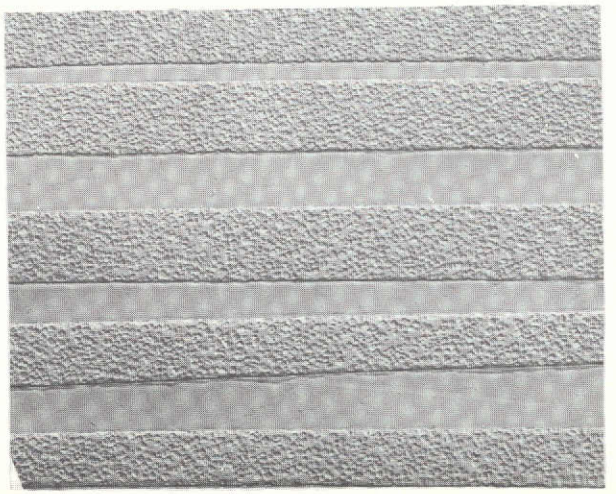

d) 1016° C max/360° C min
(1860° F) (680° F)

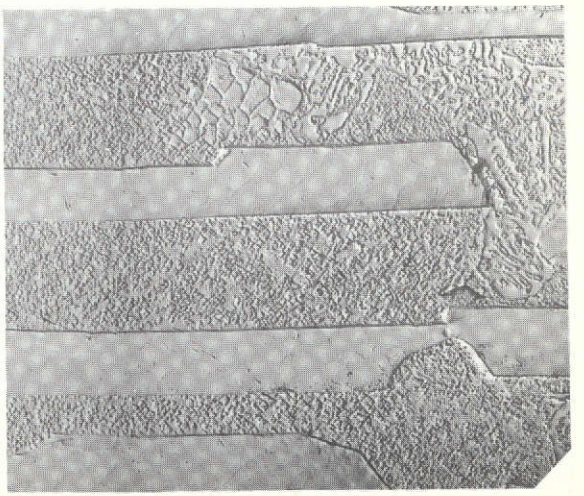

e) 1121° C max/416° C min
(2050° F) (780° F)

FIG. 50

Table XII

Transverse Tensile Properties of Quaternary $\gamma/\gamma'-\delta$ Alloys

Specimen No.	Composition w/o	Temp °C	Temp °F	UTS $10^7 N/m^2$	UTS ksi	E $10^{10} N/m^2$	E msi	Elong. %	R.A. %	$\dot{\varepsilon}$ min^{-1}
A73-148-01	Ni-20.0Cb-6.0Cr-2.5Al	20	68	43.5	63.1	231.0	33.5	.34	nil	.01
A73-148-03	"	20	68	53.2	77.2	228.1	33.1	.52	nil	.01
A73-229-01	"	20	68	58.3	84.6	217.9	31.6	.75	nil	.01
A73-148-02	"	760	1400	50.1	72.6	-	-	1.9	nil	.05
A73-148-05	"	760	1400	47.2	68.5	-	-	0.8	nil	.05
A73-148-06	"	760	1400	55.1	79.9	-	-	0.9	nil	.05
A73-148-04	"	1093	2000	20.6	29.9	-	-	3.9	3.8	.05
A73-229-02	"	1093	2000	21.9	31.9	-	-	2.8	2.7	.05
A73-229-03	"	1093	2000	19.6	28.4	-	-	3.8	2.6	.05
A72-234-03	Ni-19.5Cb-9.0Cr-1.0Al	20	68	54.8	79.6	189.7	27.5	0.5	nil	.01
A72-234-02	"	760	1400	54.0	78.3	-	-	2.8	nil	.05
A72-234-01	"	1093	2000	12.4	18.0	-	-	7.2	6.1	.05
A72-348-02	Ni-21.0Cb-2.5Al	20	68	72.4	105.0	213.7	31.0	0.8	nil	.01
A72-348-01	"	760	1400	59.2	85.9	-	-	1.5	1.1	.05

TRANSVERSE TENSION FRACTURE SURFACES OF $\gamma/\gamma'-\delta$ Ni–20.0 w/o Cb–6.0 w/o Cr–2.5 w/o Al

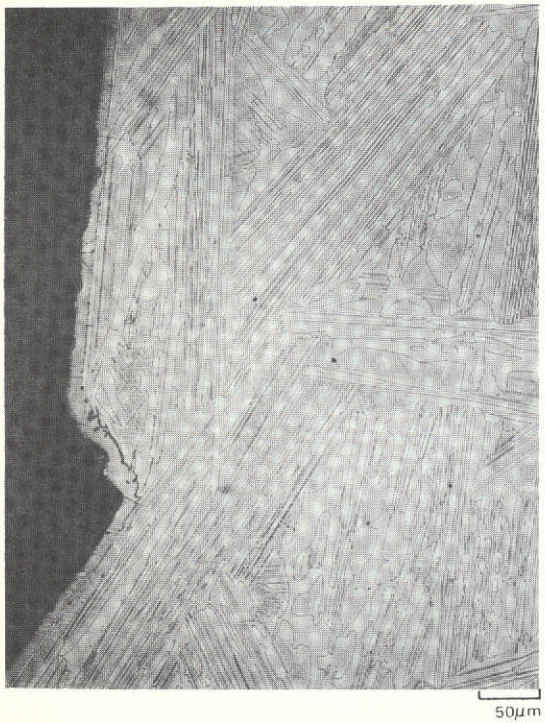

a) ROOM TEMP.

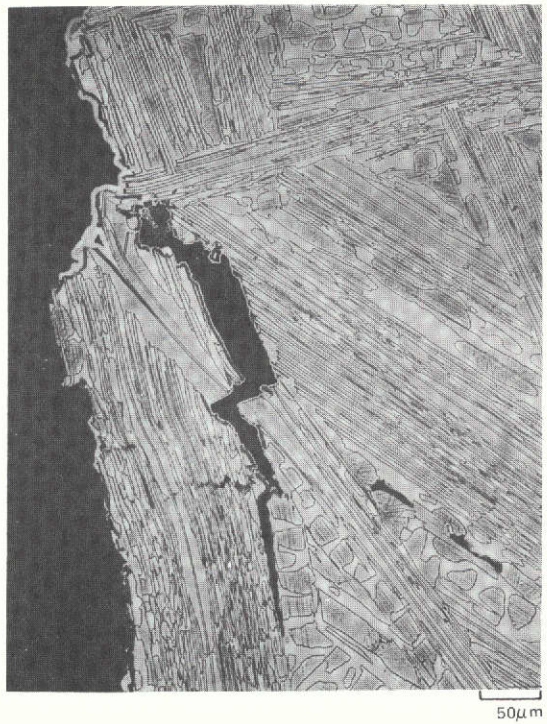

b) 760°C

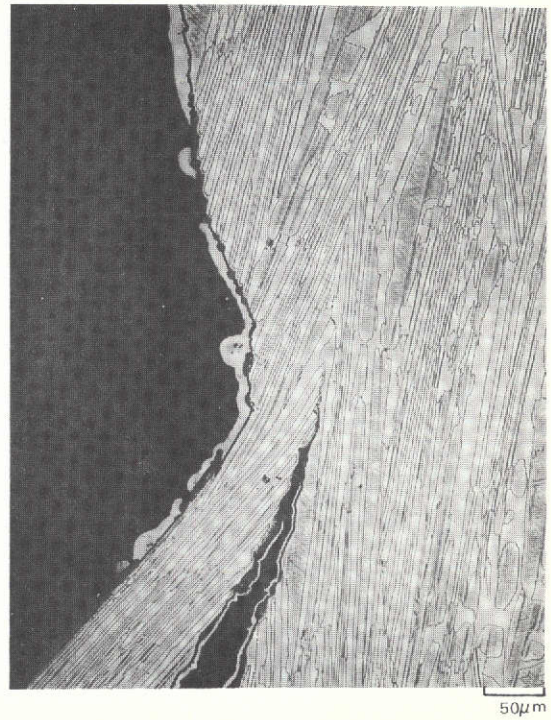

c) 1093°C

FIG. 51

N07-146-2

indicated intergranular as well as intragranular decohesion as shown in Fig. 52b. The evidence of grain boundary related failure modes in all the γ/γ'-δ alloys studied indicates the future requirement of an alloy modification which substantially strengthens these boundaries to meet the eighth goal of this program.

3.6 Mechanical Characterization of an Improved γ/γ'-δ Alloy

From the mechanical property screening tests of the tensile, shear, rupture, thermal fatigue, and oxidation behavior of the quaternary and quinary modified γ/γ'-δ alloys, only one composition appeared to exhibit improvements in both the shear and creep strength together with gains in the intrinsic oxidation resistance as is described below. The tantalum modified γ/γ'-δ alloy (Ni-17.8 w/o Cb-6.0 w/o Cr-2.5 w/o Al-3.0 w/o Ta) was selected to be more extensively tested and compared against the eight goals of the program.

3.6.1 Tensile

The strength and ductility of the tantalum modified γ/γ'-δ alloy (Ni-17.8 w/o Cb-6.0 w/o Cr-2.5 w/o Al-3.0 w/o Ta) is presented in Table XIII and plotted as a function of temperature in Fig. 53. The tensile strength of the γ/γ'-δ alloy exceeds all comparison nickel base superalloys at all temperatures (Ref. 48). The ductility of the γ/γ'-δ specimens measured as gage length elongation and reduction in area indicated a slight minimum near 900°C for a strain rate of 0.05 min^{-1}. This reduction in ductility at intermediate temperatures was considered to be associated with the intrinsic γ/γ' ductility minimum characteristic of most nickel-base superalloys. Metallographic examination of the room temperature fracture indicated that uniform deformation occurred throughout the gage. Copious twinning and cleavage of δ lamellae on assummed $\{211\}_\delta$ was characteristic of the deformation process as shown in Fig. 54. At elevated temperature, deformation was characterized by more intense translamellar shear bands concentrated in the necked region of the gage. Above 1000°C extensive local δ-Ni_3Cb lamellae damage occurred over wide deformation bands.

The average measured tensile strength of 244 MN/m^2 at 1200°C virtually meets the first goal of the program which required a tensile strength of 250 MN/m^2. The ductility criteria of at least 5% over the entire temperature range is met for all temperatures except room temperature (i.e. ~3%).

3.6.2 Creep Rupture

The results of vacuum creep rupture tests performed at temperatures between 815-1100°C are presented in Table XIV. Larson Miller parameters (constant = 20) were computed and a curve drawn for the data as shown in Fig. 55. The grey band between the solid lines represents the range in strength for the base line

TRANSVERSE TENSION FRACTURE SURFACES OF $\gamma/\gamma'-\delta$ Ni–21.0 w/o Cb–2.5 w/o Al

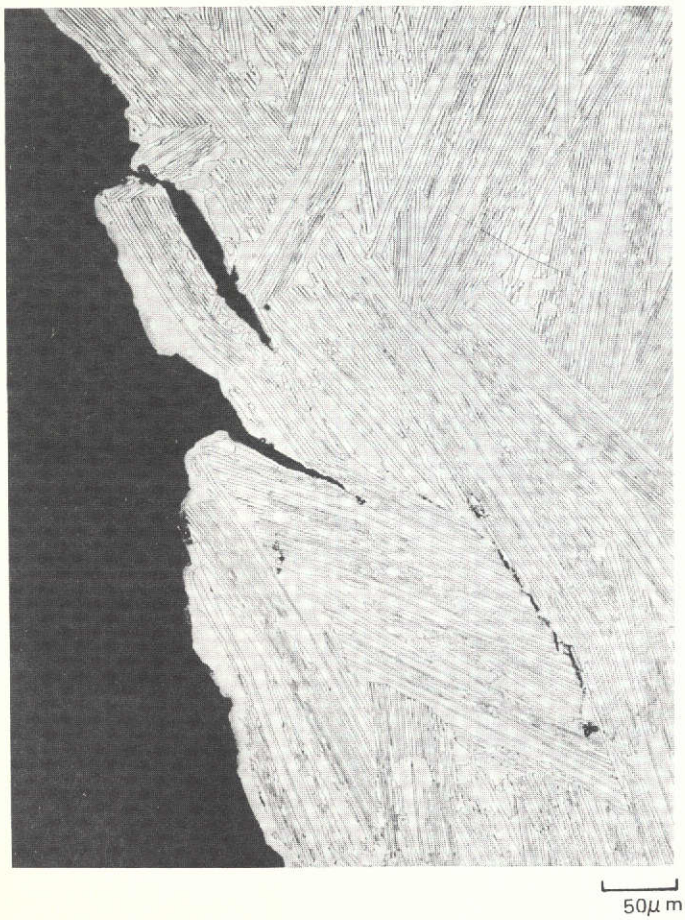

a) ROOM TEMP.

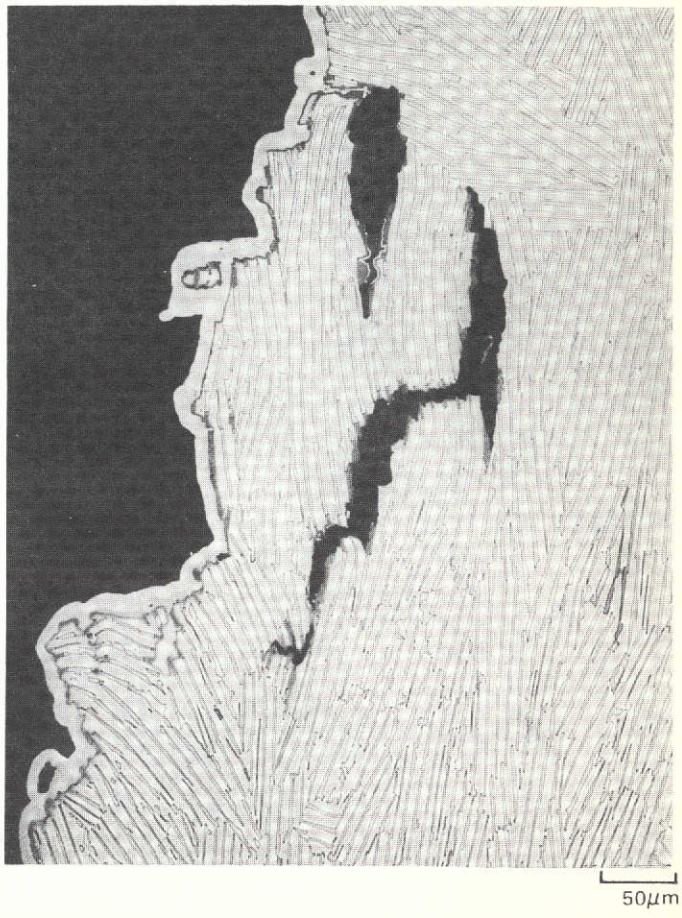

b) 760°C

N07–146–1

Table XIII

Tensile Properties of Directionally Solidified Ni - 17.8 w/o Cb - 3 w/o Ta - 6 w/o Cr - 2.5 w/o Al
Specimens Tested in Air

Specimen No.	Temperature °F	Temperature °C	0.2% Y.S. $10^7 N/m^2$	0.2% Y.S. ksi	E $10^{10} N/m^2$	E msi	UTS $10^7 N/m^2$	UTS ksi	Elong. %	R.A. %	$\dot{\varepsilon}$ min^{-1}
A74-575-03	68	20	119.7	173.5	208.4	36.2	120.1	174.0	2.4	3.2	.01
A74-186-03	68	20	121.2	175.7	254.6	36.9	124.2	180.0	2.6	3.5	.01
A74-550-03	1202	650	95.9	139.0	169.7	24.6	118.3	171.5	7.5	13.6	.05
A74-511-01	1202	650	99.4	144.0	189.1	27.4	119.0	172.5	8.2	14.1	.05
A74-511-02	1400	760	96.7	140.1	-	-	111.8	162.1	10.8	15.3	.05
A74-550-02	1400	760	97.3	141.0	158.7	23.0	109.0	158.0	12.0	18.8	.05
A74-186-02	1472	800	97.3	141.0	190.4	27.6	101.4	147.0	*	*	.05
A74-605-03	1598	870	91.4	132.5	154.6	22.4	91.8	133.0	7.3	13.6	.05
A74-511-03	1598	870	92.6	134.2	160.8	23.3	95.4	138.2	6.8	12.1	.05
A74-511-04	1832	1000	63.1	91.4	-	-	69.8	101.2	10.7	8.9	.05
A74-605-02	1832	1000	64.9	94.0	-	-	74.2	107.5	5.6	7.2	.05
A74-186-01	2012	1100	44.9	65.0	-	-	46.6	67.5	27.4	28.1	.05
A74-605-01	2192	1200	24.1	34.9	-	-	24.1	34.9	21.0	26.8	.05
A74-563-01	2192	1200	24.8	35.9	-	-	24.8	35.9	18.8	24.1	.05

*specimen failed outside gage

TENSILE PROPERTIES OF DIRECTIONALLY SOLIDIFIED Ni–17.8 w/o Cb–3.0 Ta–6.0 Cr–2.5 w/o Al SPECIMENS TESTED IN AIR

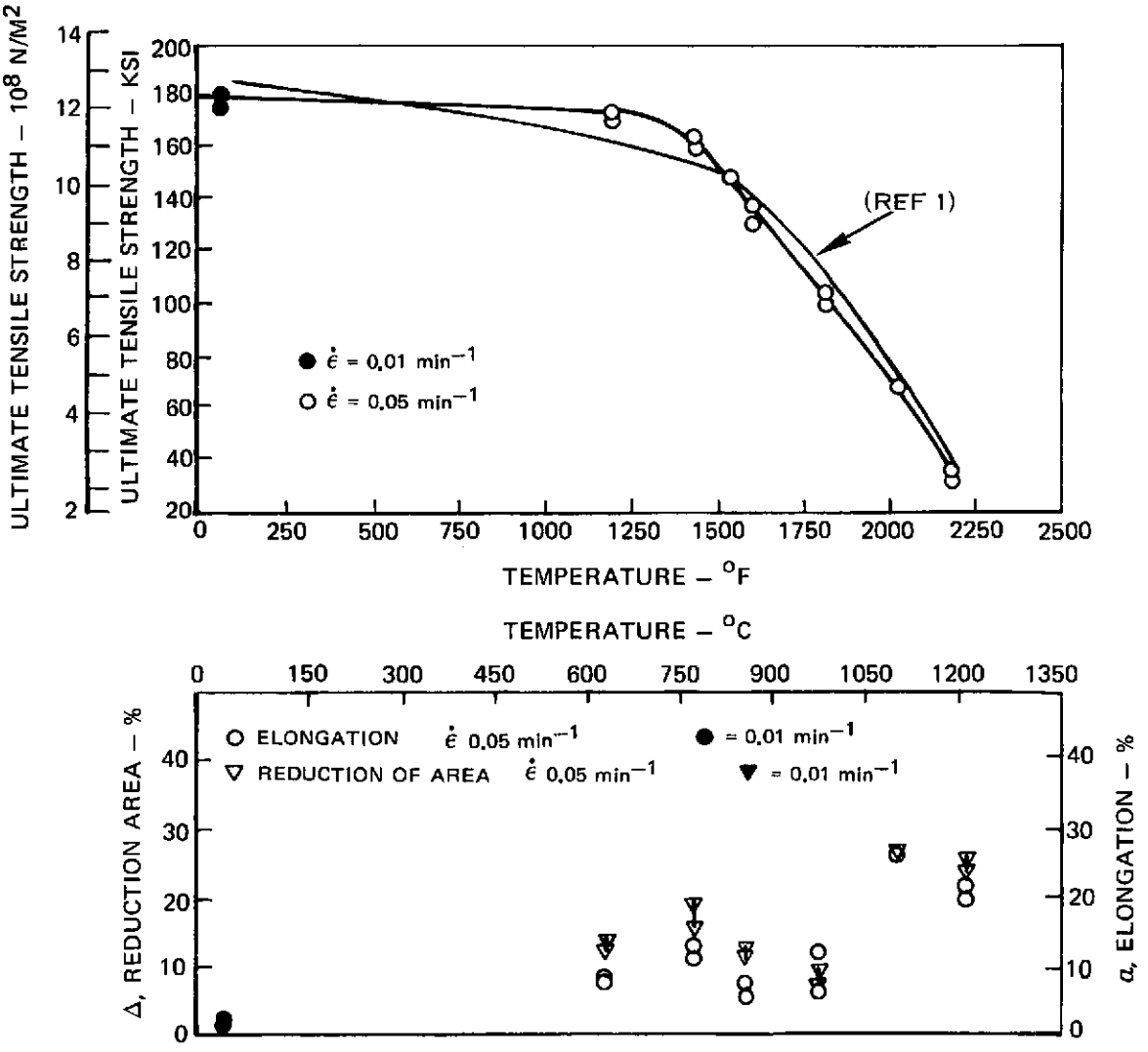

N09–10–1

DEFORMATION TWINNING AND TWIN BOUNDARY CRACKING IN Ni_3Cb OF THE
$\gamma/\gamma' - \delta$ EUTECTIC (Ni–17.9 w/o Cb–3.0 w/o Ta–6.0 w/o Cr–2.5 w/o Al)
AFTER TENSILE LOADING AT ROOM TEMPERATURE

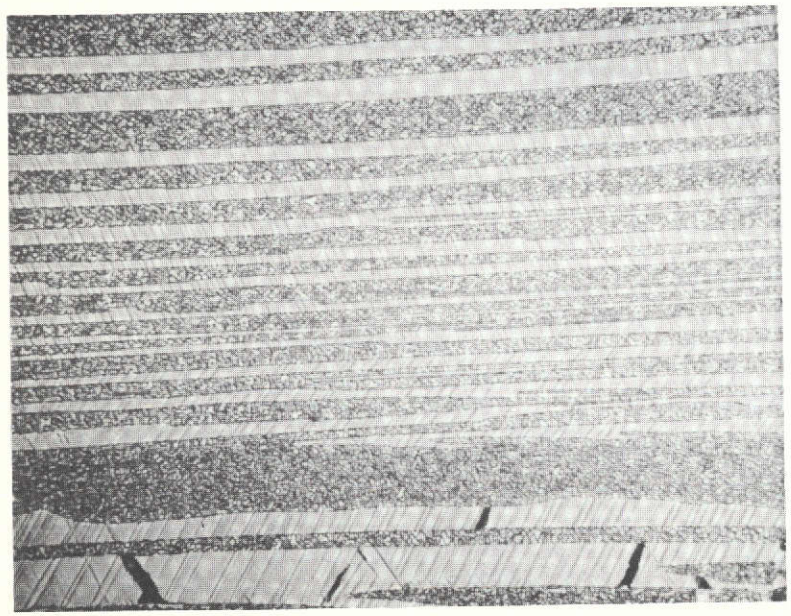

IN GAGE AWAY FROM FRACTURE

10 μm

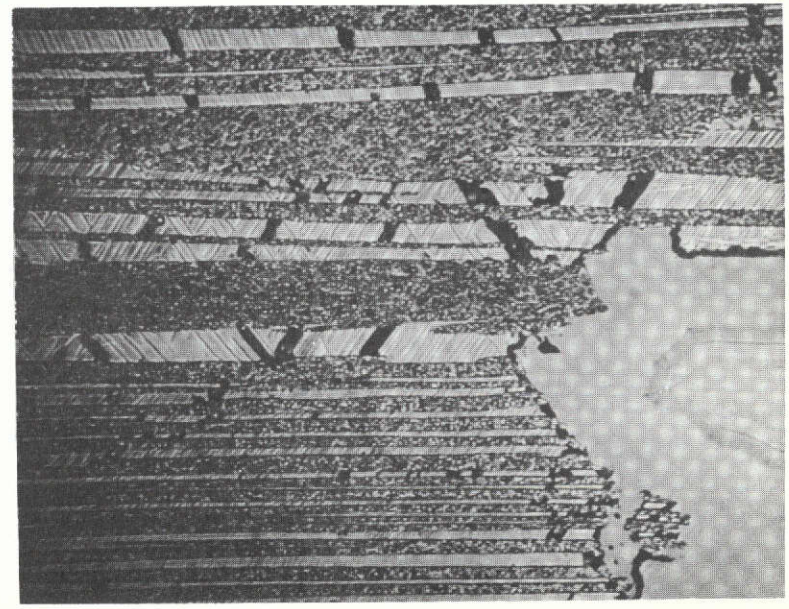

ADJACENT FRACTURE SURFACE

10 μm

N10–291–1

FIG. 54

Table XIV

Stress Rupture Properties of Directionally Solidified Tantalum Modified $\gamma/\gamma'-\delta$

Specimen No.	Composition w/o	Freezing Rate cm/hr	Temp °C	Stress $10^7 N/m^2$	ksi	Time to Rupture hrs	Time to 0.1% hrs	Time to 0.2% hrs	Time to 0.5% hrs	RT Elong. %	R.A. %	LMP $x10^{-3}$	Environment
A74-610-01	Ni-17.8Cb-3Ta-6Cr-2.5Al	3	1100	13.1	19	*	-	-	-	-	-	*	vacuum
A74-575-01		2	1100	13.1	19	407.7	5	10	30	9.8	11.0	55.89	vacuum
A74-177-01		3	1100	13.8	20	71.5	-	-	-	14.8	>20	53.98	air
A74-633-02		3	1100	13.8	20	76.8	10	22	38	8.7	12.3	54.06	vacuum
A74-633-03		3	1000	27.6	40	65.1	3	5	15	9.8	10.5	50.00	vacuum
A74-633-01		3	1000	27.6	40	56.9	4	6	13	14.6	17.4	49.86	vacuum
A74-610-03		3	900	48.3	70	61.0	2	7	58	14.0	9.0	46.01	vacuum
A74-575-03		2	900	48.3	70	109.7	34	58	80	4.2	3.5	46.55	vacuum
A74-610-02		3	815	75.9	110	17.0	>17	>17	>17	**	**	**	vacuum
A74-575-02		2	815	75.9	110	>500	>500	>500	>500	>.04	***	>44.47	vacuum

*premature failure due to equipment malfunction
**failure at undercut adjacent extensometer ridge
***test discontinued after 500 hrs, retested in tension

FIG. 55

LARSON MILLER CURVE FOR $\gamma/\gamma' - \delta$

(Ni–17.8 w/o Cb–3 w/o Ta–6 w/o Cr–2.5 w/o Al)

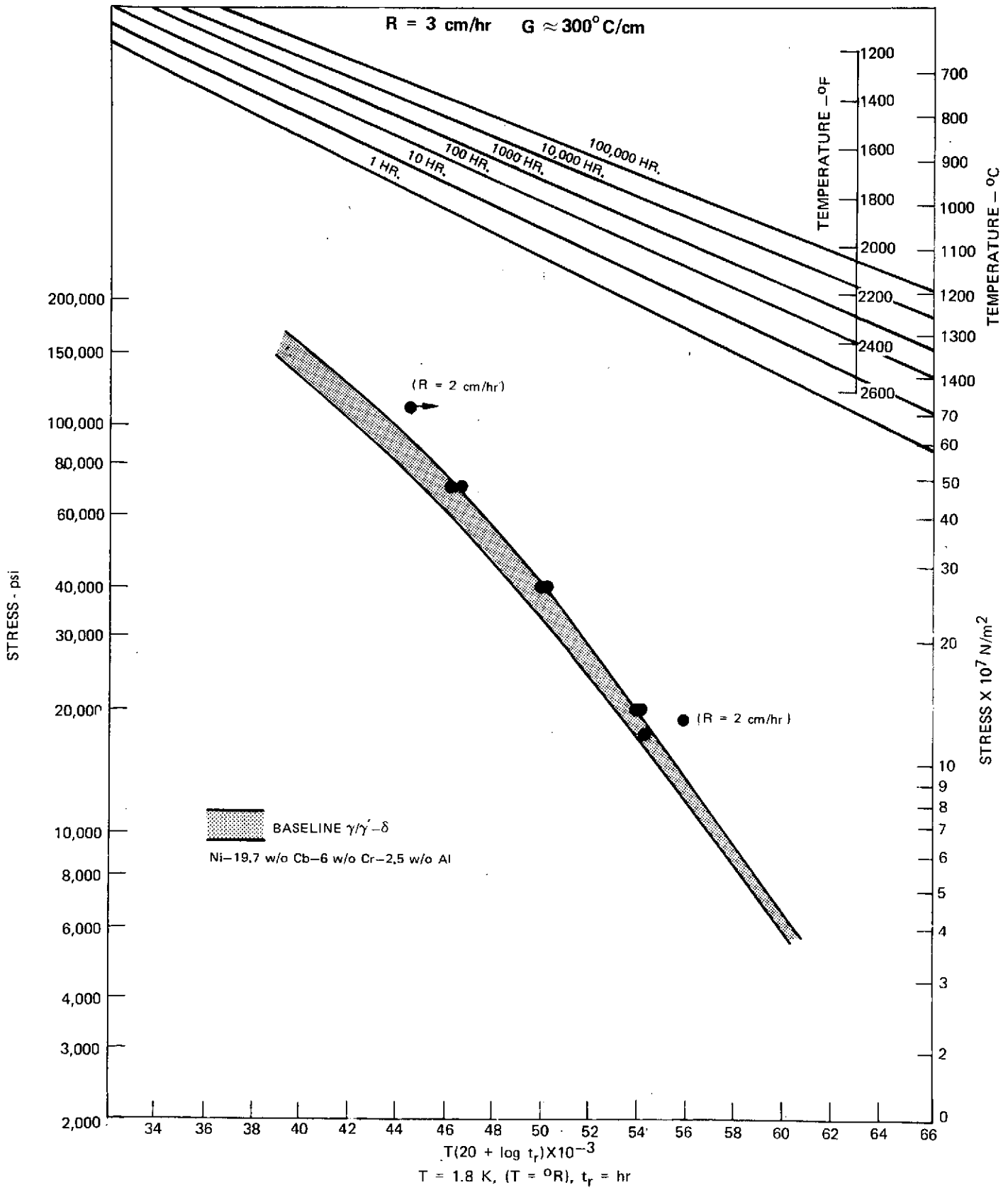

CREEP CURVE OF $\gamma/\gamma - \delta$ (Ni–17.8 w/o Cb–3 w/o Ta – 6 w/o Cr – 2.5 w/o Al)

A74–575–01 AT 1100°C (2012°F) AND 13.11×10^7 n/m^2 (19,000 PSI) IN VACUUM

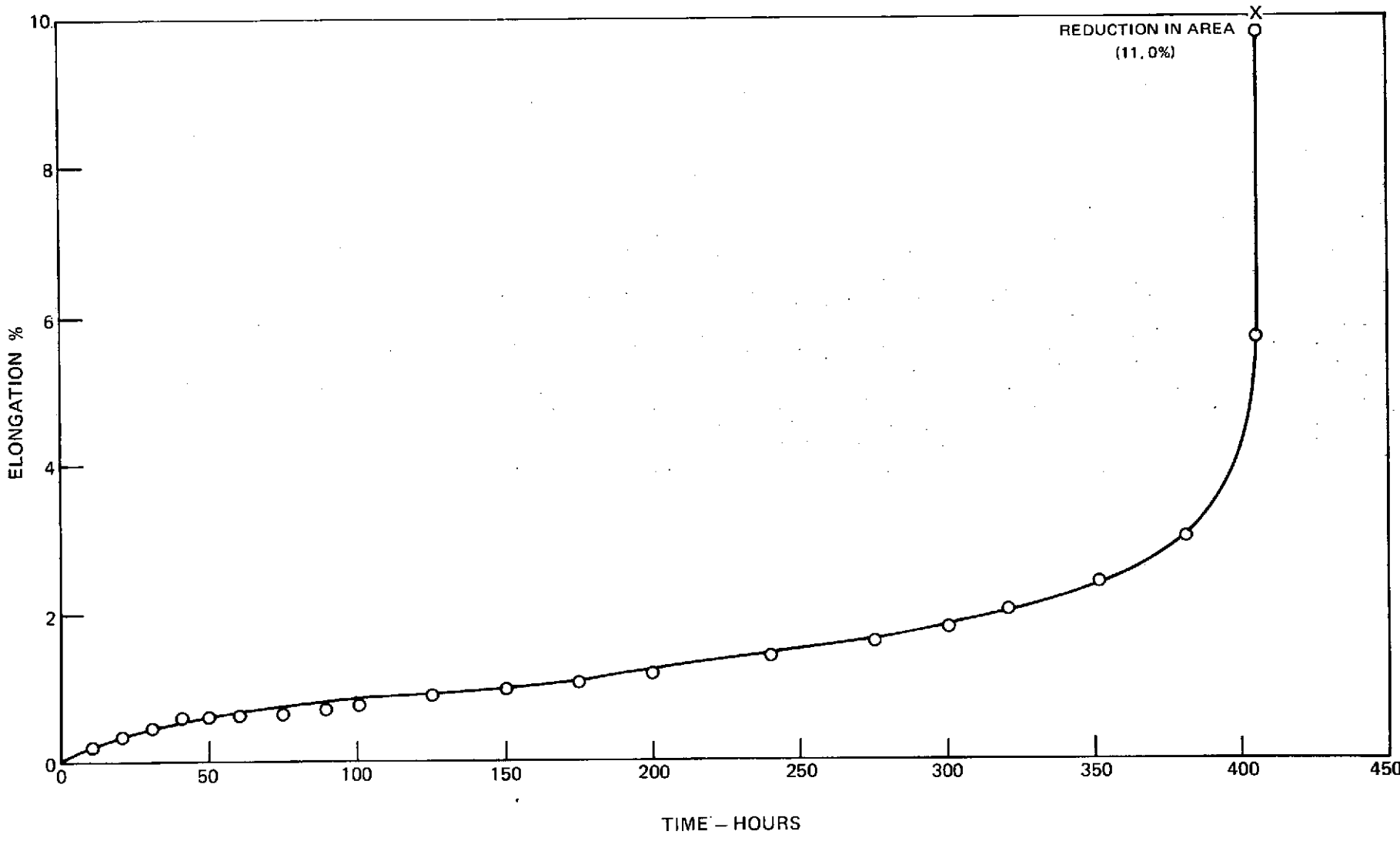

FIG. 56

N10–164–1

THE EFFECT OF 3000 CYCLES (2 MIN) ON THE PHYSICO–CHEMICAL STABILITY OF $\gamma/\gamma - \delta$

(Ni–17.9 w/o Cb–3.0 w/o Ta–6.0 w/o Cr–2.5 w/o Al)

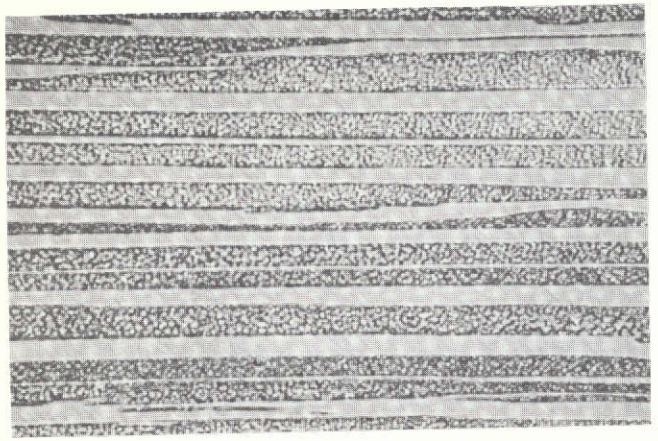

20 μm

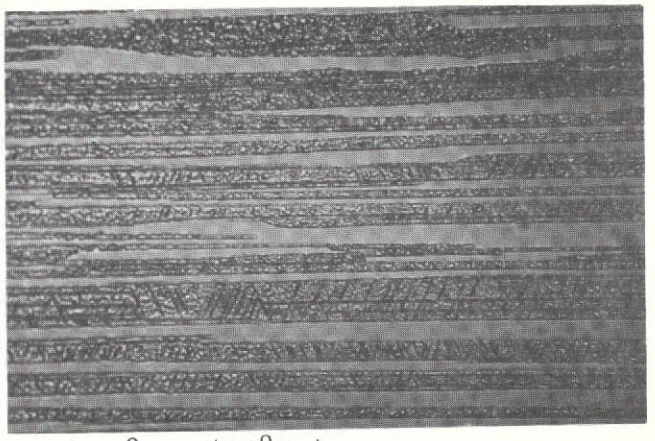

a) AS DIRECTIONALLY SOLIDIFIED:
R = 3 cm/hr, GL = 300°C/cm

b) 716°C max/254°C min
(1320°F) (490°F)

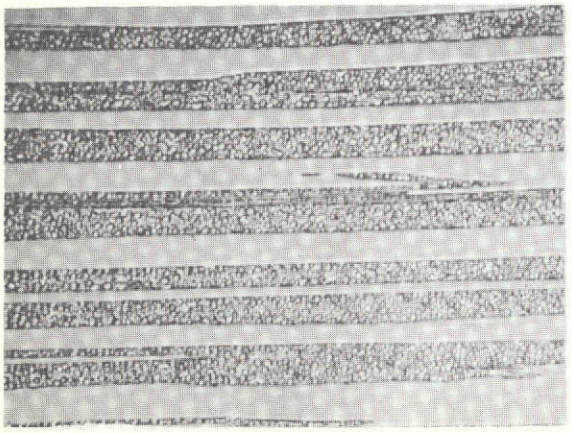

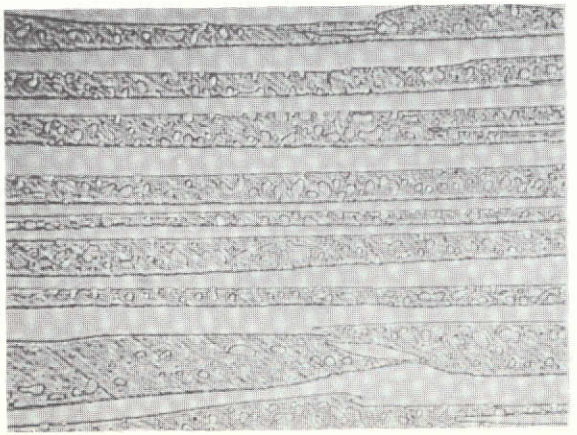

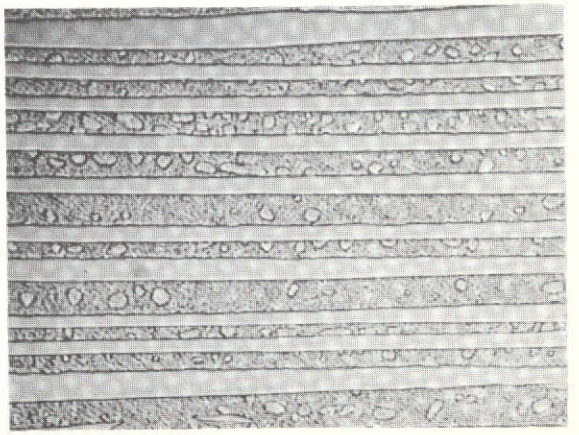

c) 899°C max/316°C min
(1650°F) (600°F)

d) 1016°C max/360°C min
(1860°F) (680°F)

e) 1121°C max/416°C min
(2050°F) (780°F)

FIG. 57

THE EFFECT OF 3000 CYCLES (2 MIN) ON THE PHYSICO–CHEMICAL STABILITY OF $\gamma/\gamma - \delta$

(Ni–17.9 w/o Cb–3.0 w/o Ta–6.0 w/o Cr–2.5 w/o Al)

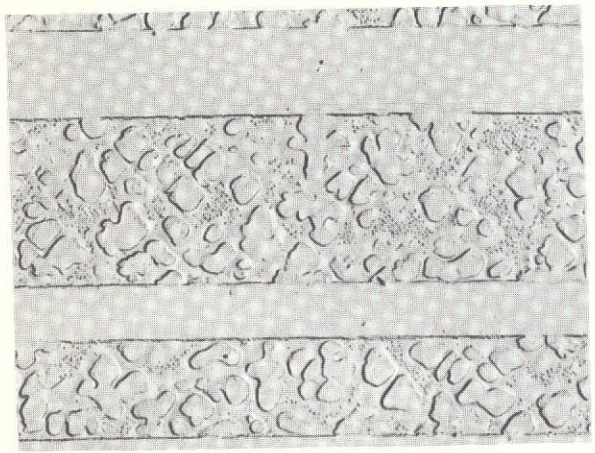

10 μm

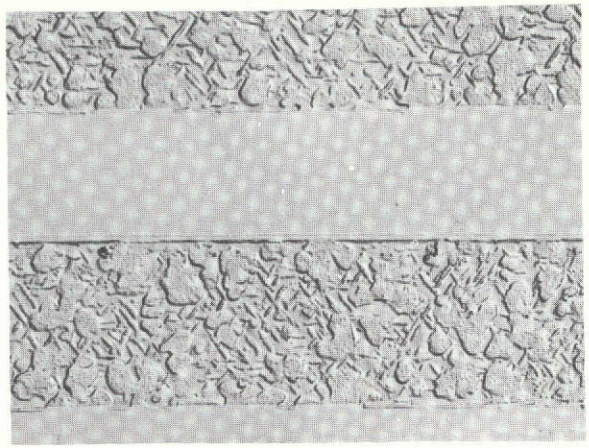

a) AS DIRECTIONALLY SOLIDIFIED:
R = 3 cm/hr, GL = 300°C/cm

b) 716°C max/254°C min
(1320°F) (490°F)

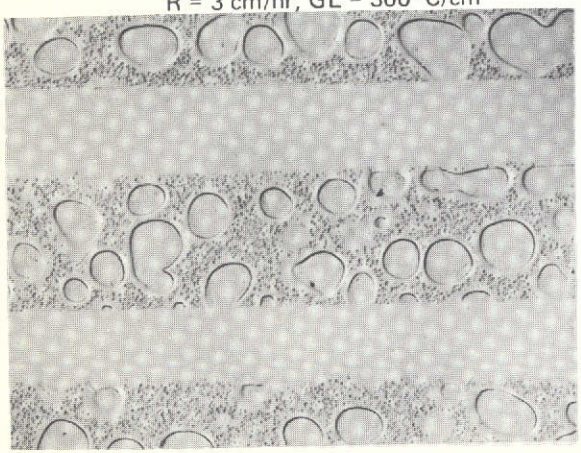

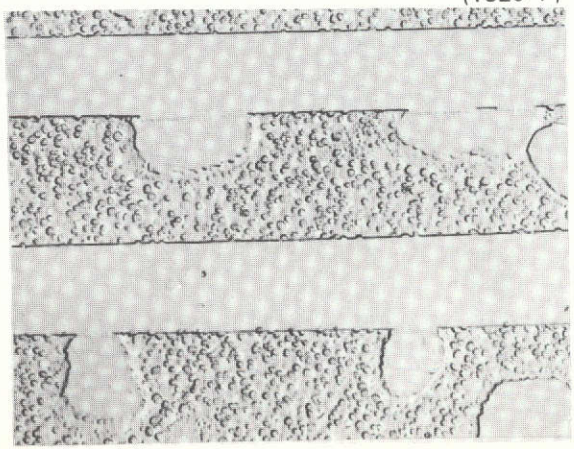

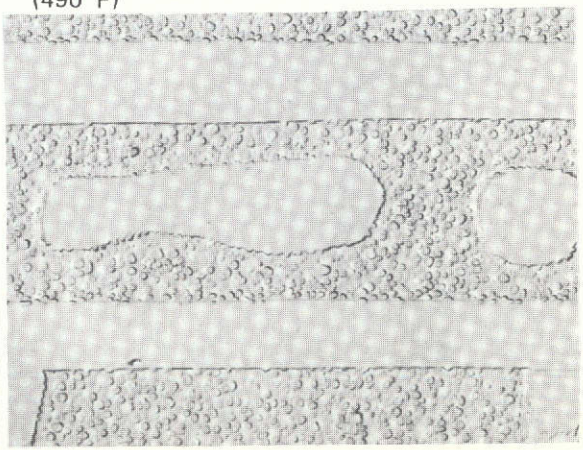

c) 899°C max/316°C min
(1650°F) (600°F)

d) 1016°C max/360°C min
(1860°F) (680°F)

e) 1121°C max/416°C min
(2050°F) (780°F)

FIG. 58

WIDMANSTATTEN δ PRECIPITATION AND REDUCED DEFORMATION TWINNING IN LAMELLAR δ Ni_3Cb OF THE $\gamma/\gamma'-\delta$ EUTECTIC (Ni–17.9 w/o Cb–3.0 w/o Ta–6.0 w/o Cr–2.5 w /o Al) AFTER 1500 HR EXPOSURE AT 900°C (1650°F) AND ROOM TEMPERATURE TENSION TESTING

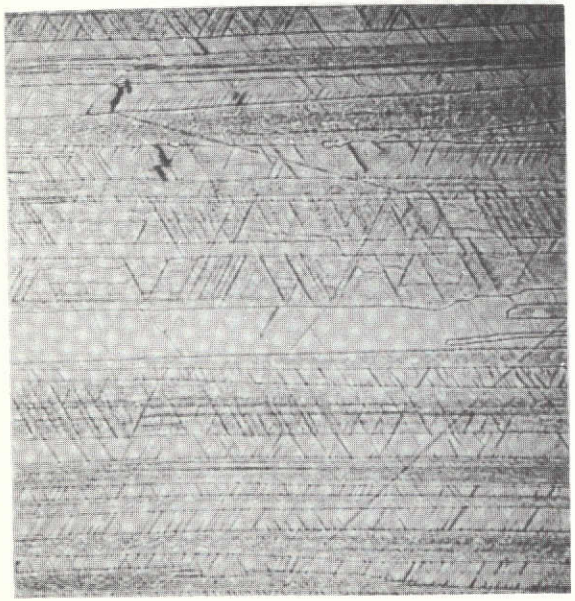

IN GAGE AWAY FROM FRACTURE

10 μm

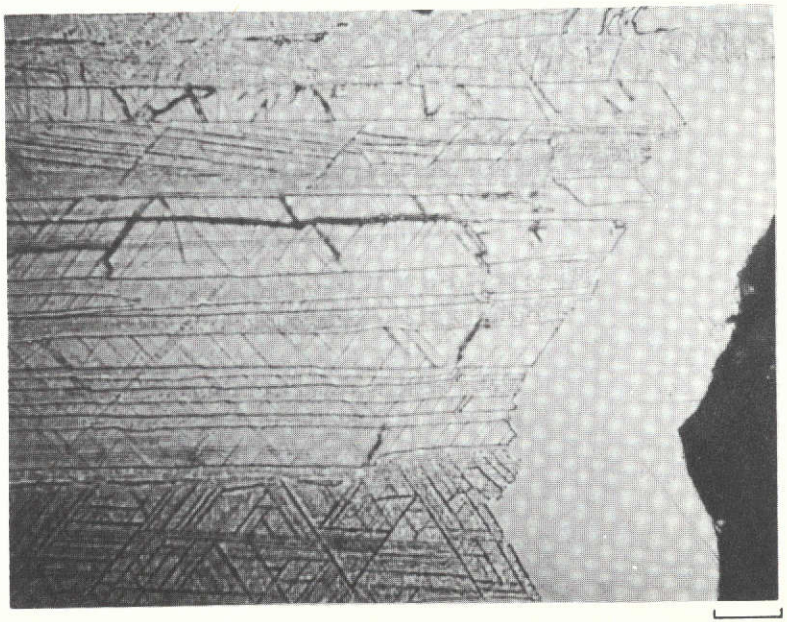

ADJACENT FRACTURE SURFACE

10 μm

N10–291–2

FIG. 59

Since a small but detectable decrease in impact strength after a 1500 hr exposure to 850°C (1560°F) was noted in the previous contract (Ref. 1) for both the Ni-19.7 w/o Cb-6.0 w/o Cr-2.5 w/o Al and Ni-21.75 w/o Cb-2.55 w/o Al, further microscopic examinations were undertaken to examine for δ precipitation. Previously (Ref. 1) examinations by both optical and scanning electron microscopy revealed no change in the microstructure due to exposure for 1500 hrs at 850°C. In the high resolution electron transmission examination of the two γ/γ'-δ alloys of the previous contract we found some δ precipitates within γ/γ'. This experiment indicated that if chromium is present in γ/γ'-δ, Widmanstätten δ does precipitate (Fig. 60) within the γ/γ' matrix to relieve Cb atoms supersaturation. In contrast in the nonchromium containing alloy, γ/γ'-δ alloy, no δ-precipitation was found as shown in Fig. 61. The presence of Widmanstätten δ within γ/γ' was somewhat deleterious on the low temperature toughness and ductility of the γ/γ'-δ alloy. The reaction kinetics for the δ precipitation in the nonchromium γ/γ'-δ alloy was inferred to be much slower than that for the base line quaternary γ/γ'-δ.

3.6.6 Transverse Tension

Tests to characterize the transverse strength of the Ta modified quinary γ/γ'-δ alloy were performed on right cylindrical slugs electron discharge machined from an ~3.5 cm diameter ingot and ground into standard Hounsfield tensile specimens. The results of triplicate test specimens at three temperature intervals are presented in Table XV. For comparison purposes the results of the base line quaternary γ/γ'-δ alloy are presented in Table XII. Small improvements in the strength and high temperature ductility are noted. However, the plastic strain to failure at room temperature as measured on the load-displacement curve was nil. The mode of fracture was again principally intergranular in that each fracture path wound around eutectic grain boundaries.

3.7 Oxidation

3.7.1 Isothermal

Oxidation tests in still air were performed on γ/γ'-δ alloy modifications listed below:

Ni-20.1 w/o Cb-6.0 w/o Cr-2.5 w/o Al-2 w/o Co
Ni-19.7 w/o Cb-6.0 w/o Cr-2.5 w/o Al-1.0 w/o Mo
Ni-18.6 w/o Cb-6.0 w/o Cr-2.5 w/o Al-0.87 w/o Ti
Ni-19.7 w/o Cb-6.0 w/o Cr-2.5 w/o Al-1.0 w/o W
Ni-17.9 w/o Cb-6.0 w/o Cr-2.5 w/o Al-3.0 w/o Ta
Ni-20.3 w/o Cb-4.0 w/o Cr-2.8 w/o Al

at 1000, 1100 and 1200°C for periods of 5, 50, 200 and 500 hrs. The results of these tests are presented in Table XVI. One feature of oxidation was present

quaternary alloy. The data obtained from specimens directionally solidified at 3 cm/hr fall on the top line of the γ/γ'-δ base line alloy. Thus, the Ta modified γ/γ'-δ alloy's Larson Miller parameters exceed NASA VIA by at least two units above 815°C which is the goal of the program. Furthermore, data obtained on two specimens directionally solidified at 2 cm/hr indicated that this alloy modification exceeds the LM parameters of NASA VIA by more than three parameters above 815°C and satisfies the longitudinal rupture strength goal of the program. A vacuum creep curve for one of these specimens is presented in Fig. 56.

3.6.3 Shear

The shear properties of the Ta modified alloy were presented in Table X discussed previously. The goal of not less than 40% of the longitudinal yield strength (0.2% offset) could only be met at intermediate temperature (800°C). At room and elevated temperature the measured shear strengths were approximately 20% of the longitudinal yield strength (Ref. 1).

3.6.4 Thermal Cyclic Fatigue

The effect of three thousand (3000) thermal cycles on the physico-chemical stability of the aligned microstructure of the modified γ/γ'-δ, Ni-17.8 w/o Cb-6.0 w/o Cr-2.5 w/o Al-3.0 w/o Ta is shown in Figs. 57 and 58. Both the size and distribution of the γ' precipitates undergo similar changes from cyclic heat treatment as did the base line γ/γ'-δ alloy (Fig. 44). The interfaces of the δ-Ni_3Cb lamellae displayed no signs of coarsening or decohesion resulting from thermally induced stresses. The 68.2 hr rupture life at 13.8×10^7 N/m^2 and 1100°C measured after cyclic exposure compared favorably with that determined for virgin directionally solidified specimens reported in Table XIV.

3.6.5 Extended Thermal Exposure

The tantalum modified γ/γ'-δ alloy was exposed in vacuum for 1500 hrs to 900°C (1650°F). After air cooling two ridged tensile specimens (Fig. 3) were ground from the d.s. ingot and tested to failure at a strain rate of 0.01 min^{-1}. The two values of strength measured after exposure exceeded those measured on unheat-treated but directionally solidified specimens, i.e. 188,000 psi UTS/183,000 psi, 0.2% Y.S. and 200,500 psi UTS/198,700 psi, 0.2% Y.S. versus 183,500 psi UTS/178,000 psi, 0.2% Y.S. The elastic modulus increased from 36.6 to 38.1 while the elongation decreased from ~4% to ~2%. Failure was associated in both thermally exposed specimens adjacent to the curved ridges. Longitudinal metallographic examination after failure indicated that Widmanstätten precipitation had taken place within γ/γ' as shown in Fig. 59. Furthermore, no extensive twinning and microcracking of δ-Ni_3Cb was observed as is also shown in Fig. 54.

WIDMANSTÄTTEN δ PRECIPITATION WITHIN γ/γ' AND γ' PRECIPITATION WITHIN δ AFTER 1500 HRS AT 850°C (Ni–19.7 w/o Cb–6.0 w/o Cr–2.5 w/o Al; A72–604–02)

5 μm

ARROWS INDICATE WIDMANSTATTEN PRECIPITATION

FIG. 60

γ' Ni_3Al PRECIPITATION WITHIN δ Ni_3Cb LAMELLAE AND COARSENED γ' PRECIPITATES WITHIN γ AFTER 1500 HR EXPOSURE AT 850°C (Ni–21.75 w/o Cb–2.55 w/o Al, A72–807)

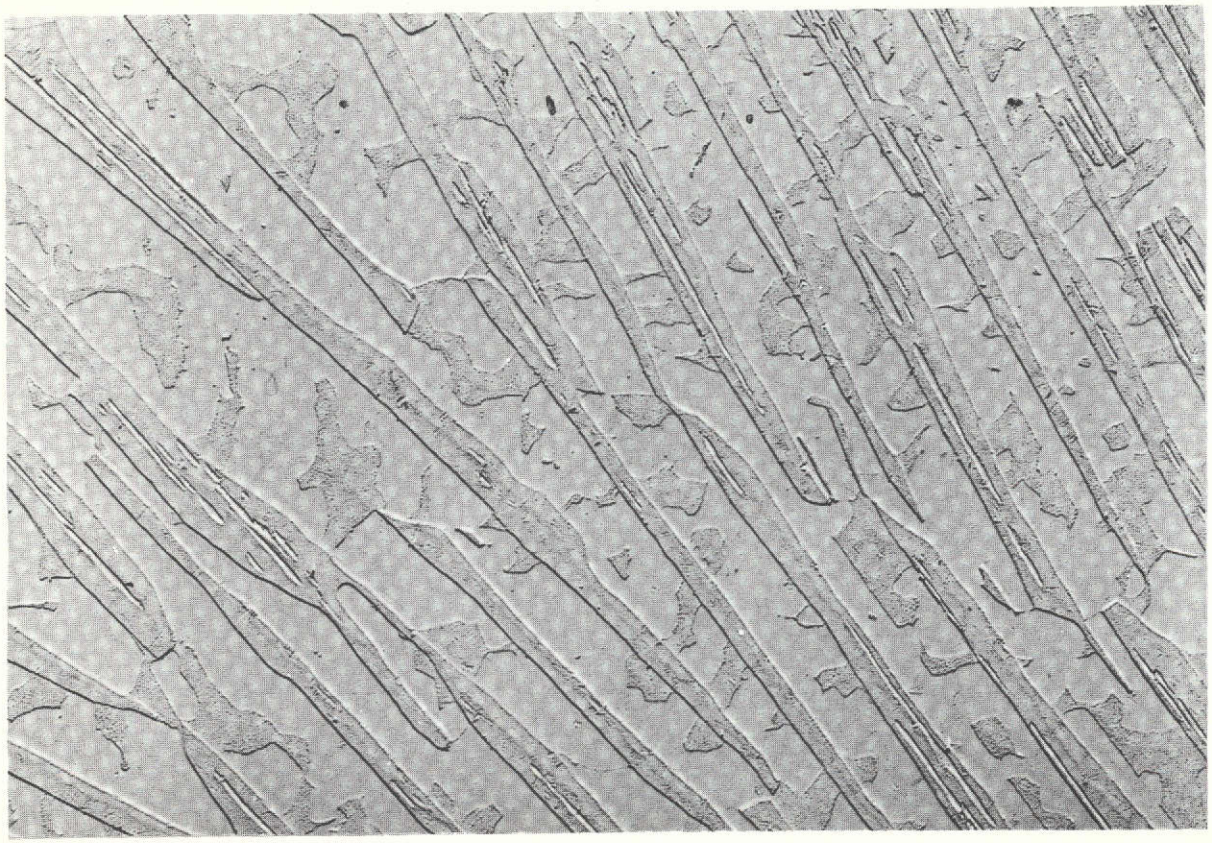

5 μm

N11-9-1

FIG. 61

Table XV

Transverse Tensile Properties of γ/γ'-δ
(Ni-17.8 w/o Cb-3.0 w/o Ta-6.0 w/o Cr-2.5 w/o Al)

Specimen No.	Composition w/o	Temp °C	Temp °F	UTS 10^7 N/m^2	UTS ksi	E 10^{10} N/m^2	E msi	Elong. %	$\dot{\varepsilon}$ min^{-1}
A74-639-01	Ni-17.8Cb-3Ta-6Cr-2.5Al	20	68	50.6	73.3	195.9	28.4	0.31	.01
-02	↓	20	68	58.4	84.6	193.9	28.1	0.47	.01
-03	↓	20	68	58.0	84.0	233.2	33.8	0.33	.01
A74-639-04	↓	760	1400	61.2	88.7	-	-	3.68	.05
-05	↓	760	1400	61.8	89.5	-	-	4.20	.05
-06	↓	760	1400	61.1	88.5	-	-	4.44	.05
A74-639-07	↓	1093	2000	23.1	33.5	-	-	6.88	.05
-08	↓	1093	2000	23.5	34.1	-	-	3.10	.05
-09	↓	1093	2000	21.7	31.5	-	-	4.40	.05

Table XVI

Specific Weight Change (mg/cm^2) (Inclusive of Spall) of Various γ/γ'-δ Alloys after Isothermal Oxidation

	5 hrs	50 hrs	200 hrs	500 hrs
		- 1100°C -		
Ni-20.1Cb-6.0Cr-2.5Al-2.0Co	.994	1.977	2.396	2.551
Ni-19.7Cb-6.0Cr-2.5Al-1.0Mo	1.058	2.226	2.000	1.868
Ni-18.6Cb-6.0Cr-2.5Al-.87Ti	1.192	2.387	2.148	2.626
Ni-19.7Cb-6.0Cr-2.5Al-1.0W	1.640	2.521	2.115	2.749
Ni-17.9Cb-6.0Cr-2.5Al-3.0Ta	1.797	2.939	3.056	2.926
Ni-20.3Cb-4.0Cr-2.8Al	2.090	3.165	3.196	2.753
		- 1000°C -		
Ni-20.1Cb-6.0Cr-2.5Al-2.0Co	.818	1.250	2.034	1.790
Ni-19.7Cb-6.0Cr-2.5Al-1.0Mo	.679	1.374	1.710	1.575
Ni-18.6Cb-6.0Cr-2.5Al-.87Ti	.692	1.302	2.317	1.807
Ni-19.7Cb-6.0Cr-2.5Al-1.0W	.862	1.741	1.931	2.220
Ni-17.9Cb-6.0Cr-2.5Al-3.0Ta	1.521	2.106	2.993	2.133
Ni-20.3Cb-4.0Cr-2.8Al	1.409	2.164	3.537	3.458
		- 760°C -		
Ni-20.1Cb-6.0Cr-2.5Al-2.0Co	.698	1.361	1.512	1.470
Ni-19.7Cb-6.0Cr-2.5Al-1.0Mo	.793	1.140	1.118	1.762
Ni-18.6Cb-6.0Cr-2.5Al-.87Ti	.432	.695	.726	.788
Ni-19.7Cb-6.0Cr-2.5Al-1.0W	.891	1.590	1.755	2.163
Ni-17.9Cb-6.0Cr-2.5Al-3.0Ta	1.640	2.536	3.482	4.240
Ni-20.3Cb-4.0Cr-2.8Al	1.178	2.345	2.844	4.144

for all the γ/γ'-δ modifications. This was the spallation of the external scale on cooling to room temperature. At elevated temperatures the addition of Mo had the most beneficial effect. In general the quinary additions had little effect on modifying the isothermal oxidation behavior of the base quaternary alloy Ni-19.7 w/o Cb-6.0 w/o Cr-2.5 w/o Al (Ref. 1).

3.7.2 Cyclic

Cyclic oxidation tests were performed on the base line quaternary and on two groups of γ/γ'-δ alloy modifications at 1100°C. The compositions tested included:

Ni-19.7 w/o Cb-6.0 w/o Cr-2.5 w/o Al
Ni-20.0 w/o Cb-8.0 w/o Cr-2.5 w/o Al
Ni-19.8 w/o Cb-6.0 w/o Cr-2.8 w/o Al
Ni-20.3 w/o Cb-4.0 w/o Cr-2.8 w/o Al
Ni-20.0 w/o Cb-6.0 w/o Cr-2.5 w/o Al-1.0 w/o Re
Ni-17.9 w/o Cb-6.0 w/o Cr-2.5 w/o Al-3.0 w/o Ta
Ni-19.7 w/o Cb-6.0 w/o Cr-2.5 w/o Al-1.0 w/o Mo
Ni-18.6 w/o Cb-6.0 w/o Cr-2.5 w/o Al-0.87 w/o Ti
Ni-19.7 w/o Cb-6.0 w/o Cr-2.5 w/o Al-1.0 w/o W
Ni-20.1 w/o Cb-6.0 w/o Cr-2.5 w/o Al-2.0 w/o Co

The results of the base line and the quaternary modifications cycled for 100 and 200 hrs at 1100°C respectively are presented in Figs. 62 and 63. The improvement in cyclic oxidation resistance by increasing the chromium content of the quaternary γ/γ'-δ base line alloy is noteworthy.

The results of more extensive cyclic oxidation tests at 1100°C are presented in Fig. 64. Only the tantalum containing γ/γ'-δ alloy could be cycled to 500 hrs as the remaining alloys indicated near complete consumption of the sheet specimen after ~325 hrs. As is noted in Fig. 64, the weight loss versus time data become erratic as complete penetration from oxidation was approached and in some instances the specimens fell from their hooks thereby terminating the usefulness of the test.

X-ray diffraction studies of the oxide scale from the tantalum containing specimen indicated the presence of $CbCrO_4$, Cr_2O_3 and other more complex oxides but no definitive conclusions were drawn to explain the markedly improved cyclic oxidation behavior derived from this quinary addition.

CYCLICAL OXIDATION BEHAVIOR OF Ni–19.7 W/O Cb –6.0 W/O Cr–2.5 W/O Al ($\gamma/\gamma'-\delta$) AT 1100 °C

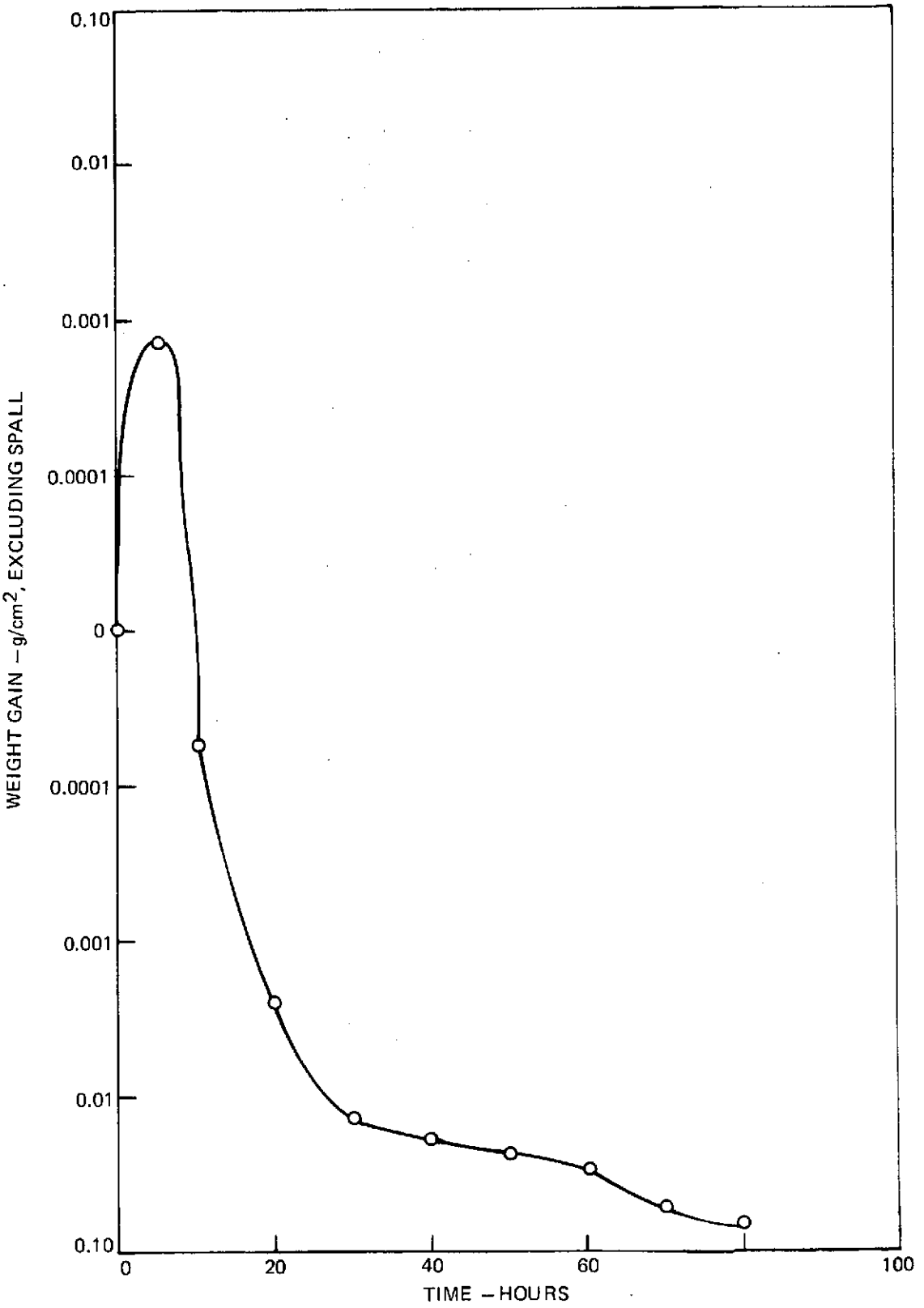

N01–83 – 1

CYCLICAL OXIDATION BEHAVIOR OF VARIOUS $\gamma/\gamma'-\delta$ ALLOYS AT 1100°C

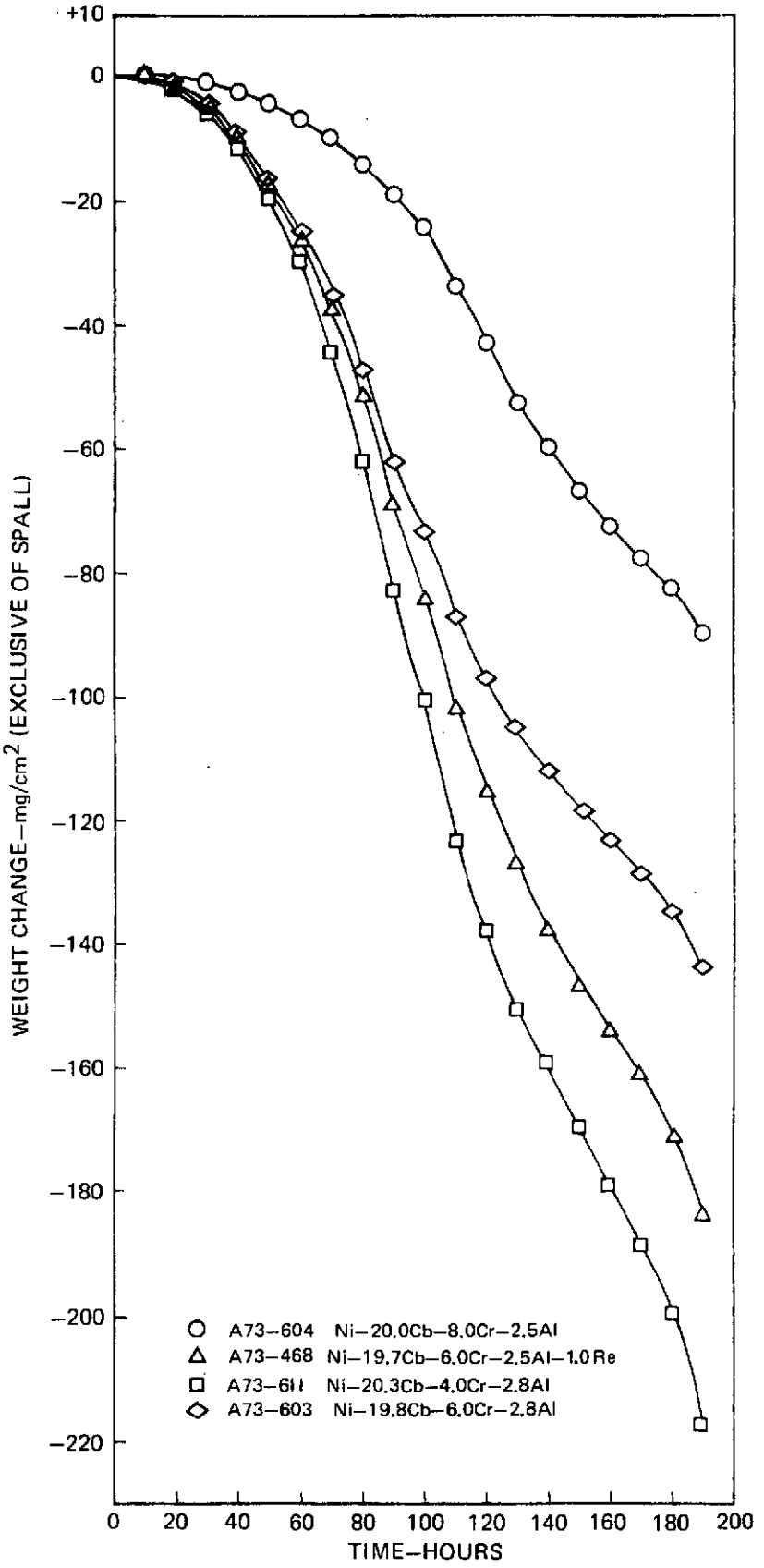

N03−219−1

FIG. 64

CYCLICAL OXIDATION BEHAVIOR OF VARIOUS $\gamma/\gamma'-\delta$ ALLOYS AT 1100°C

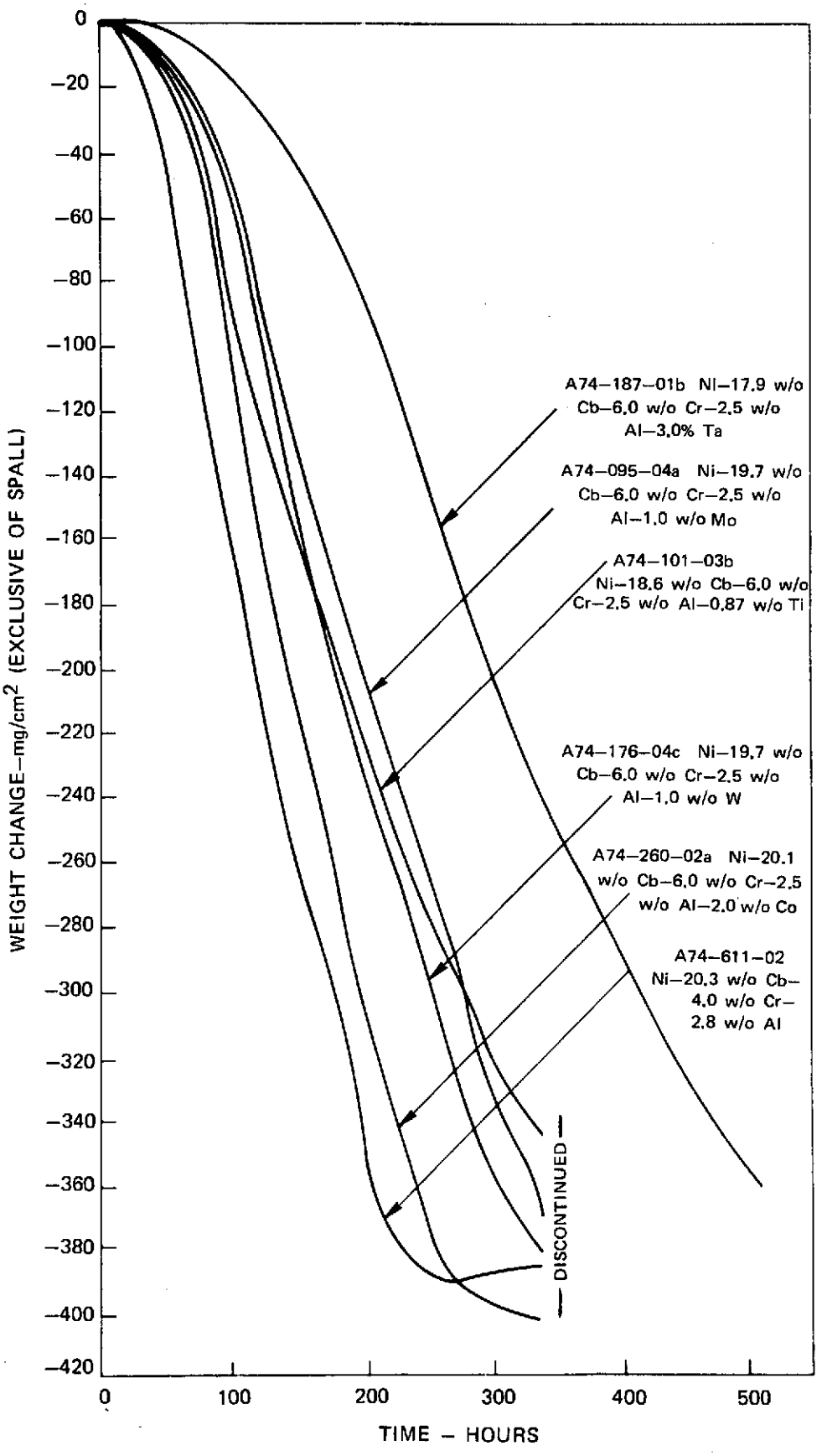

N06–175–1

IV. CONCLUSIONS

1. Considerable latitude in composition modification exists not only for alloys located on the γ-δ liquidus surface within the Ni-Cb-Cr-Al system but for quinary and higher order additions which modify this liquidus surface. This alloy freedom permits changes in the chemistry and volume fraction of both γ/γ' and δ phases.

2. Extensive alloying of the γ/γ'-δ base line quaternary is possible for elements (e.g. Co, Ti, and Ta) which exhibit a wide solubility range in both phases. Limited substitution of W, Mo, Re, Si, and B on the other hand is possible for elements with restricted solid solubility especially in the δ phase.

3. The lattice parameter difference between γ and γ' can be reduced below 1 percent but a zero misfit alloy composition containing six percent by weight chromium remains to be defined since uncertainties in the partitioning of alloyed elements in each phase and the negative compositional dependence of the lattice parameter of γ' on chromium have not been resolved.

4. More uniformity in longitudinal composition can be observed for ingots produced with induction heating equipment modified to minimize power fluctuations in the load coil. Macrosegregation can be suppressed from quaternary γ/γ'-δ alloys directionally solidified under a steep thermal gradient (~300°C/cm) and at a slow freezing velocity (~3 cm/hr).

5. Heat treatment of the quaternary γ/γ'-δ alloy indicates that useful alterations in the strength and ductility at low and intermediate temperatures can be effected. However, at elevated temperature (1100°C) no improvement has been observed.

6. The transverse tensile strength and ductility program goals (>80% of longitudinal) have not been met by any alloy modification and their achievement presents a great challenge to the alloy metallurgist.

7. The creep rupture strength of the tantalum modified γ/γ'-δ alloy (Ni-17.9 w/o Cb-6.0 w/o Cr-2.5 w/o Al-3.0 w/o Ta) after directional solidification at 2 cm/hr exceeds NASA VIA by approximately three and one-half Larson-Miller parameters (C=20) above 1000°C and exceeds the program goal by two parameters.

8. The addition of tantalum provides improvement in longitudinal shear strength compared with the base line quaternary alloy but falls short of the program goal (>40% of longitudinal yield strength) except near 850°C.

9. Widmanstatten precipitates can be observed in both the tantalum modified and base line γ/γ'-δ alloys after extended (1500 hr) thermal exposures to 850 and 900°C respectively. The presence of Widmanstätten δ within γ/γ' was somewhat deleterious to the low temperature fracture ductility. No reduction in rupture life at 1100°C was observed for a specimen thermally cycled 3000 times to 1121°C.

10. The addition of 3 w/o tantalum or a 2 w/o increase in the chromium content of the γ/γ'-δ base line alloy results in improved cyclic oxidation resistance at 1100°C.

V. RECOMMENDATIONS FOR FURTHER EVALUATION

Although the longitudinal mechanical properties of the γ/γ'-δ alloy family of directionally solidified eutectic superalloys are outstanding, further improvements in transverse strength are envisioned through quaternary additions to the monovariant γ/γ'-δ eutectic. In addition a zero lattice γ/γ' misfit composition is achievable through quaternary alloy additions to the chromium free monovariant eutectic composition. Finally, as δ precipitation within γ/γ' was observed after prolonged ~1500 hr exposures to intermediate temperatures, it would be desirable to construct a T-T-T curve describing the Ni_3Cb transformation kinetics to assist turbine designers. Because of the processing advantage (no) low chromium γ/γ'-δ alloys possess, alloy additions to this base composition are warranted to achieve rupture properties superior to NASA VI A.

VI. REFERENCES

1. F. D. Lemkey: "Eutectic Superalloys Strengthened by δ, Ni_3Cb Lamellae and γ', Ni_3Al Precipitates", NASA CR-2278, Final Report NAS3-15562, Nov. 1973.

2. K. Sheffler and R. Barkalow: Private communication.

3. R. L. Ashbrook: "Directionally Solidified Composite Systems Under Evaluation", AGARD Specialists Meeting on Directionally Solidified (In Situ) Composites, Washington, D.C., April 1974.

4. W. A. Tiller, K. A. Jackson, J. W. Rutter, and B. Chalmers: Acta Met., 1, 1953, p. 428.

5. E. R. Thompson, F. D. George, and E. M. Breinan: "The Influence of Interlamellar Spacing on the Strength of the Ni_3Al-Ni_3Cb Eutectic", Proceedings of the Conference on In Situ Composites, NMAB-308-II, Printing & Publishing Office, National Academy of Sciences, Washington, D.C., pp 71-81.

6. E. M. Breinan, E. R. Thompson, and F. D. Lemkey: "The Effect of Thermal Cycling on High Temperature Eutectic Composites", Ibid., pp 201-222.

7. I. J. Duerden and W. Home-Rothery: "The Equilibrium Diagram of the System Niobium-Nickel, J. Less Common Metals, 11, 1966, p. 381.

8. I. I. Kornilov and Ye. N. Pylayeva: Russian Metallurgy (Izv. Akad, Nauk SSSR Metally) (1972-73) 69 UDC 669,293,5'24.

9. R. S. Mints, G. F. Belyayeva, Yu. S. Malkov: "Interaction Between the Intermetallic Phases Ni_3Al-Ni_3Cb", Doklady AN SSSR (1962) 143, 4, 871.

10. J. S. Benjamin, W. C. Giessen, and N. J. Grant: "Intermediate Phase in the Ternary System Nb-Ni-Al at 1140°C", Met. Trans. 236, 1966, p. 224.

11. V. Ya. Markiv, N. F. Matushevskaya, Yu. B. Kuzima: "X-ray Investigation of the Nb-Ni-Al System", Isv. AN SSSR, Metally, 1966, No. 6, 127.

12. V. N. Svechnikov, V. M. Pan, and V. G. Korobeynikova: "Phase Diagram of the Niobium-Nickel System", Sb. nauchn. tr. In-Ta met. fiz. AN-UKr SSR 19, 1964, p. 199.

13. S. N. Pogodin and A. P. Zelikman: "Phases of Variable Composition in the Ni-Nb System", Izv. SFKhN, 16, 1943, p. 1158.

14. J. Cisse and R. G. Davies: "Nickel-Rich Portion of the Ni-Al-Nb Phase Diagram", Met. Trans., 1, 1970, p. 2003.

15. D. S. Duvall and M. J. Donachie, Jr.: "Phase Equilibria in Nickel-Rich Ni-Al-Nb Alloys", J. Inst. of Metals, 98, 1970, p. 182.

16. L. N. Guseva, R. S. Mintx, Yu. S. Malkov: "Phase Equilibria in the Ni-Ni_3Al-Ni_3Nb System in the Temperature Range 800-1200°C", Izv. Akad Nauk SSSR Metally, 1968, p. 120.

17. Cbeyhnkob and V. M. Pan in Z. M. Rogachevskaya, Structural Diagrams of Metallic Systems, Vol. 8, Moscow, 1960, p 211.

18. G. A. Sveshnikova and A. M. Borzdyka, "Solubility of Niobium in Nickel-Chromium Solid Solution", Izv. AN SSSR Metally, 6, 1966, p. 137.

19. V. I. Malkin and V. V. Pokidyshev: "Effect of a Third Component Added to Ni-Al Alloys on the Thermodynamic Properties of γ/γ'", DoKv Akad Nauk SSSR, 166, 1966, p. 1390.

20. N. E. Collins, R. J. Quigg, and R. L. Dreshfield: "Development of a Nickel-Base Superalloy Using Statistically Designed Experiments", ASM Trans., 61, 1968, p. 711.

21. G. E. P. Box and K. B. Wilson: "On the Experimental Attainment of Optimum Conditions", J. Roy. Stat. Soc. Series B, 13, 1951, p. 1.

22. C. S. Giggins and F. S. Pettit: "Oxidation of Ni-Cr-Al Alloys Between 1000° and 1200°C", J. Electrochem. Soc. Solid State Science, Nov. 1971, p 1787.

23. R. M. N. Pelloux and N. G. Grant: Trans. AIME, 218, 1960, p. 232.

24. E. R. Parker and T. H. Hazlett: "Principles of Solution Hardening", Relation of Properties to Microstructure, ASM (1954) p 30.

25. M. V. Pridantsev, G. V. Estulin, and L. N. Zimina: "Influence of Molybdenum and Tungsten on the Properties of High Temperature Nickel Alloys", Stal', 1964, 4, p 349.

26. L. M. Mirskiy: "Diffusional Changes in Alloys", Oborongiz, 53, 1959, p. 54.

27. G. A. Sveshnikova and A. M. Borzdyka: "Influence of Mo and W on the Properties of Ni-Cr-Cb Alloys", Russian Metallurgy, 1972-73, p. 170.

28. I. I. Kornilov and E. N. Pylaeva: "Investigation of the Phase Diagrams of the Ternary System Ni-Ni_3Nb-Ni_3Ta", Zhurnal Neorganicheska Khimii, 1, No. 2 1956, p. 308-16.

29. L. I. Pryakhina, K. P. Myasnikova, V. V. Burnashova, E. E. Cherkashin, and V. Ya. Markiv: "Ternary Intermetallic Compounds in the System Ni-Ti-Nb", Poroshkovaya Metallurgiya, 44, 1966, p. 61-69.

30. C. E. Lowell and R. V. Miner: Improvement in Cyclic Oxidation of the Nickel-Base Superalloy B-1900 by Addition of One Percent Silicon", NASA TM X-68191, Jan. 1973.

31. R. G. Davies and T. L. Johnston: "Ordered Alloys-Structural Application and Physical Metallurgy", Proc. 3rd Bolton Landing Conf., B. H. Kear, et al, eds, Claitor's Publishing Div., Baton Rouge, La., 1970.

32. C. Wagner: "Theorie de Aelterung von Niederschlagen durch Unlosen", (1961) 65, 581-91.

33. R. T. Quinn, R. W. Kraft, and R. W. Hertzberg: Trans. ASM, 62, 1969, p. 38.

34. W. B. Pearson: A Handbook of Lattice Spacing and Structures of Metals and Alloys, Vol. 2, Pergamon Press, Oxford, 1967.

35. A. V. Karg, B. H. Kear, A. F. Giamei, and D. E. Fornwalt: Pratt and Whitney Aircraft, Middletown, Ct., Unpublished Research.

36. R. B. Golubtsova: Separation of the Intermetallide Phase Ni_3Al from a Ni-Cr-Al Alloy", Izv Akad Nauk SSSR Metally, 1966, p. 99-101.

37. E. H. Kraft and E. R. Thompson: Final Report, Contract N00019-72-C-0192, Nov. 1972.

38. R. Barkalow and M. Donachie: Pratt and Whitney Aircraft, East Hartford, Ct., Unpublished Research.

39. E. Felten, T. E. Strangeman and R. Ulion: NAS3-16792, Quarterly Technical Progress Narrative, Jan. 1974.

40. E. H. Kraft, E. R. Thompson, V. M. Patarini: Final Report, Contract N62269-73-C-0310, April 1974.

41. R. E. Reed Hill: "A Rapid Graphical Single Surface Orientation Technique for Face Centered Metals", Trans. Met. Soc. AIME, 236, 1966, p. 1283.

42. C. Grossiard, G. Lesoult, and M. Turpin: "Slip and Mechanical Twinning in Ni-Ni_3Cb Directionally Solidified Eutectic Alloy", Proceedings of the International Materials Symposium, Univ. of California, Berkeley, 1971.

43. F. D. George: "Development of High Temperature Fasteners Using Directionally Solidified Eutectic Alloys", Final Report, NAS8-27358, NASA CR-123919.

44. P. H. Thornton, R. G. Davies and T. L. Johnston: "The Temperature Dependence of the Flow Stress on the γ' Phase Based Upon Ni_3Al", Met. Trans., 1, 1970, p 270.

45. M. Gell and R. H. Barkalow: The Microstructure and Design of Alloys, Proc. of Third Int. Conf. on Strength of Metals and Alloys, Inst. of Metals, 1973, Paper 53.

46. E. R. Thompson, F. D. George, and E. M. Breinan: "The Influence of Interlamellar Spacing on the Strength of the Ni_3Al-Ni_3Cb Eutectic", Proceedings of the Conf. on In Situ Composites, Lakeville, Ct., Sept. 1972, National Academy of Science and Engineering, Washington, D.C., NMAB 308-II, p. 71-82.

47. E. M. Breinan, E. R. Thompson, and F. D. Lemkey: Proc. Conf. on In Situ Composites, NMAB 208-II, Nat. Mats. Adv. Bd. (1973) p 201-222.

48. F. D. Lemkey and E. R. Thompson: Proc. Conf. on In Situ Composites, NMAB 208-II, Nat. Mats. Adv. Bd. (1973) p 105-120.

DISTRIBUTION LIST FOR NASA CR-134678

NAS3-17785

MR. J. ACUAIO
MS 77-5
NASA LEWIS RESEARCH CTR.
21000 BROOKPARK ROAD
CLEVELAND, OHIO 44135

DR. C.W. ANDREWS
MS 49-3
NASA LEWIS RESEARCH CTR.
21000 BROOKPARK ROAD
CLEVELAND, OHIO 44135

DR. R.L. ASHBROOK
MS 49-3
NASA LEWIS RESEARCH CTR.
21000 BROOKPARK ROAD
CLEVELAND, OHIO 44135

MR. G.M. AULT
MS 3-5
NASA LEWIS RESEARCH CTR
21000 BROOKPARK ROAD
CLEVELAND, OHIO 44135

MR. P.T. BIZON
MS 49-1
NASA LEWIS RESEARCH CTR
21000 BROOKPARK ROAD
CLEVELAND, OHIO 44135

MR. C.P. BLANKENSHIP
MS 105-1
NASA LEWIS RESEARCH CTR
21000 BROOKPARK ROAD
CLEVELAND, OHIO 44135

DR. R.L. DRESHFIELD
MS 49-1
NASA LEWIS RESEARCH CTR.
21000 BROOKPARK ROAD
CLEVELAND, OHIO 44135

MR. J.C. FRECHE
MS 49-1
NASA LEWIS RESEARCH CTR
21000 BROOKPARK ROAD
CLEVELAND, OHIO 44135

DR. H.R. GRAY
MS 49-1
NASA LEWIS RESEARCH CTR.
21000 BROOKPARK ROAD
CLEVELAND, OHIO 44135

MR. S.J. GRISAFFE
MS 49-3
NASA LEWIS RESEARCH CTR
21000 BROOKPARK ROAD
CLEVELAND, OHIO 44135

MISS T.D. GULKO
MS 49-3
NASA LEWIS RESEARCH CTR.
21000 BROOKPARK ROAD
CLEVELAND, OHIO 44135

MR. R.W. HALL
MS 49-1
NASA LEWIS RESEARCH CTR
21000 BROOKPARK ROAD
CLEVELAND, OHIO 44135

MR. P.H. HARF (10)
MS 49-3
NASA LEWIS RESEARCH CTR
21000 BROOKPARK ROAD
CLEVELAND, OHIO 44135

MR. M.H. HIRSCHBERG
MS 49-1
NASA LEWIS RESEARCH CTR.
21000 BROOKPARK ROAD
CLEVELAND, OHIO 44135

MR. B.H. KEMP
MS 49-3
NASA LEWIS RESEARCH CTR.
21000 BROOKPARK ROAD
CLEVELAND, OHIO 44135

MR. J.P. MERUTKA
MS 49-3
NASA LEWIS RESEARCH CTR
21000 BROOKPARK ROAD
CLEVELAND, OHIO 44135

MR. T.J. MOORE
MS 105-1
NASA LEWIS RESEARCH CTR
21000 BROOKPARK ROAD
CLEVELAND, OHIO 44135

DR. H.E. PROBST
MS 49-3
NASA LEWIS RESEARCH CTR.
21000 BROOKPARK ROAD
CLEVELAND, OHIO 44135

MR. M. QUATINETZ
MS 49-3
NASA LEWIS RESEARCH CTR.
21000 BROOKPARK ROAD
CLEVELAND, OHIO 44135

MR. N.T. SAUNDERS
MS 105-1
NASA LEWIS RESEARCH CTR
21000 BROOKPARK ROAD
CLEVELAND, OHIO 44135

MR. C. SCHEUERMANN
MS 49-1
NASA LEWIS RESEARCH CTR.
21000 BROOKPARK ROAD
CLEVELAND, OHIO 44135

MR. R.A. SIGNORELLI
MS 106-1
NASA LEWIS RESEARCH CTR.
21000 BROOKPARK ROAD
CLEVELAND, OHIO 44135

MR. J.L. SMIALEK
MS 49-3
NASA LEWIS RESEARCH CTR
21000 BROOKPARK ROAD
CLEVELAND, OHIO 44135

MR. J.W. WEETON
MS 49-3
NASA LEWIS RESEARCH CTR.
21000 BROOKPARK ROAD
CLEVELAND, OHIO 44135

CONTRACTS SECTION 6
MS 500-313
NASA LEWIS RESEARCH CTR
21000 BROOKPARK ROAD
CLEVELAND, OH 44135

LIBRARY (2)
MS 60-3
NASA LEWIS RESEARCH CTR
21000 BROOKPARK ROAD
CLEVELAND, OHIO 44135

PATENT COUNSEL
MS 500-113
NASA LEWIS RESEARCH CTR
21000 BROOKPARK ROAD
CLEVELAND, OHIO 44135

REPORT CONTROL OFFICE
MS 5-5
NASA LEWIS RESEARCH CTR
21000 BROOKPARK ROAD
CLEVELAND, OHIO 44135

TECHNOLOGY UTILIZATION
MS 3-19
NASA LEWIS RESEARCH CTR
21000 BROOKPARK ROAD
CLEVELAND, OHIO 44135

IT.COL. H.L. STAUBS
AFSC LIAISON MS 501-3
NASA LEWIS RESEARCH CTR
21000 BROOKPARK ROAD
CLEVELAND, OHIO 44135

DR. Y.G. KIM
MS 49-1
NASA LEWIS RESEARCH CTR
21000 BROOKPARK ROAD
CLEVELAND, OHIO 44135

DR. S.K. TEWARI
MS 49-3
NASA LEWIS RESEARCH CTR
21000 BROOKPARK ROAD
CLEVELAND, OHIO 44135

CAPT. D.W. ZABIEREK
AFAPL/TBP
HEADQUARTERS
WRIGHT PATTERSON AFB.
OH 45433

DR. D.J. VIECHNICKY ARMMR
ARMY MATERIALS AND
MECHANICS RESEARCH CTR.
WATERTOWN, MA 02172

MR G. C. DEUTSCH / RW
NASA HEADQUARTERS
WASHINGTON, DC
20546

MR. J. MALTZ / RWM
NASA HEADQUARTERS
WASHINGTON, DC
20546

MR. N.C. KALLOS
SAVDL-EU-PP
US ARMY AIR MOBILITY
R&D LABORATORY
FORT EUSTIS, VA 23604

MR. I. MACHLIN AIR-520318
NAVAL AIR SYSTEMS COMMAND
NAVY DEPARTMENT
WASHINGTON, DC 20361

LIBRARY
NASA
GODDARD SPACE FLIGHT CTR
GREENBELT, MARYLAND 20771

LIBRARY MS 185
NASA
LANGLEY RESEARCH CENTER
LANGLEY FIELD, VA 23365

MR. H.J. SCHAEFER
CODE 6350
U.S. NAV. RES. LAB.
WASHINGTON, DC 20390

MR. F.S. GARDNER
OFFICE OF NAVAL RESEARCH
495 SUMMER STREET
BOSTON, MA 02210

MR. R. HASEMEYER
NASA S&E-PE-RMM
MARSHALL SPACE FLIGHT
CENTER
HUNTSVILLE, AL 35812

LIBRARY
NASA
MARSHALL SPACE FLIGHT
CENTER
HUNTSVILLE, AL 35812

MR. R.E. TRABOCCO
PHYSICAL METALL. BRANCH
NAV. AIR DEV. CENTER
WARMINSTER, PA 18974

MR. H.D. FITZSIMMONS
NATIONAL AERONAUTICS AND
SPACE COUNCIL
EXEC OFF OF THE PRESIDENT
WASHINGTON, DC 20502

TECHNICAL LIBRARY / JM6
NASA
JOHNSON SPACE CENTER
HOUSTON, TX 77058

LIBRARY - ACQUISITIONS
JET PROPULSION LAB.
4800 OAK GROVE DRIVE
PASADENA, CA 91102

TECHNICAL REPORTS LIBRARY
ATOMIC ENERGY COMMISSION
WASHINGTON D.C. 20545

MR. J.P. HAMMOND
OAK RIDGE NATIONAL LAB
OAK RIDGE, TN 37830

LIBRARY
NASA FLIGHT RESEARCH CTR
P.O. BOX 273
EDWARDS, CALIFORNIA 93523

LIBRARY - REPORTS
MS 202-3
NASA AMES RESEARCH CENTER
MOFFETT FIELD, CA 94035

MR. G.P. BATES RD-70C
DEPT. OF TRANSPORTATION
FAA
WASHINGTON, DC 20590

MR. E. FLINT
DEPT. OF INTERIOR
BUREAU OF MINES
WASHINGTON, DC 20240

ACQUISITIONS BRANCH (10)
NASA SCIENTIFIC & TECHN.
INFORMATION FACILITY
BOX 33
COLLEGE PARK, MD 20740

DEFENCE DOCUMENTATION CTR
CAMERON STATION
5010 DUKE STREET
ALEXANDRIA, VIRGINIA
22314

MR. F. WOOD
DEPT. OF INTERIOR
BUREAU OF MINES
P.O. BOX 70
ALBANY, OR 97321

MR. J.R. LANE
MATERIALS ADV. BD.
NAT. ACAD. OF SCIENCES
2101 CONSTITUTION AVE.
WASHINGTON, DC 20418

CAPT. S. DUNCO
AFML/LLC
HEADQUARTERS
WRIGHT PATTERSON AFB.
OH 45433

MR. W. SCHULZ
AFSC/
HEADQUARTERS
WRIGHT PATTERSON AFB.
OH 45433

DR. C.W. SPENCER
MATERIALS ADV. BD.
NAT. ACAD. OF SCIENCES
2101 CONSTITUTION AVE.
WASHINGTON, DC 20418

DR. D.R. ROSSINGTON
SUNY COLLEGE OF CERAMICS
ALFRED UNIVERSITY
ALFRED, NY 14802

MR. H.E. BOYER
AM. SOCIETY FOR METALS
METALS PARK
NOVELTY, OH 44073

DR. R.I. JAFFEE
BATTELLE MEMORIAL INST.
505 KING AVENUE
COLUMBUS OHIO 43201

DR. E. WILCOX
BATTELLE MEMORIAL INST.
505 KING AVENUE
COLUMBUS, OHIO 43201

DR. A. YUE
DEPARTMENT OF METALLURGY
UNIVERSITY OF CALIFORNIA
LOS ANGELES, CALIFORNIA
90024

MR. T.Z. KATTAMIS
SCHOOL OF ENGINEERING
UNIVERSITY OF CONNECTICUT
STORRS, CT 06268

PROF. A. LEWLEY
DEPT. OF METALL. ENGRG.
DREXEL UNIVERSITY
PHILADELPHIA, PA
19104

DR. J.F. PENZEL
SCH. OF CERAMIC ENGRG.
GEORGIA INST. OF TECHN.
ATLANTA, GA 30080

PROF. J.D. VERHOEVEN
DEPARTMENT OF METALLURGY
IOWA STATE UNIVERSITY
AMES, IOWA 50010

MR. N. GRIESENAUER
BATTELLE MEMORIAL INST.
505 KING AVENUE
COLUMBUS, OHIO 43201

NCIC
BATTELLE MEMORIAL INST.
505 KING AVENUE
COLUMBUS, OHIO 43201

MR. J.M. DICKINSON
UNIVERSITY OF CALIFORNIA
LOS ALAMOS SCI. LAB.
P.O. BOX 1663
LOS ALAMOS, NM 87544

PROF. J.F. WALLACE
DEPT. OF MET. & MAT. SCI.
CASE - WESTERN RESERVE U.
CLEVELAND, OH 44106

PROF. J.E. DAVISON
UNIVERSITY OF DAYTON
RESEARCH INSTITUTE
300 COLLEGE PARK AVE
DAYTON, OHIO 45409

DR. F.H. COCKS
SCHOOL OF ENGINEERING
DUKE UNIVERSITY
DURHAM, NC 27706

DR. D.L. ALBRIGHT
DEPT. MET. & MATL. ENGRG.
ILL. INST. OF TECHN.
CHICAGO, IL 60616

DR. W. HERTZBERG
DEPT. MET. & MATL. SCI.
LEHIGH UNIVERSITY
BETHLEHEM, PA 18015

DR. W.R. KRAFT
DEPT. MET. & MATL. SCI.
LEHIGH UNIVERSITY
BETHLEHEM, PA 18015

PROF. N.J. GRANT
DEPT. OF METALLURGY
MASS. INST. OF TECHNOLOGY
CAMBRIDGE, MA 02139

DR. S.A. DAVID
DEPT. OF METALLURGY
UNIVERSITY OF PITTSBURGH
PITTSBURGH, PA 15213

PROF. G.S. ANSELL
RENSSELAER POLYTECHNICAL
INSTITUTE
TROY, NY 12180

DR. E.P. OLIVER
DEPT. CHEM. & MET. ENGRG
UNIVERSITY OF TENNESSEE
KNOXVILLE, TE 37916

MR. D.M. GODDARD
AEROSPACE CORPORATION
PO BOX 95085
LOS ANGELES, CA 90045

MR. L.J. FIEDLER
AVCO LYCOMING DIV.
550 S.MAIN STREET
STRATFORD, CT 06497

LIBRARY
BJORKSTEN RES. LAB.
P. O. BOX 265
MADISON, WI 53701

PROF. M.C. FLEMINGS
DEPT. OF METALLURGY
MASS. INST. OF TECHNOLOGY
CAMBRIDGE, MA 02139

PROF. M.J. SINNOTT
COLLEGE OF ENGINEERING
UNIVERSITY OF MICHIGAN
ANN ARBOR, MI 48104

PROF. P. WINCHELL
MATL. SCI. & MET. ENG.
PURDUE UNIVERSITY
WEST LAFAYETTE, IN
47906

PROF. O. SHERBY
DEPT. OF MATERIALS SCI.
STANFORD UNIVERSITY
PALO ALTO, CALIF. 94305

DR. T.T. COURTNEY
UNIVERSITY OF TEXAS
MATLS.SCI. LAB.
AUSTIN, TX 78712

MR. G.B. BARTHOLD
ALUMINUM CO. OF AMERICA
1200 RING BLDG
WASHINGTON, DC 20036

DR. K.A. JACKSON
BELL TELEPHONE LABS.
600 MOUNTAIN AVENUE
MURRAY HILL, NJ 07974

MR. E.C. BOVIE
BOEING COMPANY
P.O. BOX 3733
SEATTLE, WA 98124

DR. S.T. WLODEK
STELLITE DIVISION
CABOT CORPORATION
1020 W. PARK AVE
KOKOMO, IN 46901

DR. D.L. SPONSELLER
CLIMAX MOLYBDENUM COMPANY
1600 HURON PARKWAY
ANN ARBOR, MICHIGAN 48106

MR. R.E. ENGDAHL
DEPOSITS & COMPOSITES INC
1821 MICHAEL FARADAY DR.
RESTON, VA 22090

DR. H.F. KIRBY
GARRETT AIRESEARCH
DEPT. 93-393
402 S. 36TH STREET
PHOENIX, AR 85034

DR. M.F. HENRY
CRD
GENERAL ELECTRIC COMPANY
P.O. BOX 8
SCHENECTADY, N.Y. 12301

MR. J.L. WALTER
CRD
GENERAL ELECTRIC COMPANY
P.O. BOX 8
SCHENECTADY, N.Y. 12301

MR. G.H. WASIELEWSKI
MATERIALS & PROCESSES LAB
GENERAL ELECTRIC COMPANY
SCHENECTADY, N.Y. 12345

DR. C.A. BRUCH
AEG/GED
GENERAL ELECTRIC COMPANY
CINCINNATI, OHIO 45215

LIBRARY
CHRYSLER CORPORATION
DEFENSE-SPACE GROUP
P.O. BOX 757
DETROIT, MI 48231

MR. J. MOGUL
DIR - MATLS ENGRG
CURTISS-WRIGHT
1 PASSAIC ST
WOOD-RIDGE, NJ 07075

DR. T.P. TSIANG
MATERIALS DEVELOPMENT
FORD MOTOR COMPANY
ONE PARKLANE BOULEVARD
DEARBORN, MICHIGAN 48126

DR. E.G. ZEMZ
CRD
GENERAL ELECTRIC COMPANY
P.O. BOX 8
SCHENECTADY, N.Y. 12301

LIBRARY
CRD
GENERAL ELECTRIC COMPANY
P.O. BOX 8
SCHENECTADY, N.Y. 12301

LIBRARY
ADVANCED TECHNOLOGY LAB
GENERAL ELECTRIC COMPANY
SCHENECTADY, NY 12345

TECHN. INFORMATION CENTER
AEG
GENERAL ELECTRIC COMPANY
CINCINNATI, OHIO 45215

DR. J.W. SEMMEL
AEG/GED
GENERAL ELECTRIC COMPANY
CINCINNATI, OHIO 45215

DR. M. HERMAN
DETROIT DIESEL ALLISON DV
P.O. BOX 894
INDIANAPOLIS, IN 46206

DR. E.E. REYNOLDS
TECHNICAL CENTER
GENERAL MOTORS CORP.
WARREN, MI 48090

MR. F. JAEGER
HOMMET CORPORATION
AUSTENAL DIVISION
DOVER, NJ 07801

DR. R.F. DECKER
INTERNATIONAL NICKEL CO.
ONE NEW YORK PLAZA
NEW YORK, NY 10004

MR. T. MILES
KELSEY HAYES CORPORATION
7250 WHITMORE LAKE ROAD
BRIGHTON, MI 48116

TECHNICAL INFORMATION CTR.
MATLS. & SCIENCE LAB.
LOCKHEED RESEARCH LABS
3251 HANOVER STREET
PALO ALTO, CAL. 94304

DR. S. WEINIG
MATERIALS RESEARCH CORP.
ORANGEBURG, NY 10962

DR. J.C. WILLIAMS
ROCKWELL INTERNATIONAL
SCIENCE CENTER
THOUSAND OAKS, CALIFORNIA
91360

LIBRARY
MATERIALS SCIENCE LAB.M5
DETROIT DIESEL ALLISON
GENERAL MOTORS
INDIANAPOLIS,IN 46206

DR. F.M. DUNLEVEY
GOULD LABORATORIES
GOULD INC.
540 EAST 105TH STREET
CLEVELAND, OH 44108

MR. W.H. FREEMAN
SUPERALLOY GROUP
HOMMET CORPORATION
WHITEHALL, MI 49461

MR. R.C. GIBSON
INTERNATIONAL NICKEL CO.
MERICA RESEARCH LAB
STERLING FOREST
SUFFERN, NY 10901

DR. W.S. CHEMENS
RESEARCH LABORATORY
LOCKHEED-GEORGIA COMPANY
MARIETTA, GEORGIA 30060

DR. I. KAUFMAN
MANLABS, INC
21 ERIE STREET
CAMBRIDGE, MA 02139

DR. G. GABRONG
ROCKWELL INTERNATIONAL
SCIENCE CENTER
THOUSAND OAKS, CALIFORNIA
91360

DR. M. SUTTON
SPECIAL METALS
CORPORATION
NEW HARTFORD, N.Y. 13413

DR. T. RIVONKA
MATERIALS TECHNOLOGY
TRW EQUIPMENT GROUP
23555 EUCLID AVENUE
CLEVELAND, OHIO 44117

LIBRARY
MATERIALS TECHNOLOGY
TRW EQUIPMENT GROUP
23555 EUCLID AVENUE
CLEVELAND,OH 44117

DR. E.A. STEIGERWALD
TRW METALS DIVISION
NINEVA, OH 44657

DR. G.F. HURLEY
TYCO LABORATORIES, INC
16 HICKORY DRIVE
WALTHAM, MA 02154

DR. A.I. MLAVSKY
TYCO LABORATORIES, INC
16 HICKORY DRIVE
WALTHAM, MA 02154

DR. P.S. KOTVAL
UNION CARBIDE
RESEARCH INSTITUTE
TARRYTOWN, NY 10591

DR. D.R. HOPKINS
WESTINGHOUSE RESEARCH LAB
BEULAH ROAD
PITTSBURGH, PENNSYLVANIA
15235